

Filip Karlsen  
Steinar Sund-Olsen

# A Laboratory Study on the Use of Non-Destructive Testing for Evaluation of the Strength and Deformation Properties of Stabilized Soil

Master's thesis in Bygg- og miljøteknikk  
Supervisor: Priscilla Paniagua  
Co-supervisor: Sølve Hov  
June 2023





Filip Karlsen  
Steinar Sund-Olsen

# **A Laboratory Study on the Use of Non-Destructive Testing for Evaluation of the Strength and Deformation Properties of Stabilized Soil**

Master's thesis in Bygg- og miljøteknikk  
Supervisor: Priscilla Paniagua  
Co-supervisor: Sølve Hov  
June 2023

Norwegian University of Science and Technology  
Faculty of Engineering  
Department of Civil and Environmental Engineering





# Preface

This master's thesis is written as the final part of our master's degree in geotechnical engineering at Norges Teknisk-Naturvitenskapelige Universitet (NTNU) during the spring of 2023. The study is written in collaboration with Norges Geotekniske Institutt (NGI) as a part of the Green sOil stAbiLization (GOAL) research project. The study is a continuation of our project thesis from 2022 which was a literature study about the comparison of apparatuses to measure seismic wave velocities.

We would like to thank NGI for facilitating the material and some of the equipment for the laboratory work. Special appreciation goes to our main supervisor, Priscilla Paniagua for her guidance throughout the study and our co-supervisor Sølve Hov for interesting discussions and help at the laboratory. We would also like to thank Stefan Ritter and the other people involved in the GOAL project for their help and discussions regarding the study.

A special thanks to the people working at the geotechnical department at NTNU for assistance at the laboratory and for helping in creating and fixing the equipment that was needed for the laboratory work in this study.

Lastly, we would like to thank people of *Geohjørnet 2023* for contributing to a motivating and enjoyable working atmosphere throughout the entire period.

  
Filip Karlsen

---

  
Steinar Sund-Olsen

Trondheim, 8th June 2023



# Abstract

The process of stabilizing the ground with binders is a widely used method to improve the strength and deformation properties of soft soils in Norway. The current methods of testing the strength in stabilized soil piles are usually destructive. By relating geophysical properties such as seismic wave velocities and electrical resistivity to the strength and stiffness of stabilized soils, the use of non-destructive testing can be applied as a more sustainable method of testing. In this master's thesis, a laboratory study has been carried out to investigate the seismic wave velocity and electrical resistivity of stabilized soil and if they could be related to important soil parameters like strength and stiffness.

To study the seismic wave velocity and resistivity in stabilized soil a total of 108 samples were made in the laboratory. The samples consisted of soft clay from Onsøy and quick clay and peat from Tiller-Flotten, which was stabilized using cement combined with the by-products: ladle slag (LS1), bottom ash (BA), paper sludge ash (PSA), and biochar (BC1 and BC4). The P-wave velocity, S-wave velocity, and electrical resistivity were measured on day 3, 7, 14, 21, and 28 after preparation, to study how these properties varied with the curing time. After 28 days of curing, unconfined compression tests were performed to determine strength and stiffness to compare, and correlate, with P-wave and S-wave velocities, and electrical resistivity. The S-wave velocities were measured using bender elements and a Pundit device. The two methods of measuring S-waves were then compared to see if the Pundit device can be used as a reliable method to measure shear waves in stabilized soil. The Pundit device was also used to measure the P-wave velocities. For the resistivity measurements, a two-electrode setup was used.

The P-wave velocity generally increased with the curing time for most samples. An increase in the P-wave velocity,  $v_p$ , showed to correlate with an increase for both the unconfined compression strength,  $q_{uf}$  and the secant stiffness,  $E_{50}$ . However, the correlation is affected by much scatter. The S-wave velocity clearly showed an increasing trend with the curing time. It was found a good correlation between increasing S-wave velocities and increasing strength and stiffness of the stabilized soil samples, independent of the types of soil and binders being used. The shear wave velocities measured with the Pundit device were consistently larger than those measured with bender elements. The Pundit device equipped with 40 kHz dry-point shear wave transducers indicated a lower measuring limit at around 200 m/s when measuring shear wave velocities. Pundit measurements above 200 m/s showed clear similarities to previous studies, which indicates that the measurements are reliable. The electrical resistivity did not show consistent behavior and variations with the curing time. Measurements of electrical resistivity were not found to correlate with the strength and stiffness of the stabilized quick clay samples. The samples of soft clay and to some degree the peat samples had a tendency where an increase in resistivity correlated with an increase in strength and stiffness. The resistivity measurements are believed to be affected by varying contact resistance due to the use of a two-electrode setup.



# Sammendrag

Prosesen med å stabilisere jord ved bruk av bindemidler er en vanlig brukt metode for å forbedre styrke- og deformasjonsegenskapene til myke jordtyper i Norge. De vanlige metodene for å teste den oppnådde styrken i stabiliserte jordpeler er normalt destruktive. Ved å relatere geofysiske egenskaper som seismisk bølgehastighet og elektrisk resistivitet til styrke og stivhet til stabilisert jord kan man ta i bruk ikke-destruktive metoder for en mer bærekraftig måte å teste styrke på. I denne masteroppgaven har det blitt utført en laboratoriestudie for å undersøke seismiske bølgehastigheter og elektrisk resistivitet i stabilisert jord, og om disse parametrene kan relateres til styrke og stivhet.

For å undersøke seismiske bølgehastigheter og resistivitet i stabilisert jord ble det laget 108 prøver i laboratoriet. Prøvene bestod av myk leire fra Onsøy og kvikkleire og torv fra Tiller-Flotten som var stabilisert med sement kombinert med bi-produktene: *ladle slag* (LS1), *bottom ash* (BA), *paper sludge ash* (PSA) og *biochar* (BC1 og BC4). P-bølge hastighet, S-bølge hastighet og elektrisk resistivitet ble målt dag 3, 7, 14, 21 og 28 etter prøvene ble preparert for å undersøke hvordan disse parameterne varierer med herdetiden. Etter 28 dager herding ble enaksiale trykkforsøk utført for å bestemme styrke og stivhet til prøvene. Deretter ble det undersøkt om styrke og stivhet korrelerte med P-bølge og S-bølge hastighetene og elektrisk resistivitet. S-bølge hastighetene ble målt med både bender elementer og med et Pundit-apparat. Disse to metodene for å måle S-bølge hastighet ble deretter sammenlignet for å se om bruken av et Pundit-apparat er en pålitelig metode for å måle skjærbølgehastighet i stabilisert jord. Pundit-apparatet ble også brukt til å måle P-bølge hastighetene. For å måle elektrisk resistivitet ble et oppsett med to elektroder brukt.

Generelt økte P-bølge hastigheten med herdetiden for de fleste prøvene. Det ble funnet en korrelasjon hvor en økning i P-bølge hastighet korrelerer med økning i styrke og stivhet. Denne korrelasjon er derimot påvirket av stor spredning. Skjærbølgehastigheten hadde en klart økende trend over herdetiden. Det ble også funnet en god korrelasjon mellom økende skjærbølgehastigheter og økende styrke og stivhet i de stabiliserte prøvene, for alle typer jord og bindemidler. Skjærbølgehastighetene målt med Pundit-apparatet var konsekvent høyere enn de som ble målt med bender elementene. Pundit-apparatet utstyrt med 40 kHz tørr-punkt skjærbølgetransdusere indikerte en nedre grense på rundt 200 m/s for måling av skjærbølgehastigheter. Pundit-målingene over 200 m/s viste tydelige likhetstrekk sammenlignet med tidligere studier, noe som indikerer at målingene er pålitelige. Elektrisk resistivitet viste ikke konsekvent oppførsel og variasjon med herdetiden. Resistiviteten korrelerte ikke med styrke og stivhet for de stabiliserte kvikkleireprøvene. For prøvene av stabilisert myk leire og til en viss grad torv var det en trend hvor økende resistivitet korrelerte med økende styrke og stivhet. Resistivitetsmålingene i denne studien er antatt påvirket av varierende kontaktmotstand på grunn av oppsettet med to elektroder som ble brukt til målingene.





# Contents

<b>Preface</b> . . . . .	<b>iii</b>
<b>Abstract</b> . . . . .	<b>v</b>
<b>Sammendrag</b> . . . . .	<b>vii</b>
<b>Contents</b> . . . . .	<b>ix</b>
<b>Figures</b> . . . . .	<b>xiii</b>
<b>Tables</b> . . . . .	<b>xvii</b>
<b>Acronyms</b> . . . . .	<b>xix</b>
<b>List of Symbols</b> . . . . .	<b>xxi</b>
<b>1 Introduction</b> . . . . .	<b>1</b>
1.1 Background . . . . .	1
1.2 Objective . . . . .	2
1.3 Research approach . . . . .	2
1.4 Limitations . . . . .	2
1.5 Disposition . . . . .	3
<b>I Theoretical Framework</b> . . . . .	<b>4</b>
<b>2 Soil Stabilization</b> . . . . .	<b>5</b>
2.1 Soil Behavior Prior to Stabilization . . . . .	5
2.1.1 Clay . . . . .	5
2.1.2 Peat . . . . .	7
2.2 Main Principles of Soil Stabilization . . . . .	8
2.3 Binders . . . . .	9
2.3.1 Cement . . . . .	10
2.3.2 Ladle Slag (LS1) . . . . .	13
2.3.3 Bottom Ash (BA) . . . . .	14
2.3.4 Paper Sludge Ash (PSA) . . . . .	14
2.3.5 Biochar (BC1 and BC4) . . . . .	15
2.4 Stabilization by Ion Exchange . . . . .	17
2.5 Factors Affecting Achieved Strength and Stiffness . . . . .	17
2.5.1 Properties of the Soil . . . . .	17
2.5.2 Mixing Procedure . . . . .	18
2.5.3 Amount of Binder . . . . .	18

<b>3</b>	<b>Background Theory of Seismic Waves</b>	<b>19</b>
3.1	Introduction to Seismic Waves	19
3.2	P-waves	19
3.3	Shear waves	20
3.4	Relationship between P-waves and S- waves	21
3.5	Stiffness from Seismic Measurements	22
3.6	Strength from Seismic Measurements	24
3.7	Measuring Seismic Velocities	25
3.7.1	In Situ Measurements	25
3.7.2	Laboratory Measurements	26
<b>4</b>	<b>Laboratory Measurements of Seismic Waves</b>	<b>27</b>
4.1	Pundit Device	27
4.2	Bender Elements	28
4.2.1	Design and Mechanisms	28
4.2.2	Travel Time Determination	30
4.2.3	Near-Field Effect	32
4.2.4	Frequency	33
4.2.5	Contact between Probe and Specimen	34
<b>5</b>	<b>Electrical Resistivity</b>	<b>35</b>
5.1	Resistivity Theory	35
5.2	Resistivity for Soil Materials	35
5.3	Resistivity for Stabilized Soil	36
5.4	Measurement of Resistivity	37
5.4.1	Field Measurements	37
5.4.2	Laboratory Measurements	37
<b>6</b>	<b>Test Sites</b>	<b>39</b>
6.1	Norwegian Geo-Test Sites	39
6.2	Tiller-Flotten Testing Site	40
6.2.1	Location and Quaternary Geology	40
6.2.2	Stratigraphy	41
6.2.3	Shear Wave Velocity and Stiffness	42
6.2.4	Electrical Resistivity	43
6.2.5	Tiller-Flotten Peat	44
6.3	Onsøy Testing Site	45
6.3.1	Location and Quaternary Geology	45
6.3.2	Stratigraphy	46
6.3.3	Shear Wave Velocity and Stiffness	47
6.3.4	Electrical Resistivity	48
<b>II Lab and Results</b>		<b>49</b>
<b>7</b>	<b>Laboratory Work</b>	<b>51</b>
7.1	Preparation of Samples	51
7.2	Pundit Test	56

7.3	Bender Element Testing . . . . .	58
7.3.1	Preparation of Samples for the Bender Element Test . . . . .	58
7.3.2	Procedure for Testing . . . . .	60
7.4	Electrical Resistivity Testing . . . . .	62
7.5	Uniaxial Testing . . . . .	62
7.6	Index Testing . . . . .	64
7.6.1	Density . . . . .	64
7.6.2	Water Content . . . . .	64
<b>8</b>	<b>Results . . . . .</b>	<b>65</b>
8.1	Variation of Wave Velocities over Time . . . . .	65
8.1.1	P-wave Velocity Variation over Time . . . . .	65
8.1.2	Shear Wave Velocity Development over Time . . . . .	68
8.2	Development of Electrical Resistivity over Time . . . . .	70
8.3	Wave Velocities vs. Strength and Stiffness . . . . .	73
8.3.1	P-wave Velocity vs. Strength and Stiffness . . . . .	73
8.3.2	Shear Wave Velocity vs. Strength and Stiffness . . . . .	75
8.4	Electrical Resistivity vs. Strength and Stiffness . . . . .	78
8.5	Densities and Water Content of Stabilized Samples . . . . .	80
<b>9</b>	<b>Discussion . . . . .</b>	<b>81</b>
9.1	Handling and Preparation of Samples . . . . .	81
9.1.1	Sample Molding and Layer Separation . . . . .	81
9.2	P-wave Velocity for Stabilized Soil . . . . .	82
9.2.1	Limitations and Noise with the Pundit Device . . . . .	83
9.2.2	Dynamic Poisson’s Ratio . . . . .	85
9.3	Shear Wave Velocity for Stabilized soil . . . . .	86
9.3.1	Shear Wave Velocity versus Curing Time . . . . .	86
9.3.2	Shear Wave Velocity versus Strength . . . . .	87
9.3.3	Shear Wave Velocity versus Strength and Stiffness from Pundit Test . . . . .	88
9.3.4	Limitation of Shear Wave Velocity Measurements with the Pundit Device . . . . .	88
9.3.5	Shear Wave Velocity from Bender Element Testing . . . . .	88
9.3.6	Effect of the Carved Slots Filled with gypsum . . . . .	88
9.3.7	Effect of Frequency . . . . .	90
9.3.8	Near-field Effect . . . . .	91
9.3.9	Peak-to-Peak method . . . . .	92
9.4	Comparison of bender element and Pundit results . . . . .	93
9.5	Electrical Resistivity . . . . .	94
9.5.1	Effect of Contact Resistance . . . . .	95
9.5.2	Effect of Different Soils and Binders on the Resistivity . . . . .	95
9.5.3	Effect of Voltage . . . . .	96
9.5.4	Difference Between Resistivity in Laboratory and In Situ . . . . .	96
9.5.5	Comparing Stabilized Soil Samples Mixed in the Laboratory and Field . . . . .	97
9.6	Effect of Different By-products and Binder Ratios . . . . .	98

<b>III Conclusion and further work</b>	<b>101</b>
<b>10 Conclusion and Further Work</b> . . . . .	<b>103</b>
10.1 Conclusion . . . . .	103
10.2 Further Work . . . . .	104
<b>Bibliography</b> . . . . .	<b>107</b>
<b>A Complete Sample Review</b> . . . . .	<b>113</b>
<b>B Interpretation of Unconfined Compression Strength Testing</b> . . . . .	<b>127</b>
<b>C Sample Densities</b> . . . . .	<b>139</b>
<b>D Water Content of Stabilized Samples</b> . . . . .	<b>141</b>

# Figures

2.1	Illustration of tetrahedral and octahedral (Jordan, 2014) . . . . .	6
2.2	Clay minerals based on the composition of tetrahedral- and octahedral sheets (Negrón-Mendoza, 2020) . . . . .	6
2.3	Stabilization of soil (NGF, 2012) . . . . .	9
2.4	Effect of stabilization in different soil types (Janz & Johansson, 2002) . . . . .	10
2.5	Hydration development over time (Jacobsen et al., 2023) . . . . .	12
2.6	Curing time and strength development for different clinkers (Jacobsen et al., 2023) . . . . .	12
2.7	Development of compressive strength with the use of Ladle Slag, from Shi (2002) . . . . .	14
2.8	Effect of biochar quantities on the shear strength in cement treated (a) quick clay and (b) peat (Ritter et al., 2022, 2023) . . . . .	16
2.9	Illustration of the effect of ion exchange in clay (Janz & Johansson, 2002) . . . . .	17
2.10	A generalized relation between binder quantity and shear strength (Janz & Johansson, 2002) . . . . .	18
3.1	Illustration of the P-wave propagation, modified after Shearer (2010) . . . . .	20
3.2	Illustration of the shear wave propagation, modified after Shearer (2010) . . . . .	21
3.3	P-wave velocity compared to S-wave velocity, modified after (Nordal & Eiksund, 2021) . . . . .	21
3.4	Characteristic strain-stiffness behaviour of soils (PLAXIS, 2023) . . . . .	23
3.5	$E_0$ and $E_{50}$ for a typical soil, modified after NGF (2012) and PLAXIS (2023) . . . . .	24
3.6	Correlation between shear wave velocity, $v_s$ and unconfined compression strength, $q_{uf}$ by Åhnberg and Holmén (2011) from Bender Element (BE) and Resonance Column free-free (RCff) tests . . . . .	25
3.7	Field measurements of shear wave velocity: a) invasive techniques, b) MASW (L'Heureux & Long, 2017) . . . . .	26
4.1	Illustration of a typical Pundit setup, modified after Andi et al. (2019) . . . . .	27
4.2	Illustration of the bender elements and the testing setup, modified after VJTECH (2020) . . . . .	29
4.3	Interpretation of travel time using peak-to-peak method . . . . .	30
4.4	Demonstration of first arrival determination, modified from Morawska (2019) . . . . .	31
4.5	Demonstration of the ambiguously first arrival determination, modified after (Lee & Santamarina, 2005) . . . . .	31

4.6	Variation of shear wave velocity with the frequency for two types of bender elements on an acrylic sample (Xiao et al., 2018)	33
4.7	Effect on using infilling material in over-cut slots (Xiao et al., 2018)	34
5.1	Typical resistivity for earth materials, modified after (Samouëlian et al., 2005)	36
5.2	Schematic of two-electrode probe method, modified after Liu et al. (2008)	38
6.1	NGTS locations (SINTEF, 2017)	39
6.2	Location of Tiller-Flotten testing site (Kartverket, 2023)	40
6.3	Map of quaternary geology at the Tiller-Flotten testing site, modified from (NGU, 2023b)	41
6.4	Interpreted soil profile from Tiller-Flotten testing site, modified from (L'Heureux et al., 2019)	42
6.5	$V_s$ and $G_{max}$ with depth (L'Heureux et al., 2019)	43
6.6	Electrical resistivity tomography of Tiller-Flotten (L'Heureux et al., 2019)	44
6.7	Tiller-Flotten peat characterized with Von Post log (Ritter et al., 2022)	44
6.8	Location of Onsøy testing site (Kartverket, 2023)	45
6.9	Map of quaternary geology at the Onsøy testing site, modified from (NGU, 2023b)	46
6.10	Interpreted soil profile from Onsøy testing site, modified from (Gundersen et al., 2019a)	47
6.11	$V_s$ and $G_{max}$ with depth (Gundersen et al., 2019a)	48
6.12	Electrical resistivity tomography of Onsøy (Gundersen et al., 2019b)	48
7.1	Process of mixing unstabilized material with binders	54
7.2	Illustration of finished moulded sample and how they got stored	55
7.3	Demonstration of sample extrusion with explaining text-boxes	56
7.4	Overview of the Pundit setup in this study	56
7.5	Example of a Pundit Proceq 200 file	58
7.6	Used setup for carving slots in samples, made by the laboratory at NTNU	59
7.7	Process of filling carved slots with gypsum	59
7.8	Setup of bender element testing, with the three different types of stabilized soil	60
7.9	Procedure of performing bender element tests with several different frequencies in order to calculate the shear wave velocity	61
7.10	Overview of the resistivity test setup that was used in this study	62
7.11	Setup of the uniaxial test, with sample before test and failure lines after testing	63
7.12	Example of interpretation from uniaxial test	63
8.1	P-wave velocity variation over time for quick clay (Tiller-Flotten) with binder combinations: <b>(a)</b> CEM/LS1, <b>(b)</b> CEM/BA, <b>(c)</b> CEM/PSA and <b>(d)</b> CEM/BC1	66
8.2	P-wave velocity variation over time for soft clay (Onsøy) with binder combinations: <b>(a)</b> CEM/LS1, <b>(b)</b> CEM/BA, <b>(c)</b> CEM/PSA and <b>(d)</b> CEM/BC1	67
8.3	Shear wave velocity variation over time for quick clay (Tiller-Flotten) with binder combinations: <b>(a)</b> CEM/LS1, <b>(b)</b> CEM/BA, <b>(c)</b> CEM/PSA and <b>(d)</b> CEM/BC1	68
8.4	Shear wave velocity variation over time for soft clay (Onsøy) with binder combinations: <b>(a)</b> CEM/LS1, <b>(b)</b> CEM/BA, <b>(c)</b> CEM/PSA and <b>(d)</b> CEM/BC1	69

8.5	Electrical resistivity variation over time for quick clay (Tiller-Flotten) with binder combinations: <b>(a)</b> CEM/LS1, <b>(b)</b> CEM/BA, <b>(c)</b> CEM/PSA and <b>(d)</b> CEM/BC1 . . . . .	70
8.6	Electrical resistivity variation over time for soft clay (Onsøy) with binder combinations: <b>(a)</b> CEM/LS1, <b>(b)</b> CEM/BA, <b>(c)</b> CEM/PSA and <b>(d)</b> CEM/BC1 . . . . .	71
8.7	Electrical resistivity variation over time for peat (Tiller-Flotten) with binder combinations: <b>(a)</b> CEM/LS1, <b>(b)</b> CEM/BA, <b>(c)</b> CEM/PSA and <b>(d)</b> CEM/BC4 . . . . .	72
8.8	P-wave velocity versus: <b>(a)</b> unconfined compressive strength, $q_{uf}$ and <b>(b)</b> secant modulus, $E_{50}$ . . . . .	73
8.9	P-wave velocity versus: <b>(a)</b> unconfined compressive strength, $q_{uf}$ and <b>(b)</b> secant modulus, $E_{50}$ . . . . .	74
8.10	Shear wave velocity from Pundit tests versus: <b>(a)</b> unconfined compressive strength, $q_{uf}$ and <b>(b)</b> secant modulus, $E_{50}$ . . . . .	75
8.11	Shear wave velocity from bender element tests versus: <b>(a)</b> unconfined compressive strength, $q_{uf}$ and <b>(b)</b> secant modulus, $E_{50}$ . . . . .	76
8.12	Shear wave velocity from Pundit and bender element tests versus: <b>(a)</b> unconfined compressive strength, $q_{uf}$ and <b>(b)</b> secant modulus, $E_{50}$ . . . . .	77
8.13	Electrical resistivity versus: <b>(a)</b> unconfined compressive strength, $q_{uf}$ and <b>(b)</b> secant modulus, $E_{50}$ . . . . .	78
8.14	Electrical resistivity versus: <b>(a)</b> unconfined compressive strength, $q_{uf}$ and <b>(b)</b> secant modulus, $E_{50}$ . . . . .	79
8.15	Electrical resistivity versus: <b>(a)</b> unconfined compressive strength, $q_{uf}$ and <b>(b)</b> secant modulus, $E_{50}$ . . . . .	80
9.1	Fracture between two compaction layers in a sample. Fracture happened between to separate compacted layers . . . . .	82
9.2	Comparison between a clear wave arrival and what is suspected to be noise . . . . .	83
9.3	Illustration of how the water content might affect the correlation . . . . .	85
9.4	Unconfined compression strength versus Poisson's ratio . . . . .	86
9.5	Shear wave velocity vs. strength for stabilized soil found in this study compared to previous studies by both Åhnberg and Holmén (2011) and Dannewitz et al. (2005) . . . . .	87
9.6	Comparison of received signals by: <b>(a)</b> pushing bender elements directly into the sample and <b>(b)</b> cutting a slot filled with gypsum . . . . .	89
9.7	Variation of S-wave velocity with frequency for three different samples . . . . .	90
9.8	Presentation of each input frequency and the respective calculated shear wave velocity for all samples in this study, and the belonging trendline . . . . .	91
9.9	Plot of the $L_{tt}/\lambda$ ratio for all the samples that were tested with bender elements to see if the requirement to prevail the near-field effect is fulfilled. Values within the green zone are considered sufficient . . . . .	92
9.10	Illustration of several peaks arriving in the received signal . . . . .	93
9.11	Shear wave velocities from the bender element test versus shear wave velocities from the Pundit test. The dashed line illustrates where the values from both method are equal . . . . .	94

9.12 Electrical resistivity,  $\rho$  versus unconfined compression strength,  $q_{uf}$  for all samples in this study . . . . . 96

9.13 Effect on biochar quantity compared to other binder combinations in **(a)** stabilized Tiller-Flotten quick clay and **(b)** stabilized Onsøy soft clay . . . . . 99

9.14 Comparison of **(a)** Unconfined Compression Strength (UCS) vs. binder combinations and **(b)**  $v_s$  vs. binder combinations for stabilized Tiller-Flotten peat . . . . 100



# Tables

2.1	Notations of clay based on undrained shear strength (SSV, 2018). . . . .	7
2.2	Clinker phases in CEM I (Jacobsen et al., 2023) . . . . .	11
2.3	Chemical and mineralogical composition, modified from I.Vegas et al. (2006) . .	15
2.4	Soil properties impacting the stabilization . . . . .	17
5.1	Parameters affecting the resistivity for stabilized soil . . . . .	37
7.2	Complete overview of prepared stabilized samples, including which type of soil, binder- combinations and ratios that are used, number of samples made, and belonging plot ID . . . . .	53



# Acronyms

AC	Alternating Current. 37, 62
AG	Airborne Geoscanning. 37
BA	Bottom Ash. vii, 10, 52, 53, 66, 72, 98
BC1	Biochar 1. vii, 10, 52, 53, 66, 69, 71, 98
BC4	Biochar 4. vii, 10, 52, 53, 72, 99
BE	Bender Element. xiii, 25, 33, 90, 91
C-S-H	Calcium-Silicate-Hydrates. 11, 14
CEM	Cement. 10, 52, 68, 69, 72, 84, 98, 99
CPT	Cone Penetration Test. 1
CSW	Continuous Surface Waves. 25
DAQ	Data Acquisition. 58, 90
DC	Direct Current. 37
ERT	Electrical Resistivity Tomography. 37, 43, 45, 48
FOPS	Forinstallert omvendt pelsonde. 1
GDS	Global Digital Systems. 33, 58
GOAL	Green sOil stAbiLization. iii, 10
KPS	Kalkpelsonde. 1
LS1	Ladle Slag 1. vii, 10, 52, 53, 66, 68, 72, 84, 98
MASW	Multichannel Analysis of Surface Waves. xiii, 25, 26, 42
NGF	Norges Geotekniske Forening. 54
NGI	Norges Geotekniske Institutt. iii, 39, 54
NGTS	Norwegian Geo-Test Sites. 39
NTNU	Norges Teknisk-Naturvitenskapelige Universitet. iii, 90

PSA	Paper Sludge Ash. vii, 10, 14, 15, 52, 53, 66, 72, 98
PUNDIT	Portable Ultrasonic Non-destructive Digital Indicating Tester. 27
RCff	Resonance Column free-free. xiii, 25
RCPTU	Resistivity Piezocone Penetration Test. 37, 43
SASW	Spectral Analysis of Surface Waves. 25
SCPTU	Seismic Cone Penetration Test. 25, 42, 47
SDMT	Seismic Dilatometer. 25, 42, 47
UCS	Unconfined Compression Strength. xvi, 100, 127

# List of Symbols

Sign	Description	Unit
$A$	Cross section of sample	$m^2$
$E_0$	Small strain Young's modulus	kPa
$E_b$	Young's modulus for bender elements	kPa
$E_{50}$	Secant modulus	kPa
$E$	Young's modulus	kPa
$G_0$	Small-strain shear modulus	kPa
$G_{max}$	Small-strain shear modulus	kPa
$G$	Shear modulus	kPa
$I$	Electrical current	A
$I$	Moment of inertia	$kg\ m^2$
$K_0$	Small-strain bulk modulus	kPa
$L_b$	Cantilever length of bender elements	m
$L_{tt}$	Tip-to-tip distance between bender elements	m
$L$	Length of sample	m
$L$	Travel distance for the shear wave	m
$M_0$	Small-strain constraint modulus	kPa
$M$	Constraint modulus	kPa
$N$	Multiple of phase differences	-
$S_t$	Sensitivity	-
$V$	Volume of a soil sample	$m^3$
$\Delta U$	Applied electrical voltage to soil	V
$\Delta t$	Time interval	s
$\alpha$	Effective length factor	-
$\beta$	Empirical constant	-
$\epsilon$	Axial strain	%
$\eta$	Mean displacement influence factor at the soil-element interface	-
$\lambda$	Lame's constant	kPa
$\lambda$	Wave length	m
$\nu$	Poisson's ratio	-
$\rho_b$	Density of bender elements	$kg/m^3$
$\rho_s$	Density of soil	$kg/m^3$

<b>Sign</b>	<b>Description</b>	<b>Unit</b>
$\rho$	Density	kg/m <sup>3</sup>
$\rho$	Electrical resistivity	$\Omega$ m
$\sigma_1$	Axial stress	kPa
$\sigma$	Electrical conductivity	S/m
$\tau_{max}$	Maximum shear stress	kPa
$\tau$	Shear stress	kPa
$b$	Bender element width	m
$f_r$	BE-soil-system resonant frequency	Hz
$f$	Frequency	Hz
$h$	Bender element thickness	m
$m_1$	Mass of cup with wet soil	g
$m_2$	Mass of cup and dry sample	g
$m_c$	Mass of empty cup	g
$m_d$	Mass of dry soil sample	g
$m_s$	Mass of soil sample	g
$m_w$	Mass of wet soil sample	g
$q_{uf}$	Unconfined compression strength	kPa
$s_r$	Remoulded shear strength	kPa
$s_u$	Undrained shear strength	kPa
$t$	Travel time of the shear wave	s
$v_p$	P-wave velocity	m/s
$v_s$	Shear wave velocity	m/s
$v$	Velocity	m/s
$w$	Water content	%

# Chapter 1

## Introduction

### 1.1 Background

Soil stabilization is a method often used to increase the stability, strength, and applicability of areas with soft ground conditions. This is commonly done by mixing binders, like lime and cement, into the soil. Chemically reactions caused by the binders increase the strength of the soil and thus stabilizing the soil and surrounding areas. Production of binders such as cement and lime causes large CO<sub>2</sub> emissions. In recent times reducing the emissions caused by soil stabilization has been given large interest. By using industrial by-products as binders and non-destructive methods to evaluate the strength of stabilized soils the potential for reducing climate emissions in soil stabilizing increases.

Today, the typical methods for measuring the achieved strength and stiffness of stabilized soil are for example the FOPS. The FOPS consists of a preinstalled prope placed at the head of the pile and is a destructive way of measuring the shear strength. Other commonly used destructive methods are the likes of KPS and CPT. According to NGF (2012) it is recommended to test up to 2 % of the stabilized columns depending on the size of the project. Using destructive tests, therefore, leads to a lot of material waste.

The conventional methods used today in order to test stabilized soils for strength are not very sustainable due to their destructiveness. There are two main advantages of using non-destructive methods to test the strength of stabilized soil. Firstly it prevents the tested stabilized soil column from getting destroyed. Secondly, non-destructive testing allows for the material to be tested several times, instead of just once. One way of using non-destructive testing methods on stabilized soil is to develop correlations between geophysical parameters such as seismic wave velocities and electrical resistivity to strength and stiffness. The correlations can be studied in the laboratory and then be applied to field-stabilized soils. If quantitative relations between these sorts of parameters are found, it is possible with the use of non-destructive quality control methods to predict/estimate the strength of stabilized soil in a sustainable way.

## 1.2 Objective

A laboratory study is performed where samples of stabilized soft clay, quick clay, and peat are made with the use of several different binders. The objective of this thesis is to investigate the use of geophysical properties for strength and stiffness estimation of stabilized Norwegian soils. More specifically, this study is based on the following objectives:

- To investigate the variation of seismic wave velocities and resistivity over the curing time.
- To compare seismic wave velocities and electrical resistivity to the unconfined compression strength,  $q_{uf}$ , and the secant stiffness  $E_{50}$ , and investigate potential correlations.
- To compare the reliability and applicability of the Pundit apparatus with bender elements for measuring shear wave velocities in stabilized soil samples.
- To evaluate best practice for the different methods used in this study.

## 1.3 Research approach

Laboratory investigations have been done in order to study the seismic wave velocities and electrical resistivity for stabilized soils. Stabilized samples of soft clay, quick clay, and peat using several different binders were prepared. The samples were prepared using a modification of the NGF rodding technique. The samples were then stored for 28 days. The P-wave velocity, S-wave velocity, and electrical resistivity were measured on day 3, 7, 14, 21, and 28 of curing. After 28 days of curing, uniaxial compression tests were performed on the samples to measure the unconfined compression strength and the secant stiffness.

## 1.4 Limitations

One limiting factor in this study was that the bender elements at the NTNU laboratory couldn't reach the desired frequency for many of the measurements. This limited the data for comparing the measured shear wave velocities obtained by the Pundit apparatus to those obtained with bender elements. Another limitation was that the frequency of the Pundit transducers was very large which increased the attenuation and lead to many samples not getting proper measurements for the wave velocities.

Many of the measurements of electrical resistivity were affected by varying contact resistance due to the use of a two-electrode setup. This type of setup makes the result very sensitive to varying amounts of conducting gel being used.



## 1.5 Disposition

The master's thesis is divided into three parts. Each part is built up of unique chapters. A brief explanation of each part is given in the following list:

- **Part I** - gives a presentation of relevant theory from available literature and previous studies.
- **Part II** - gives a presentation of the performed laboratory study. The results from the laboratory study are then presented followed by belonging discussions.
- **Part III** - gives a conclusion of the study and discussions around potential further work.

# **Part I**

## **Theoretical Framework**

## Chapter 2

# Soil Stabilization

This chapter describes the stabilization process of soils. Firstly the behavior of soils prior to stabilization is presented. Following this, the practical application of soil stabilization is described. The chemical reactions that occur when soils are stabilized are then explained. Lastly, the different types of binders that are used in this study are presented and described.

### 2.1 Soil Behavior Prior to Stabilization

Prior to understanding different aspects of soil stabilization, it is important to have knowledge of how the different soil types are built up and behave. This section describes the fundamentals of Norwegian clays and peat. The formation of the materials is described and important characteristics and properties are mentioned.

#### 2.1.1 Clay

##### Clay Mineralogy

Mineral soil types are usually defined by its grains fraction size. Clay particles are defined as the fraction of grains with a size  $< 0,002$  mm. Classification of clay is determined by considering the weight percentage of material finer than 0,002 mm (Brattli, 2015).

Clay particles have a lamellar-like structure, which is composed of a stack of layers of tetrahedral and octahedral. These are built up of oxygen and hydroxides. The tetrahedral binds to the central cation of the octahedral, which usually is magnesium or aluminum, shown in Figure 2.1. It is this binding that decides the stability of the particle (Jordan, 2014). Tetrahedral and octahedral can thereby be seen as building blocks of the clay mineral, and it is the different combinations of these that decide the clay different minerals, such as Chlorite and Illite, see Figure 2.2.

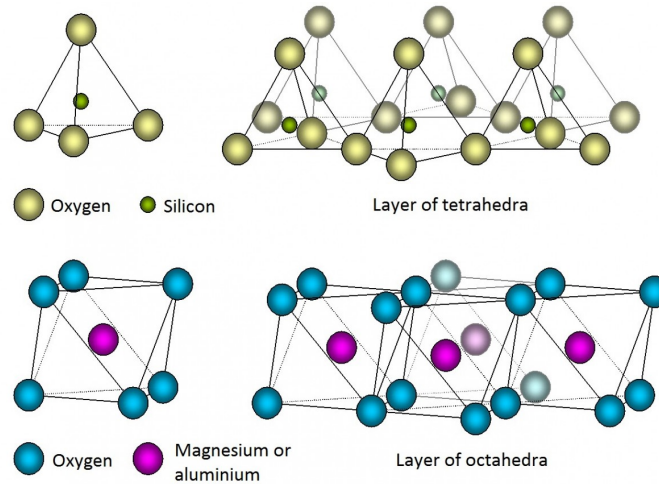


**Figure 2.1:** Illustration of tetrahedral and octahedral (Jordan, 2014)

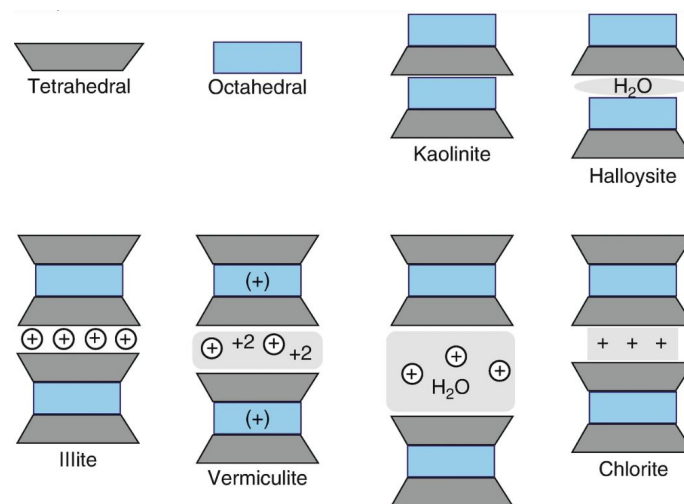


**Figure 2.2:** Clay minerals based on the composition of tetrahedral- and octahedral sheets (Negrónk-Mendoza, 2020)

A nationwide study of the mineralogy of Norwegian sensitive clays showed a dominating appearance of Chlorite and Illite for clays all over the country. Some regional differences were also identified; Northern - and Middle-Norway showed a high content of illite compared to a lower content in the more Southern and South-western areas (Syversen, 2013).

### Quick- and Soft Clay

There are several kinds of clays. As this thesis mainly focuses on soft clay and quick clay, these types of clay and their characteristics are discussed below.

### Soft Clay

Clays may be classified by its undrained shear strength,  $s_u$ . Table 2.1 shows how the classification for clays ranges.

**Table 2.1:** Notations of clay based on undrained shear strength (SSV, 2018).

Notation	$s_u$ [kPa]
Very soft	< 10
Soft	10 - 25
Medium firm	25 - 50
Firm	> 50

As seen, the notation soft clay is according to Statens Vegvesen (2016) used for clay with undrained shear strengths within the range of 10 - 25 kPa.

### Quick Clay

Quick clays mainly consist of non-swelling minerals, like the mineral illite, described earlier (Rankka et al., 2004). Middle-Norway, Trøndelag, and Southeastern Norway are known for the highest occurrences of sensitive and quick clay (NGU, 2023a). Quick clay occurs in areas where the clay has been deposited in salt water, and due to the post-glacial rebound is now located over sea level, with access to fresh water. Over time, the salt water, with its many differently charged ions, has been washed out and replaced by fresh water, leaving a more vulnerable structure. In comparison to *regular* clay built up by connecting strong layers, the quick clay is characterized by its end-to-plate structure, more popularly described as a card house structure. This card house-like structure leaves big pores, which can hold large amounts of water. If this structure goes to failure, the pore water is released and whatever strength it had built up vanishes in a highly liquid consistency (Nordal et al., 2020).

Quick clay has several characteristics. The definition of quick clay, however, is that the remoulded shear strength,  $s_r < 0,33$  kPa (NVE, 2019).

Other typical characteristics of quick clay are:

- Sensitivity,  $S_t > 50$
- Salt content < 0,5%

#### 2.1.2 Peat

Peat is an organic fine-grained soil material with its dry-weight built up of at least 30% dead and broken down remains of other organic materials, like dead leaves. The material is overflooded by water, and not more than 35 % of the weight mass consists of dry masses. It is also characterized by not having available oxygen, and therefore the breakdown of organic material moves very slowly. Peat is often formed over thousands of years and stores a high volume of carbon (Carlsten, 1988).

Peat is typically classified by the *von Post scale*, which is based on the degree of disintegration. To classify according to the von Post scale, a simple visual and manual test is performed to characterize the degree of disintegration. The scale goes from H1 - no degree of disintegration to H10 - completely disintegrated. These steps are often divided into three intervals for further classification (Blackland Centre, 2015):

- Easily visible plant residues (H1-H4): *Fibric peat*
- Some plant residues (H5-H7): *Hemic peat*
- No visible plant residues (H8-H10): *Sapric peat*

Classification of peat is also done based on its structure. Based on the peat's predominant characteristic, the peat is classified as either *Amorphous-granular*, *Fine-fibrous* or *Coarse-fibrous*. Peat will develop towards amorphous over time (Carlsten, 1988).

Peat is usually found under the groundwater table, and the undrained shear strength of peat is important for geotechnical design. Typically peat is characterized by low shear strengths and high compressibility. The peat's fibers act as reinforcements in the load direction, and fibrous peat often has higher shear strengths than amorphous peat. It is important to note that the reinforcement effect of fibers is not uniformly distributed in the soil body, due to it being anisotropic. This makes peat anisotropic in both strain and strength. This often complicates the process of understanding peat's behavior regarding strength (Berbar, 2020).

## 2.2 Main Principles of Soil Stabilization

Stabilization of soil is usually done by pushing a drill rod with a whisk mounted at the bottom down to a desired level while rotating the rod. When the rod is at the desired depth, binders start getting pumped into the soil while the whisk is being rotated and raised. The mixing ends at around 0,5-1 m below the surface and the curing process for the stabilized soil starts immediately (NGF, 2012). An illustration of how soil is stabilized in situ, is shown in Figure 2.3. The effect of the stabilization of the soil is dependent on factors such as soil type, water content, sensitivity, and shear strength. The strength is also dependent on which binders are being used, the amount of binder, as well as the curing time. For clays, studies on previous projects show that soil stabilization is most efficient when the soil has shear strengths between 5 - 30 kPa. Stabilization of peat has also been shown to improve the ground conditions (NGF, 2012).

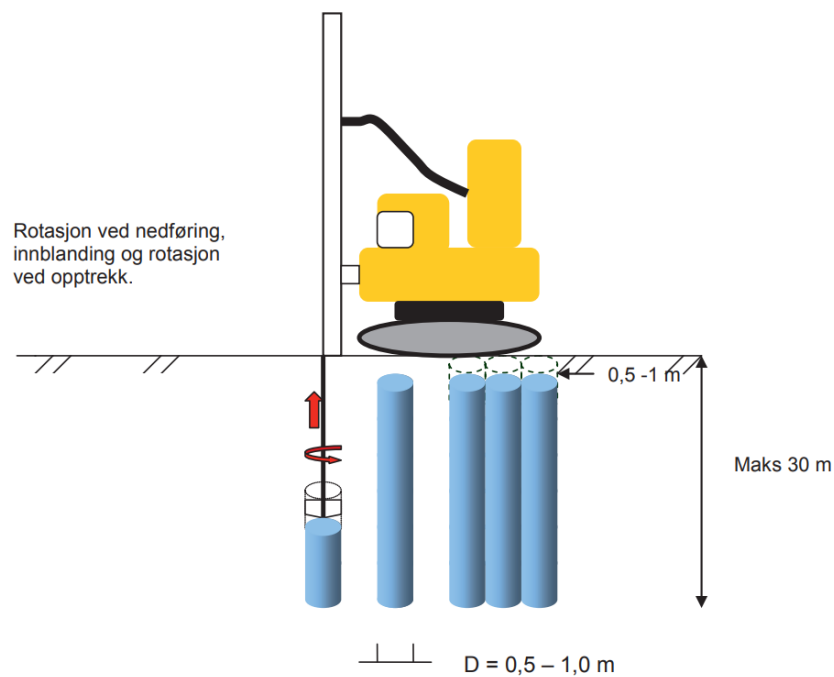


Figure 2.3: Stabilization of soil (NGF, 2012)

Stabilization of soil can also be performed in the laboratory. This is often in regards to testing the behavior and properties of the stabilized soil, and procedure principles differ from the typical field procedures. Laboratory stabilization is often a more manual process, where kitchen mixers, rodding, tapping, and hydraulic presses are used to mix and homogenize the samples. Hov and Paniagua (2022) studied how to optimize different laboratory molding techniques. One identified key property in laboratory molding was the amount of entrapped air in the stabilized samples. With the use of methods that were common at that time, the amount of entrapped air was significantly higher compared to in situ mixing. The study resulted in an improved method, done by slightly modifying a commonly used impact compaction method from NGF (2012).

## 2.3 Binders

Soil stabilization is both a physical and chemical method to improve ground conditions. The applicability and effect of the stabilization are depended on the properties of the soil and the type, amount, mixing, and curing of chosen binders. Binders can have a huge impact on the strength and stiffness of the soil. To understand how the soil will change with stabilization, it is important to understand the effect of different binders.

A simple illustration of the function of binders in different soils is given in Figure 2.4. The soils are stabilized with cement, lime-cement, and lime, and compared to unstabilized soil. It

shows the lowest achieved strengths are in soils like peat and mud, which are the most porous materials in this specific selection.

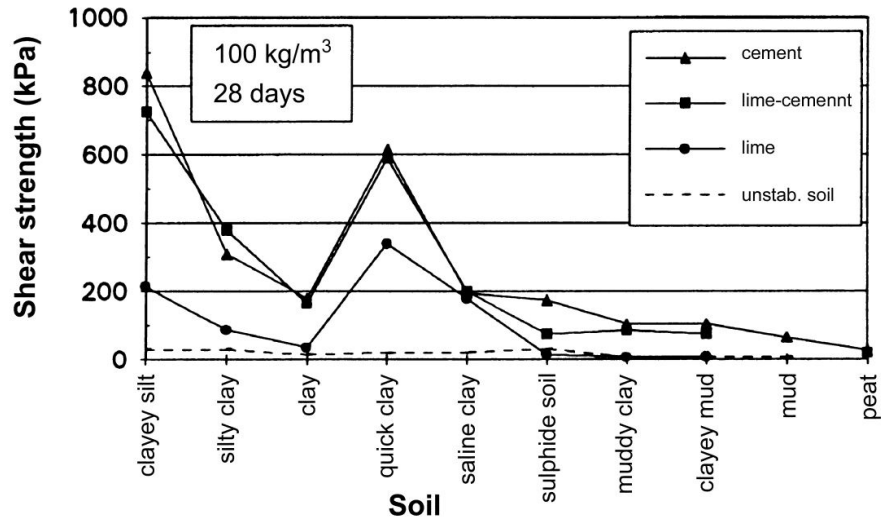


Figure 2.4: Effect of stabilization in different soil types (Janz & Johansson, 2002)

Further, this chapter aims to describe the chosen binders used for this study, which are Cement (CEM), Ladle Slag 1 (LS1), Bottom Ash (BA), Paper Sludge Ash (PSA), Biochar 1 (BC1) and Biochar 4 (BC4). These four by-products are chosen based on parallel lab investigations from the ongoing Green sOil stAbiLization (GOAL) project, which have given early identifications of positive effects with these by-products used in soil stabilization.

### 2.3.1 Cement

The first binding agent used in soil stabilization was cement, and this may be because it was early figured out that cement is not dependent on the type of soil minerals, but only the amount of available water. This makes using cement highly applicable to use in the stabilization of a large variety of soil types (Makusa, 2012).

Cement is a hydraulic binder, which means that when cement and water are mixed they start a chemical reaction, known as hydration reactions (Jacobsen et al., 2023) In this chemical reaction, the cement will hydrate and form cement paste, which is considered a microporous solid (NGF, 2012). This hardening of cement makes the soil enclose as glue (Makusa, 2012). During heating and under the induced hydration reactions, four major clinker minerals will form. All these have different impacts on how the cement work (Jacobsen et al., 2023). An overview of these clinker phases is given in Table 2.2.



**Table 2.2:** Clinker phases in CEM I (Jacobsen et al., 2023)

Mineral term	Chemical formula	Chemical term	Share
Alite	$3\text{CaO} \cdot \text{SiO}_2$	$\text{C}_3\text{S}$	55-60%
Belite	$2\text{CaO} \cdot \text{SiO}_2$	$\text{C}_2\text{S}$	14-20%
Aluminate	$2\text{CaO} \cdot \text{Al}_2\text{O}_3$	$\text{C}_3\text{A}$	5-10%
Ferrite	$4\text{CaO} \cdot \text{Al}_2\text{O}_3\text{Fe}_2\text{O}_3$	$\text{C}_4\text{AF}$	6-10%

### Hydration reactions

After mixing cement with water, a hydration process between the cement's clinker minerals and the water will begin. The forming hydrates will contain chemically bound water, whereas for Portland cement the amount of chemically bound water is proportional to the amount of reacted cement (Jacobsen et al., 2023). The different calcium silicates and calcium aluminates, known as the clinkers, play different roles in these processes:

- **Alite -  $\text{C}_3\text{S}$** 
  - The hydration of calcium silicates creates Calcium-Silicate-Hydrates (C-S-H). C-S-H is mainly built up by colloidal particles (smaller than  $1 \mu\text{m}$ ) and has a gel-like behavior. This is the most important hydration component (Jacobsen et al., 2023).
- **Belite -  $\text{C}_2\text{S}$** 
  - Hydration of Belite is almost the same as for Alite, as it creates the same reaction products, but in larger amounts. Comparisons show Belite gives better results after full hydration, while Alite performs stronger in earlier phases of the hydration. (Jacobsen et al., 2023).
- **Aluminate -  $\text{C}_3\text{A}$** 
  - Hydration of Aluminate is considered more complicated than for the calcium silicates, and many properties of the Aluminate are seen as unfavorable. At the same time, it gives several economic and technical advantages, like accessibility and ease of production. Hydration between Aluminate and water is very rapid. The rapidness is controlled by adding gypsum to the cement and is used to control the setting time (Jacobsen et al., 2023).
- **Ferrite -  $\text{C}_4\text{AF}$** 
  - Ferrite follows in many ways the same process as Aluminate. But it differs in setting and reaction time, as Ferrite reacts much slower (Jacobsen et al., 2023)

An illustration of how the hydrates develop after mixing the cement with water is illustrated in Figure 2.5, from Jacobsen et al. (2023).

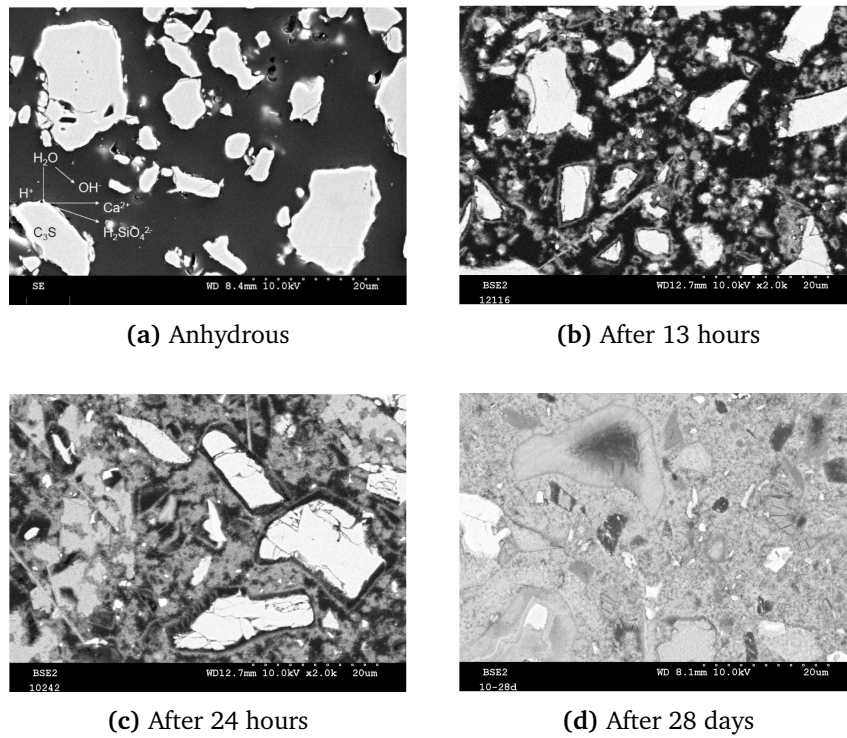


Figure 2.5: Hydration development over time (Jacobsen et al., 2023)

Figure 2.6 shows how the different clinkers contribute to the development of compressive strength, in regards to rapidness, curing time, and early and later age strengths.

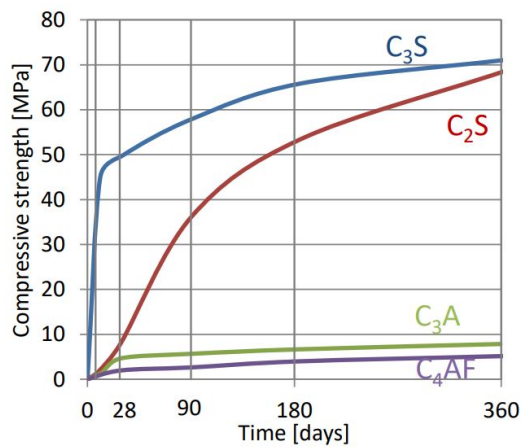


Figure 2.6: Curing time and strength development for different clinkers (Jacobsen et al., 2023)

### CO<sub>2</sub> emissions and measures

Due to its massive use, cement production itself stands for 5-8% of worldwide man-made CO<sub>2</sub> emissions. For each tonne of produced cement, approximately 0,9 tonne CO<sub>2</sub> is released. This originates mainly from two reasons (Jacobsen et al., 2023):

- $\text{CaCO}_3 \rightarrow \text{CaO} + \text{CO}_2$
- Required energy used to the heating up to ca. 1450°C

At the same time disposal of industrial by-products is a growing concern for industries worldwide, because of the steadily increasing volume of their generated waste by-products and how to handle it. Increasing environmental awareness has put effort into looking at using these products in for example concrete production. Several industrial by-products have significant cementitious properties, both in use for concrete and also soil stabilization (Siddique, 2007). By mixing by-products with cement for concrete production or in this case soil stabilization, two major problems can be reduced; CO<sub>2</sub> emissions from cement production and handling of industrial waste by-products.

The by-products that are used in this study are presented in the following subsections.

#### 2.3.2 Ladle Slag (LS1)

Further refining of steel slag by adding fluxes to the molten steel gives the by-product known as ladle slag. Ladle slag has a large portion of fine particles. The steel slag has a highly variable chemical composition, thus the mineral compositions also vary. Typical minerals in steel slag are C<sub>3</sub>S, C<sub>2</sub>S, C<sub>4</sub>AF, and free CaO among others. Whereas the ladle slag mainly consists of C<sub>2</sub>S. The presence of these minerals endorses the ladle slag with cementitious properties. These contents are much lower than in regular Portland cement, but ladle slag can be seen as a weak Portland cement clinker (Shi, 2002).

Studies also show that significantly better cementitious properties are gained by having an alkaline activator present, and the finer the ladle slag is, the better the cementitious properties are. Often the ladle slag is mixed alongside with cement, and the cement will then work as the alkaline activator. How these properties are compared to actual Portland cement are illustrated in Figure 2.7, from the study by Shi (2002).

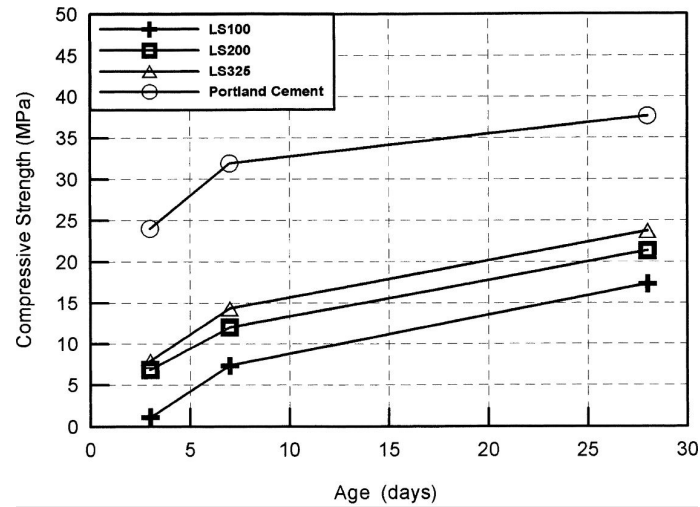


Figure 2.7: Development of compressive strength with the use of Ladle Slag, from Shi (2002)

It is worth noticing that the materials with ladle slag show low strength in the early stages, but later have a faster gain rate than the reference Portland cement (Shi, 2002). This effect correlates well with what is expected from the ladle slag's high content of Belite, and the development curve in Figure 2.6. The ladle slag used in this study comes from *Celsa Armeringsstål AS*.

### 2.3.3 Bottom Ash (BA)

The bottom ash used in this study originates from Bergene Holm's combustion plant at Brandval. It consists of biomasses from around 40% dry wood chips and 60-65 % bark which are grate-fired in temperatures from 1000-1200°C. 90% of the ashes from this process constitute the bottom ash, while the remaining 10% is known as fly ash.

Studies on the microstructure of bottom ash show its major elements are  $\text{SiO}_2$  and  $\text{Al}_2\text{O}_3$ , where these compounds create the C-S-H during hydration, as discussed in the cement theoretical Section 2.3.1. The studies showed that the incorporation of bottom ash gave lower strength in the short term compared to a regular cementitious material, like cement, but in the long term, the bottom ash mix was nearly identical (Mohammad et al., 2022).

### 2.3.4 Paper Sludge Ash (PSA)

Paper sludge ash comes as a by-product of de-inking and re-pulping of paper. It is built up of cellulose fibers, and fillers like calcium carbonate. The mineralogical composition of PSA given in Table 2.3 looks a lot like the cement mineralogical composition, back in Table 2.2. As with the ladle slag, it is also expected that the PSA has cementitious properties (I.Vegas et al., 2006).

**Table 2.3:** Chemical and mineralogical composition, modified from I.Vegas et al. (2006)

Chemical composition (% by mass)		Mineralogical composition (% by mass)	
CaO	65.5	C <sub>3</sub> S	65.29
SiO <sub>2</sub>	20.71	C <sub>2</sub> S	10.21
Al <sub>2</sub> O <sub>3</sub>	5.58	C <sub>3</sub> A	9.24
Fe <sub>2</sub> O <sub>3</sub>	3.28	C <sub>4</sub> AF	9.97

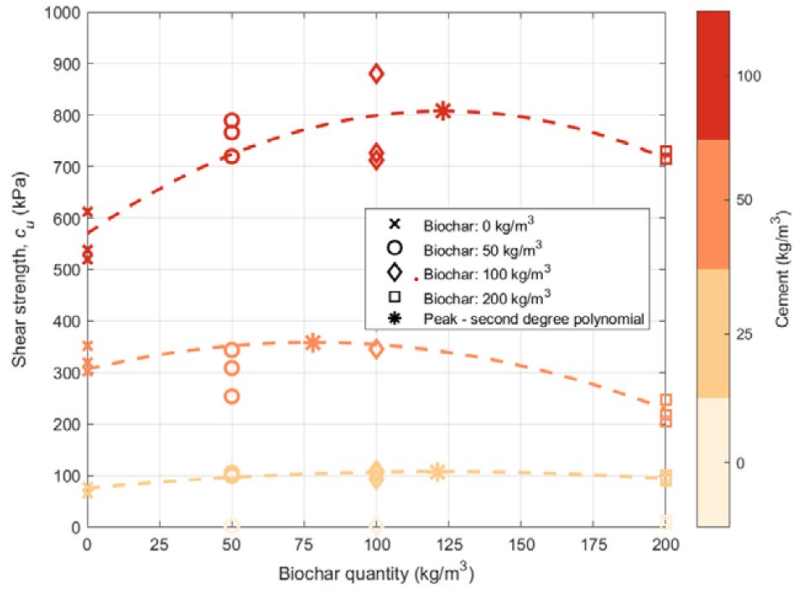
A study by Ahmad et al. (2013) showed that using waste paper sludge with cement, the percentage of water absorption increases. This will decrease the w/c ratio, and give the stabilized material higher strength (Jacobsen et al., 2023).

The PSA used in this study is obtained from the Norske Skog Skogn factory. Its composition consists of roughly 58% demolition wood, 25% de-inked pulp sludge, 14% bio sludge, and 3% plastic cartons and is combusted with a temperature of around 850°C.

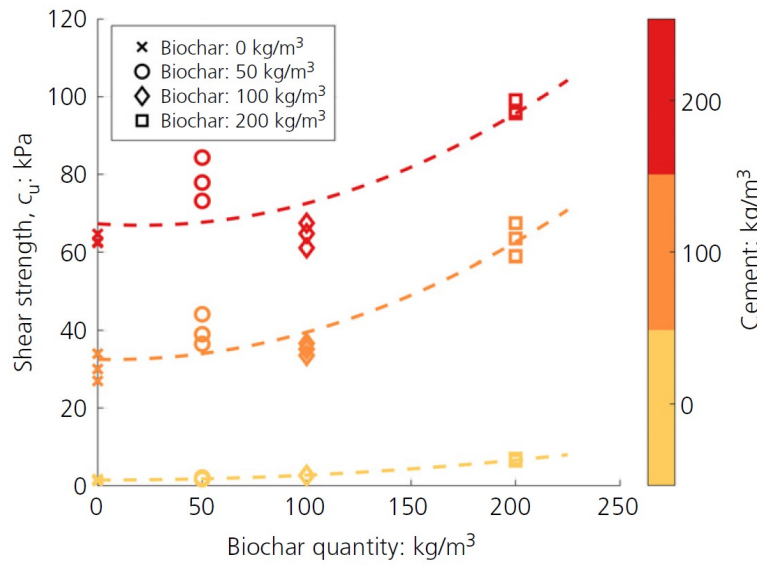
### 2.3.5 Biochar (BC1 and BC4)

By heating biomasses like plants, wood, or from waste streams, in the absence of oxygen creates biochar. The absence of oxygen helps convert roughly 50% of the stored carbon into a stable and condensed form. Two variants of biochar, both produced in a Pyreg-500 pyrolysis unit with a reactor temperature around 470-600°C are used in this study. The first variant, biochar 1, originates from demolition wood. While the second variant, biochar 4, originates from garden waste.

A study on the incorporation of biochar in cementitious materials by Hamid et al. (2021) highlights multiple factors affecting the properties of the material. As with the PSA, the biochar also absorbs a lot of water, decreasing the w/c ratio. It was shown adding biochar with cement did for some dosages increase the strength of the material, but too much would make it decrease again. This optimum dosage effect is also shown in a study by Ritter et al. (2023) on biochar in quick clay stabilization. This effect is shown for quick clay, but earlier studies on peat by Ritter et al. (2022) shows that increasing the content of biochar increases the strength. These effects are illustrated in Figure 2.8



(a) Biochar quantity vs. shear strength in Tiller-Flotten quick-clay, from Ritter et al. (2023)



(b) Biochar quantity vs. shear strength in Tiller-Flotten peat, from Ritter et al. (2022)

**Figure 2.8:** Effect of biochar quantities on the shear strength in cement treated (a) quick clay and (b) peat (Ritter et al., 2022, 2023)

## 2.4 Stabilization by Ion Exchange

One of the main principles in stabilization, is ion exchange. The soil can perform a structural change in ion exchanges, which stabilize the soil. This is maybe most prominent in soft and sensitive clay, which is shown back in Figure 2.4. The mixing of a binder with the soil introduces new ions, mainly calcium, with a different charge than the positive cations on the soil particle surfaces. An ion exchange will take place, and the new ions cause the soil particles to flocculate and create a change in particle size distribution. For Illite and Kaolinite, as mentioned in 2.1.1, this effect is demonstrated in Figure 2.9

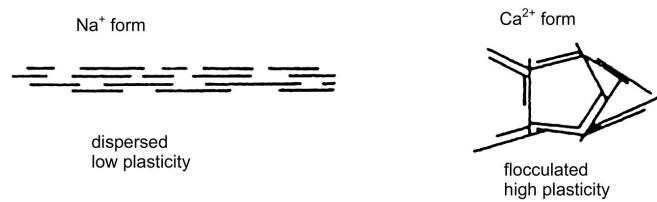


Figure 2.9: Illustration of the effect of ion exchange in clay (Janz & Johansson, 2002)

## 2.5 Factors Affecting Achieved Strength and Stiffness

The achieved gains regarding strength and stiffness in soil stabilization are depended on multiple factors. Such factors can be; binder content, soil properties, and mixing/curing procedure.

### 2.5.1 Properties of the Soil

The effect of different binders varies for different soil types. Table 2.4 discuss some important soil properties affecting the stabilization process:

Table 2.4: Soil properties impacting the stabilization

Properties	Explanation
Water content	Low water contents often give higher strength than higher water contents, due to the lower w/c ratio. At the same time, it needs to be enough available water for the cement to fully hydrate and give full effect (Jacobsen et al., 2023).
Grain size distribution	Generally higher contents of silt and sand will require more effort in mixing for achieving desired homogeneity and results (NGF, 2012). Clays, specifically sensitive clays, are much more workable in this regard.
Plasticity	Higher plasticity give a higher resistance under mixing, making it more difficult to achieve desired homogeneity and implicitly strength and stiffness (NGF, 2012).

## Mineralogy

Different clay mineralogy will react differently to the induced ion exchanges happening in soil stabilization. A study by Bell (1996) showed kaolinitic clays gave the highest strength gains, compared to montmorillonitic clays.

### 2.5.2 Mixing Procedure

For lime-cement stabilization of piles NGF (2012) describes the importance of a sufficient mixing procedure in order to achieve desired shear strengths and stiffness. Among others, factors like rotation speed and whisk type will affect the homogeneity of the mixture. This also applies to mixing stabilized soil in the laboratory. It is the different binder and their reaction products that binds soil particles together and gives the stabilizing effect, and for optimal effect it is important to evenly spread the cement in the soil, creating a homogeneous mix. In Norway, both Statens Vegvesen and NGF have developed soil mixing techniques for use in the laboratory. The use of these is further explained in Chapter 7.

### 2.5.3 Amount of Binder

Janz and Johansson (2002) show that a certain quantity of binder is needed for the binder to give any effect at all. The quantity should at minimum be sufficient for building a load-bearing skeleton, and if not, no stabilizing effect will occur. A simple sketch of this idea is demonstrated in Figure 2.10

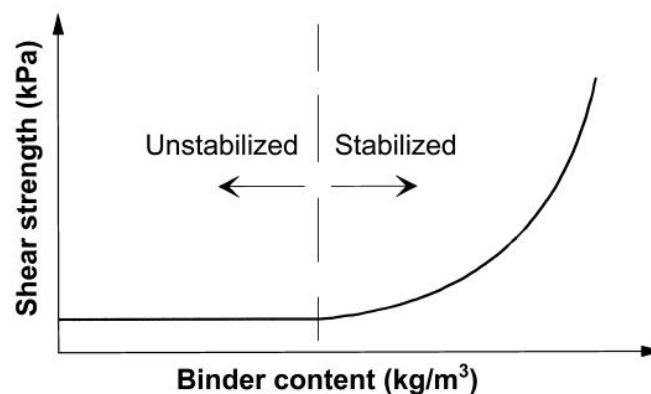


**Figure 2.10:** A generalized relation between binder quantity and shear strength (Janz & Johansson, 2002)

As for the use of biochar in Section 2.3.5, there is also an optimum quantity of binder in general, before the effect either flattens out or starts dropping. This optimum quantity varies based between soil types and used binders. For sensitive clays the quantity is usually around 80 - 110 kg/m<sup>3</sup>, and for peat values around 300 kg/m<sup>3</sup> is not unusual (Janz & Johansson, 2002).



## Chapter 3

# Background Theory of Seismic Waves

This chapter presents some theoretical background regarding seismic wave propagation. How the wave velocities in stabilized soils can correlate with strength and stiffness is then described. Methods of measuring the seismic wave velocities are also presented. Some of the theory presented is the same as for the project thesis by Karlsen and Sund-Olsen (2022).

### 3.1 Introduction to Seismic Waves

Seismic waves can be divided into two types of waves: surface waves and body waves. Surface waves travel along the surface and consist of Rayleigh waves (R-wave) and Love waves (L-waves). Body waves propagate through a body, and the two types of body waves are P-waves and shear waves (Nordal & Eiksund, 2021). In this thesis, it is the body waves that are of interest, and these are described further.

### 3.2 P-waves

P-waves (often called compression waves and primary waves) are described as a push-pull motion in the same direction as the wave propagation (Nordal & Eiksund, 2021). The P-wave velocity is denoted as  $v_p$ . Figure 3.1 shows the wave propagation of a P-wave.

Equation 3.1 shows the differential equation for the P-wave (Nordal & Eiksund, 2021):

$$\frac{\delta^2 \epsilon_{\vartheta}}{\delta t^2} = \frac{(\lambda + 2G)}{\rho} \nabla^2 \epsilon_{\vartheta} = v_p^2 \nabla^2 \epsilon_{\vartheta} \quad (3.1)$$

Where  $\lambda$  is defined as in Equation 3.2:

$$\lambda = \frac{\nu E}{(1 + \nu)(1 - 2\nu)} \quad (3.2)$$

From Equation 3.1 the P-wave velocity is determined as shown in Equation 3.3:

$$v_p = \sqrt{\frac{\lambda + 2G}{\rho}} = \sqrt{\frac{M}{\rho}} \quad (3.3)$$

where M is defined as the constraint modulus, given in Equation 3.4, which essentially is the oedometer modulus for very small strains (Nordal & Eiksund, 2021):

$$M = \lambda + 2G = \frac{E(1 - \nu)}{(1 + \nu)(1 + 2\nu)} = \frac{2G(1 - \nu)}{1 - 2\nu} \quad (3.4)$$

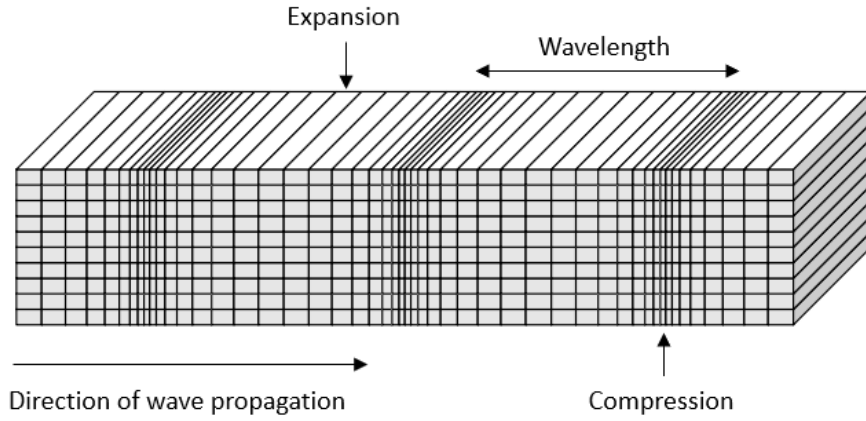


**Figure 3.1:** Illustration of the P-wave propagation, modified after Shearer (2010)

### 3.3 Shear waves

Shear waves (often called S-waves and secondary waves) are characterized by the oscillations being perpendicular to the direction that the wave propagates. The shear wave velocity is expressed as  $v_s$ . Figure 3.2 shows an illustration of the shear wave propagation.

Equation 3.5 gives the differential equation for a shear wave (Nordal & Eiksund, 2021):

$$\frac{\delta^2 \omega_x}{\delta t^2} = \frac{G}{\rho} \nabla^2 \omega_x = v_s^2 \nabla^2 \omega_x \quad (3.5)$$

where  $\omega_x$  is the rotation around the x-axis. From Equation 3.5 the shear wave velocity is determined as in Equation 3.6:

$$v_s = \sqrt{\frac{G}{\rho}} \quad (3.6)$$

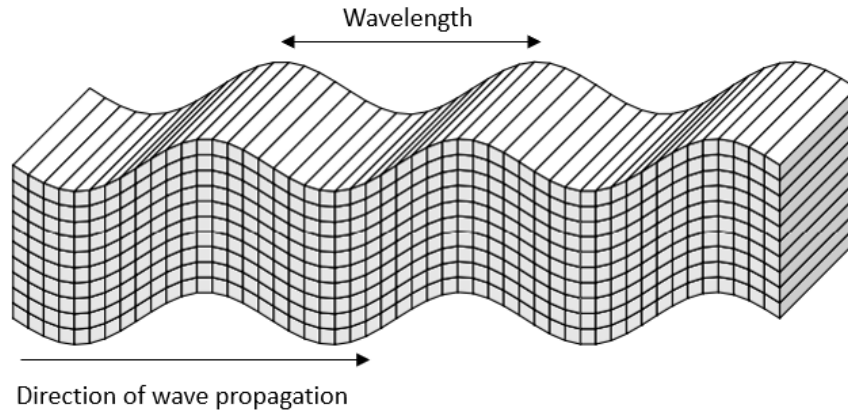


**Figure 3.2:** Illustration of the shear wave propagation, modified after Shearer (2010)

### 3.4 Relationship between P-waves and S- waves

From Equation 3.3 and 3.6 we get the relationship between P-wave velocity and S-wave velocity which is shown in Equation 3.7. This shows that the relationship of the P-wave and S-wave velocity is dependent on the Poisson’s ratio,  $\nu$ . Figure 3.3 shows how the P-wave velocity varies compared to the S-wave velocity for different Poisson’s ratios.

$$\frac{v_p^2}{v_s^2} = \frac{\left(\frac{M}{\rho}\right)}{\left(\frac{G}{\rho}\right)} = \frac{M}{G} = \frac{2(1-\nu)}{1-2\nu} \tag{3.7}$$

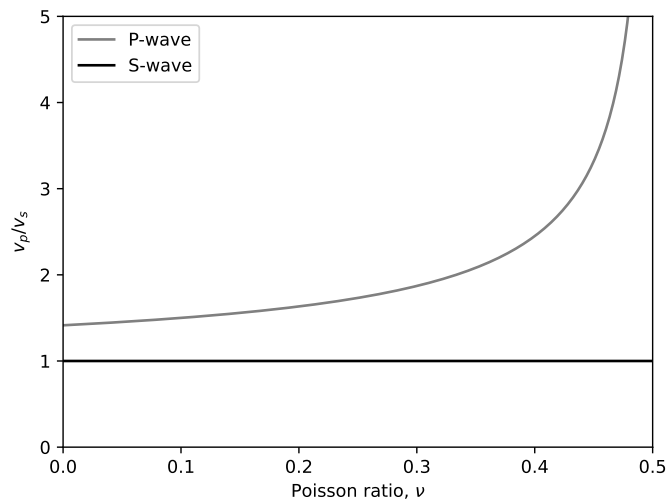


**Figure 3.3:** P-wave velocity compared to S-wave velocity, modified after (Nordal & Eiksund, 2021)

As shown in Figure 3.3 the P-wave velocity is larger than the S-wave velocity. Waves will propagate through soils along the fastest path, which is decided by the stiffness of the soil skeleton. For fully saturated soils however, the soil skeleton may have a negligible effect on the P-wave velocity, as it will almost completely be controlled by the speed of sound in water, which is about 1500 m/s, (Nordal & Eiksund, 2021). Therefore  $v_p$  is not much used in regular soil mechanics. For stabilized soils, however, the stiffness increases and the water content decreases. The P-wave velocity can therefore be of more interest in stabilized soils.

Unlike P-waves, the shear wave velocity is not affected by water and the velocity will be represented by the soil skeleton only. Therefore the use of shear waves is preferable when studying saturated soils (Aziman et al., 2016). However, the shear wave arrival can be hard to identify when doing investigations because of the earlier arrival of the P-waves.

The dynamic Poisson's ratio can be calculated knowing the P-wave and S-wave velocities. This is done using Equation 3.8 (Nordal & Eiksund, 2021).

$$\nu = \frac{1 - \frac{1}{2} \left( \frac{v_p}{v_s} \right)^2}{1 - \left( \frac{v_p}{v_s} \right)^2} \quad (3.8)$$

### 3.5 Stiffness from Seismic Measurements

Soils exhibit non-linear stress-strain behavior. The stiffness of soils varies with the strain level. Figure 3.4 shows how the shear modulus typically varies for different strains. Typically, the stiffness behavior for soils is considered to be linear and elastic for strains below 0.001%. This value is the upper threshold for the range where small-strain parameters are used. These are; the small-strain shear modulus ( $G_0$  or  $G_{max}$ ), Young's modulus ( $E_0$ ), constraint modulus ( $M_0$ ), bulk modulus ( $K_0$ ) and the dynamic Poisson's ratio ( $\nu$ ). The relationship between the small-strain parameters is given in Equation 3.9 (Gu et al., 2013).

$$G_0 = \frac{E_0}{2(1 + \nu)} = \frac{3K_0(1 - 2\nu)}{2(1 + \nu)} = \frac{M_0(1 - 2\nu)}{2(1 - \nu)} \quad (3.9)$$

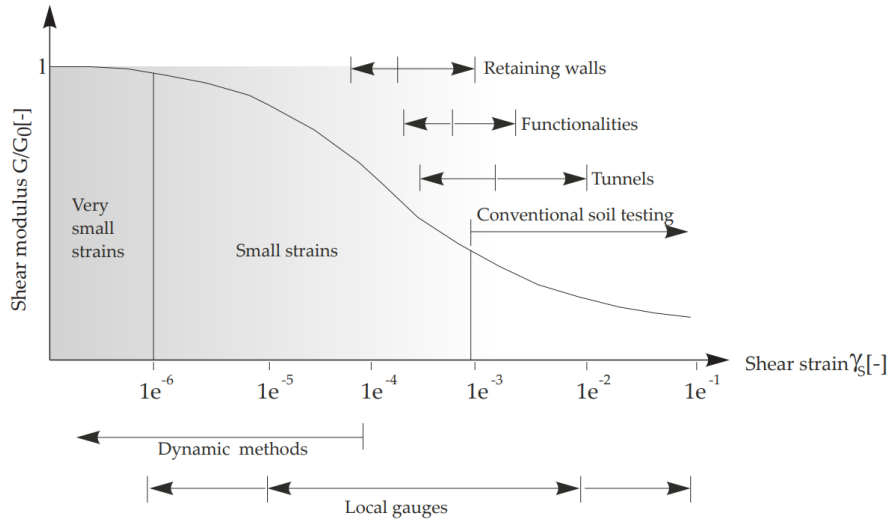


**Figure 3.4:** Characteristic strain-stiffness behaviour of soils (PLAXIS, 2023)

The dynamic small strain properties for soils are important in geotechnical problems, such as settlement calculations, soil-structure interaction, earthquake problems, and machine foundations. The small strain parameters are usually determined by measuring  $G_0$  and  $M_0$  or  $G_0$  and  $E_0$  (Gu et al., 2013). This is done by measuring the S-wave and P-wave velocities.  $G_0$  and  $M_0$  are then calculated as given in Equations 3.10 and 3.11:

$$G_0 = \rho v_s^2 \tag{3.10}$$

$$M_0 = \rho v_p^2 \tag{3.11}$$

For larger strains, the secant modulus,  $E_{50}$  might be a more relevant stiffness parameter.  $E_{50}$  can be calculated by performing a triaxial test or a uniaxial compression test. The secant modulus is defined by drawing a line between the start of the deformation curve and the point where 50% of the failure load is applied. Figure 3.5 shows how  $E_0$  and  $E_{50}$  may look for a typical soil material.

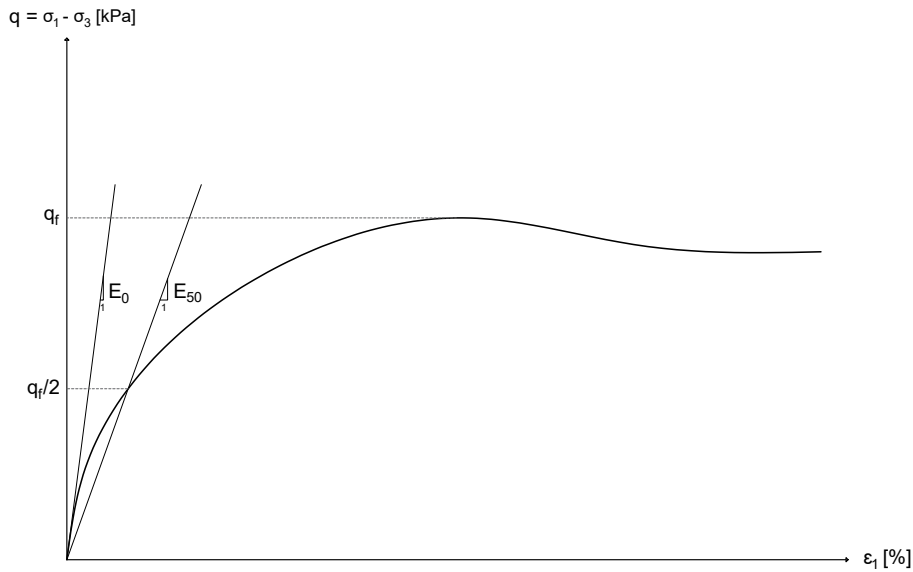


**Figure 3.5:**  $E_0$  and  $E_{50}$  for a typical soil, modified after NGF (2012) and PLAXIS (2023)

For stabilized soils the propagation of S-waves and P-waves will occur along the fastest path, which is affected by factors such as porosity, microstructure, and particle bonding (Barrett et al., 2013). As these factors also affect the general stiffness of the sample it is expected that the seismic wave velocities will have some correlation with the static stiffness, such as  $E_{50}$ .

### 3.6 Strength from Seismic Measurements

There is no theoretical basis for a relationship between strength and wave velocities in geomaterials. However, similar parameters influence both strength and stiffness, such as void ratio, particle bonding, and confining pressure (Toohey & Mooney, 2012). Due to these similarities, there could be a correlation between strength and wave velocities in soils and stabilized soils.

L'Heureux and Long (2017) measured shear wave velocity and undrained shear strength on soil samples from 28 sites. From these tests, a correlation between the undrained shear strength and shear wave velocity was observed. The correlation between strength and shear wave velocity for stabilized soil has also been investigated. Previous studies by Åhnberg and Holmén (2011) and Dannewitz et al. (2005) show a clear correlation between the shear wave velocity,  $v_s$  and the unconfined compression strength,  $q_{uf}$ , for stabilized soil. The studies show that the shear strength increases with the shear wave velocity, demonstrated by the correlation found by Åhnberg and Holmén (2011) in Figure 3.6. The studies by Åhnberg and Holmén (2011) and Barrett et al. (2013) also show a correlation between the P-wave velocity,  $v_p$  and the unconfined compression strength,  $q_{uf}$ .

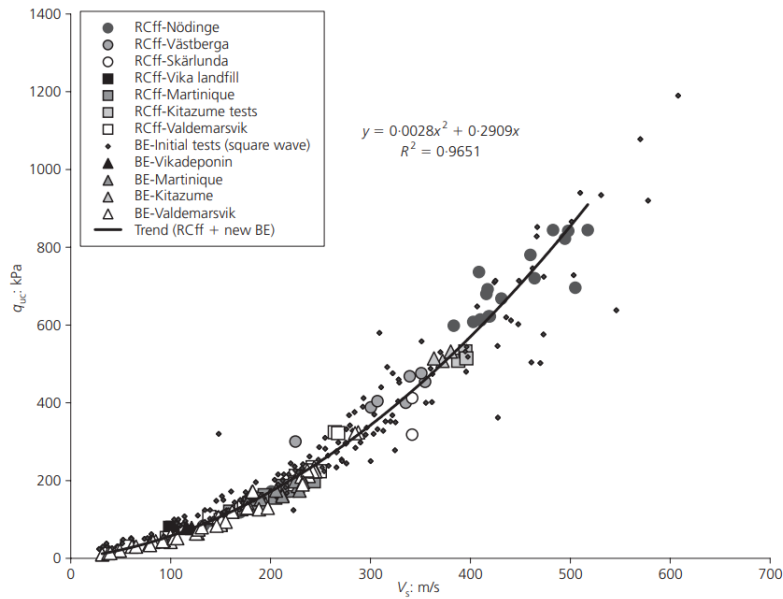


**Figure 3.6:** Correlation between shear wave velocity,  $v_s$  and unconfined compression strength,  $q_{uf}$  by Åhnberg and Holmén (2011) from Bender Element (BE) and Resonance Column free-free (RCff) tests

## 3.7 Measuring Seismic Velocities

The P-wave velocity and S-wave velocity can be measured both in the field or in the laboratory. There are several methods for in situ measurements and for laboratory measurements. Some of the relevant methods are given below.

### 3.7.1 In Situ Measurements

Measurements done in situ have the advantages of not disturbing the material, maintaining the in situ stresses, and gives the ability to measure large volumes of soil (L'Heureux & Long, 2017). In situ measurements are best suited to measure the S-wave velocity,  $v_s$ . Measurements of P-wave velocity in saturated soil could be heavily influenced by the P-wave velocity in water, as discussed in Section 3.4. Field measurements can be both invasive and non-invasive. Invasive measurements involve drilling into the ground and include methods such as up-hole logging, down-hole logging, cross-hole logging, suspension logging, Seismic Dilatometer (SDMT), and Seismic Cone Penetration Test (SCPTU) (L'Heureux & Long, 2017). Non-invasive measurements include Multichannel Analysis of Surface Waves (MASW), Spectral Analysis of Surface Waves (SASW), Continous Surface Waves (CSW), seismic refraction, and seismic reflection. Figure 3.7 shows some of these measurement techniques. Most of these methods apply to both regular soil and stabilized soil. However, for stabilized soil, the measurements may be more difficult to interpret.

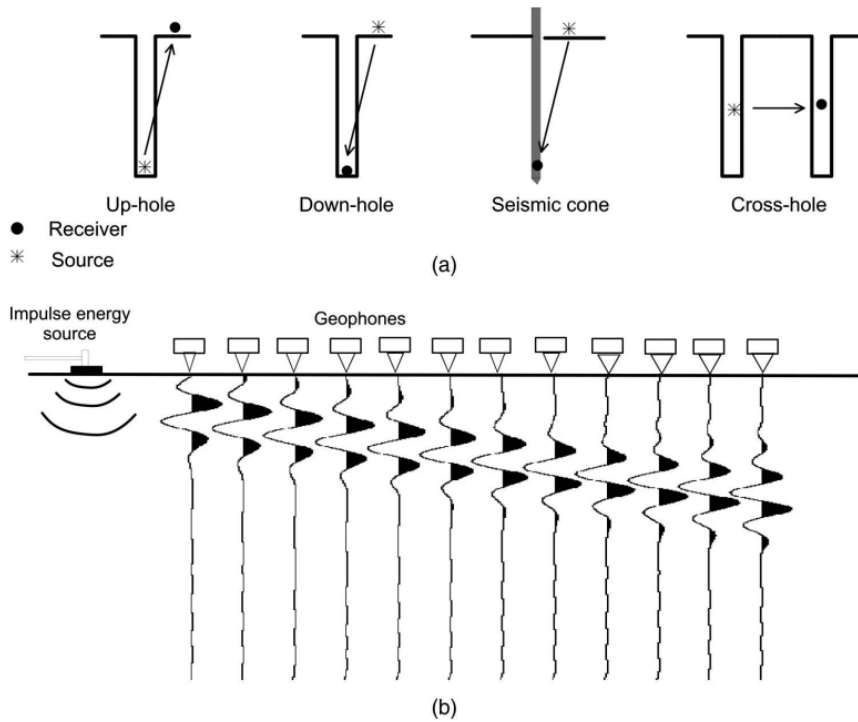


**Figure 3.7:** Field measurements of shear wave velocity: a) invasive techniques, b) MASW (L'Heureux & Long, 2017)

### 3.7.2 Laboratory Measurements

There are several techniques and methods to measure the wave velocities in the laboratory, such as the bender element test, ultrasonic test, resonance column test, and quasi-static loading at very low strains (Nordal & Eiksund, 2021). For laboratory tests, it is possible to measure both the P-wave velocity,  $v_p$ , and the S-wave velocity,  $v_s$ . The tests performed in this study are the bender element test and ultrasonic test. These are presented further in Chapter 4.



## Chapter 4

# Laboratory Measurements of Seismic Waves

This chapter describes the methods of measuring seismic wave velocities in the laboratory that are relevant to this study. The methods themselves are described along with their relevant limitations.

### 4.1 Pundit Device

The Portable Ultrasonic Non-destructive Digital Indicating Tester (PUNDIT) device is an apparatus that measures ultrasonic pulse velocity. Ultrasonic waves are stress waves with frequencies larger than 20 kHz. The Pundit device consists of a transducer and receiver that are connected to an electronic device (Andi et al., 2019). An illustration of a typical Pundit setup is shown in Figure 4.1.

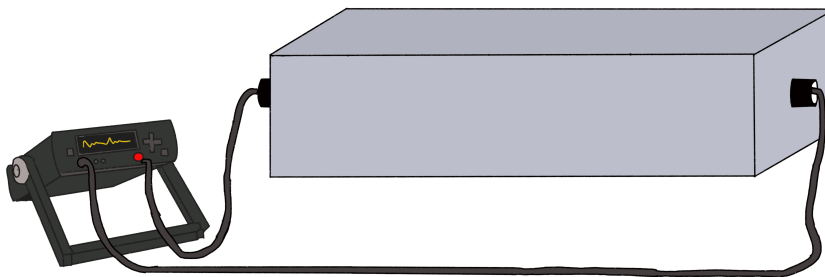


**Figure 4.1:** Illustration of a typical Pundit setup, modified after Andi et al. (2019)

The test is performed by placing the transducer and receiver on opposite sides of a sample. The transducer then generates ultrasonic pulses. Stress waves are generated by these pulses

and propagate through the sample. The electronic device that the transducer and receiver are attached to records the time interval between the pulse is generated at the transducer and when it arrives at the receiver. The ultrasonic pulse velocity is calculated by Equation 4.1.

$$v = \frac{L}{\Delta t} \quad (4.1)$$

The Pundit test can be performed with several different transducer arrangements. A pulse-echo configuration or a through-transmission configuration can be used (Yesiller et al., 2001). The pulse-echo arrangement is where a single transducer is used to both send and receive the ultrasonic waves. Through-transmission arrangement is when two transducers are used, as shown in Figure 4.1. By using different transducers it is possible to measure the P-wave velocity and the S-wave velocity with the Pundit test. Typical frequencies for the transducers vary between 20 kHz and 1000 kHz (Proceq, 2017). Generally, larger frequencies are used for stiffer materials since the transmission of stress waves in a material is affected by attenuation. Attenuation is the energy loss of a wave as it travels through a medium. In materials that are not completely uniform and homogeneous, scattering will occur due to pores and grain boundaries (Hwang et al., 2020). The attenuation is dependent on the frequency of the wave and larger frequencies generate more attenuation.

The Pundit test is fast and simple to perform and there is significant experience in using ultrasonic testing on concrete structures (Yesiller et al., 2001). It can be used to measure the change of material properties over time, thickness variations, and detection of cracks and voids in concrete structures (Proceq, 2017). For stabilized soil, however, there is a limited amount of studies.

## 4.2 Bender Elements

The background for this section is to present the bender element test and its fundamental operating principles. As well as workability, main challenges, sources of difficulties, and influencing factors for interpreting the output.

### 4.2.1 Design and Mechanisms

The bender element test is a method that measures shear wave velocities propagating through a soil sample. The shear wave velocity is an important geotechnical parameter since it can be used to calculate the small strain shear modulus. Bender element testing is a popular method due to its non-destructive nature, giving the opportunity to conduct multiple tests on the same specimen. The possibility of integrating the bender elements with a triaxial cell is also appealing.

Bender elements are built up of two piezoceramic sheets, one surface electrode on each sheet and a center electrode between the sheets. The idea is that the piezoelectric material can generate an electrical potential if it is subjected to mechanical deformation and vice versa. Meaning the bender element will deform when voltage is applied (Morawska, 2019).

For soil investigation usage, two elements are used; one transmitter and one receiver. These are placed on opposite sides of a soil specimen. A voltage pulse in the form of a sine wave is applied to the transmitter, usually mounted on the base pedestal. The voltage and the configuration of the piezoceramic sheets will then cause elongation in one sheet and contraction in the other, making the transmitter element bend, demonstrated in Figure 4.2. It is this deformation in the bender element that will generate a shear wave propagating through the specimen. When the wave reaches the receiver, the receiver will vibrate and create an electric impulse which is detected by a digital oscilloscope (VJTECH, 2020).

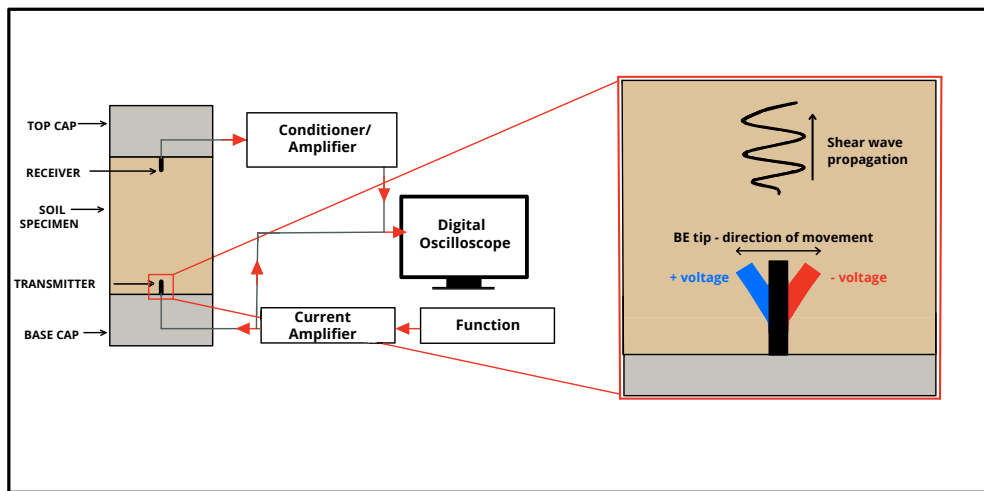


**Figure 4.2:** Illustration of the bender elements and the testing setup, modified after VJTECH (2020)

When the travel time has been determined, and knowing the travel distance, the shear wave velocity can be calculated with Equation 4.2

$$v_s = \frac{L}{t} \quad (4.2)$$

There is some discussion regarding what travel distance to use when doing bender element tests. Some of the literature suggests using the tip-to-tip length between the bender elements as the travel distance (Lee & Santamarina, 2005; Viggiani & Atkinson, 1995). However, Valsson et al. (2021) and Rio (2006) suggested using the length between the center of the dynamic pressure of the bender elements, which was estimated to be at around 60 % of the embedded bender element length.

Despite being a common method to determine the shear wave velocity and its superficial easy mechanism, the bender element measurements are affected with a lot of uncertainty. This is mostly due to it being no accepted and standardized procedure for interpretation. The following sections aim to describe the most relevant problems with the use of bender element testing and in regard to determining the shear wave velocities.

## 4.2.2 Travel Time Determination

The travel time is defined as the time interval from when the transmitter receives an electrical impulse to the waveform is recorded and logged at the receiver. Two main categories of methods are used to determine the travel time; time,- and frequency domain methods. Time domain methods use the time lag between transmitted and received signals, where the difference in used holding points gives the different methods; *peak-to-peak*, - *first arrival*, - and *cross-correlation method*. Frequency domain methods use the relationship between phase angle changes and the input frequency, like the discrete  $\pi$ -*point method* and the *continuous frequency spectral analysis method* (Y. Wang et al., 2016).

### Peak-to-Peak Method

The peak-to-peak method is based on visual inspection of the input and output signals, and is a widely applied method. The travel time is determined as the time lag between the peak of the transmitted signal and the peak of the first major wave in the received signal. It is important to be aware that the soil's size, stiffness, etc. affects the shape and frequency of the wave and makes the interpretation more difficult. Often the output signal will show more than one peak and differ in shape (Y. Wang et al., 2016). A visual demonstration of the peak-to-peak method is given in Figure 4.3.

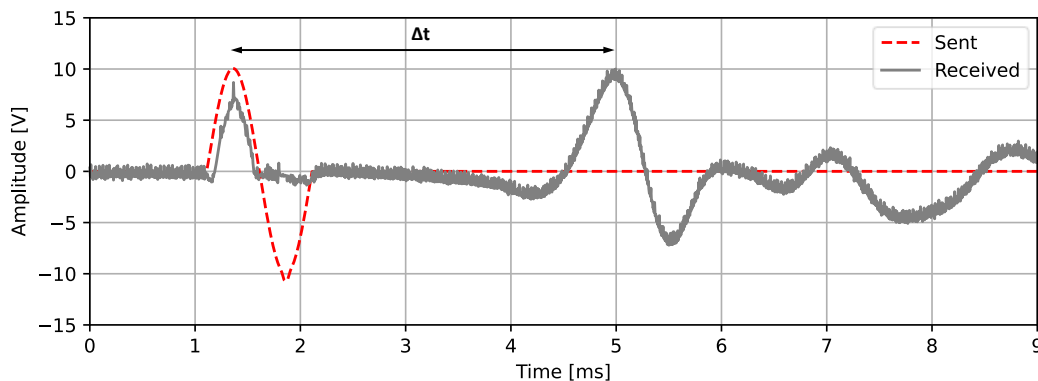
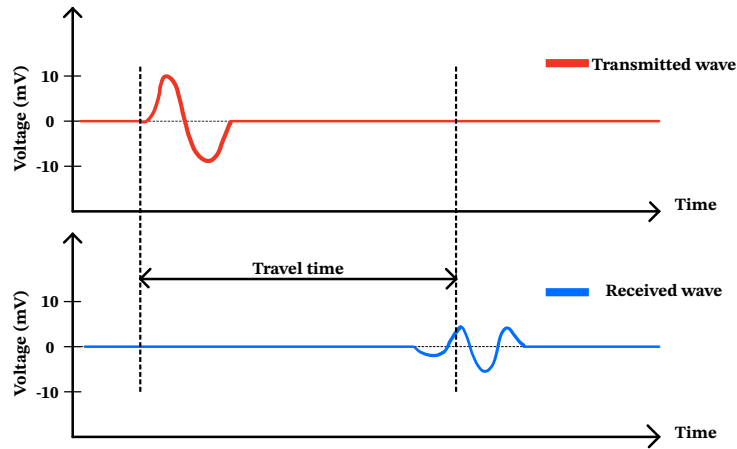


Figure 4.3: Interpretation of travel time using peak-to-peak method

### First Arrival Method

As the peak-to-peak method, the first arrival method is based on visual inspection. By inspecting the first deflection point of the received signal, the travel time is determined as the time lag between the transmitted wave and this deflection point, as demonstrated in Figure 4.4



**Figure 4.4:** Demonstration of first arrival determination, modified from Morawska (2019)

It is the most commonly used method, but at the same time quite controversial, due to being subjective in regards to interpretation. Picking the first arrival is often ambiguous due to the shape of the output signal. Often five different characteristic points are apparent for interpretation, as shown in Figure 4.5.

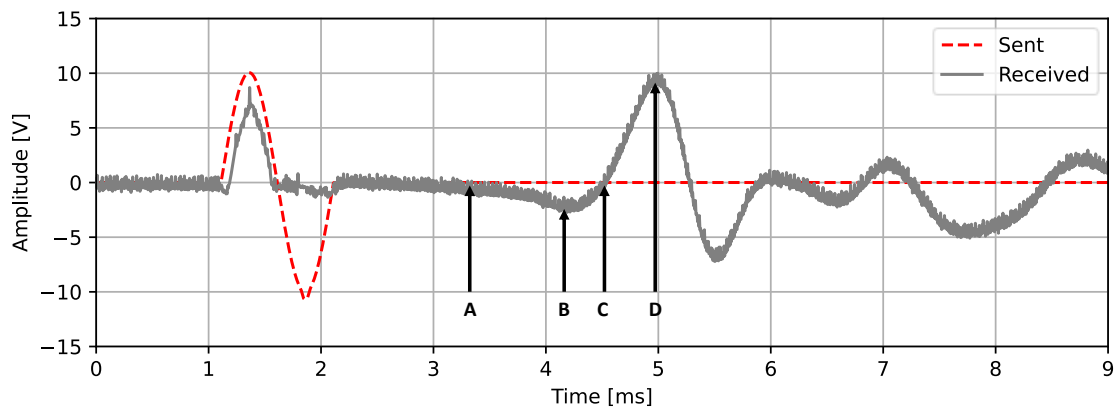


**Figure 4.5:** Demonstration of the ambiguously first arrival determination, modified after (Lee & Santamarina, 2005)

Difficulties in interpretations can be caused by the near-field effect, a wave dispersion phenomenon, discussed in Section 4.2.3. There is still no standardized procedure for working around the distortion and selection of first arrival points. Historically, point A is considered to be the arrival of the near-field effect component and is thereby neglected. Therefore it is usually point B (*the first reversal*) or C (*zero after first reversal*) that are used as the point of first arrival (Lee & Santamarina, 2005; Y. Wang et al., 2016).

### Cross-Correlation Method

Y. Wang et al. (2016) describes the cross-correlation as a method that uses a cross-correlation function,  $CR(\tau)$ , which is a measure of the similarity of two separate signals;  $x(t)$  and  $y(t)$ . These are time records of respectively input and output wave signals. The correlation is also a function of the time delay  $\tau$ . The method determines the travel time by corresponding it to the cross-relation peak. The function is given in Equation 4.3.

$$CR(\tau) = \lim_{T \rightarrow +\infty} \frac{1}{T} \int_0^T x(t)y(t + \tau)dt \quad (4.3)$$

### $\pi$ -point Method

For the  $\pi$ -point method the input signal is usually a continuous sinusoidal wave. Input and output signals are measured and displayed in an X-Y plot, where the phase shift between the two is measured. Slightly increasing the transmitter frequency induces a phase shift. Since it is a sinusoidal wave, the phase differences can be seen as a multiple,  $N$ , of  $\pi$  or  $-\pi$ , and an indication of the number of wavelengths. With corresponding frequency,  $f$ , and wave theory, the travel time is determined with Equation 4.4 (Y. Wang et al., 2016).

$$t = \frac{N}{f} \quad (4.4)$$

Equation 4.4 indicates that the travel time is the slope of an N-f plot. Results from using this method often show to be more objective than the mentioned time domain methods but the  $\pi$ -point method is often not used due to it being time-consuming and gives few interpretable points (Y. Wang et al., 2016).

### Frequency Spectral Analysis

A frequency domain method that potentially can provide more interpretable data in a shorter period of time compared to the  $\pi$ -point method, is the frequency spectral analysis method. A sweep signal with a wide frequency spectrum is used as input. A spectrum analyzer then tries to find the coherence between transmitted and received signals. Output from the spectrum analyzer is the coherence function and phase angles. Travel time is then determined as the slope of the relationship between these two. This method is often limited to results often not converging quickly enough, and further time-consuming analyses are required (Y. Wang et al., 2016).

#### 4.2.3 Near-Field Effect

The near-field effect is caused by waves that have the same particle motion but propagate at different velocities and attenuate at different rates (Sanchez-Salinero et al., 1986). The influence of the near-field effect is significant near the source of disturbance and is reduced as the waves propagate further from it, hence the name. Several studies have been done on

the near-field effect in bender element testing. According to studies by Sanchez-Salinerio et al. (1986), Arroyo et al. (2003) and Y. Wang et al. (2007) the requirement in Equation 4.5 should be fulfilled to avoid the near-field effect:

$$2 < L_{tt}/\lambda < 9 \quad (4.5)$$

Otherwise, the near-field effect may mask the arrival of the actual shear wave (Di Sante et al., 2022).

#### 4.2.4 Frequency

The interpretation of shear waves generated by the bender elements is highly dependent on the input frequency when testing. In order to optimize the readability of the signal the input frequency should ideally match the resonant frequency of the BE-soil-system (Lee & Santamarina, 2005). The resonant frequency increases with the stiffness of the soil. The BE-soil-system resonant frequency can be defined as in Equation 4.6 (Lee & Santamarina, 2005):

$$f_r = \frac{1}{2\pi} \left[ \frac{1,875^4 \frac{E_b I}{(\alpha L_b)^3} + 2\eta v_s^2 \rho_s (1 + \nu) L_b}{\rho_b b h (\alpha L_b) + (\rho_s b^2 L_b) \beta} \right]^{\frac{1}{2}} \quad (4.6)$$

Very low input frequencies can give poor results and cause too low shear wave velocities. Figure 4.6 shows how GDS bender elements gave much lower shear wave velocities than expected when low frequencies were used in the study by Xiao et al. (2018) on an acrylic sample. When the frequency increases, so does the shear wave velocity. When the frequency is above a certain level the measured shear wave velocity stabilizes somewhat.

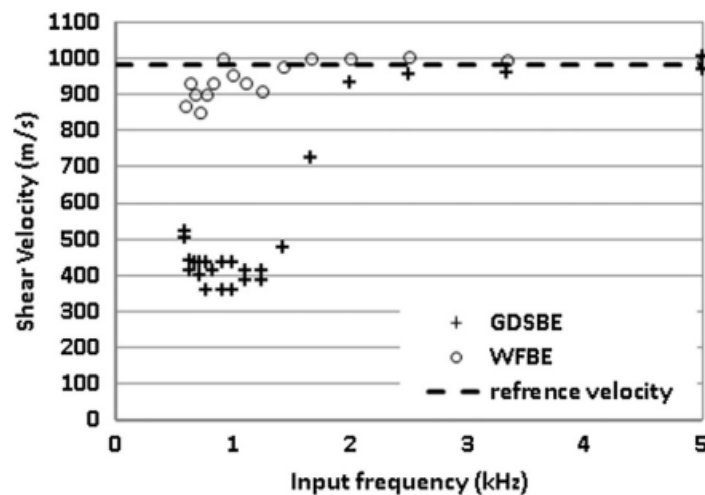


**Figure 4.6:** Variation of shear wave velocity with the frequency for two types of bender elements on an acrylic sample (Xiao et al., 2018)

#### 4.2.5 Contact between Probe and Specimen

A study by Xiao et al. (2018) on the effect of method and setup regarding bender element measurements, highlights the importance of applying sufficient contact between the soil specimen and the bender elements. When testing unstabilized soil samples with the bender elements it is easy to achieve good contact since the sample can be pushed directly onto the bender elements. This is not possible for cement-treated and stiffer soil samples. The most common method, in this case, is to pre-cut slots in the samples with dimensions to match the bender elements and place a fill material like plasticine or gypsum in the slots (Xiao et al., 2018). It was shown that the signal quality is highly sensitive to the contact between elements and soil. For example, with an over-cut slot, the bender tip will not be in full contact with the specimen, and the generated wave will not be able to clearly travel through the specimen.

Figure 4.7 shows how the results are affected by using too large dimensions on the slots, as well as the improving effect by enhancing the contact between the probe and soil with an infilling material. Different materials used for infilling have usually been fast-setting gypsum and plasticine (Åhnberg & Holmén, 2011; Baustad, 2022; Xiao et al., 2018).

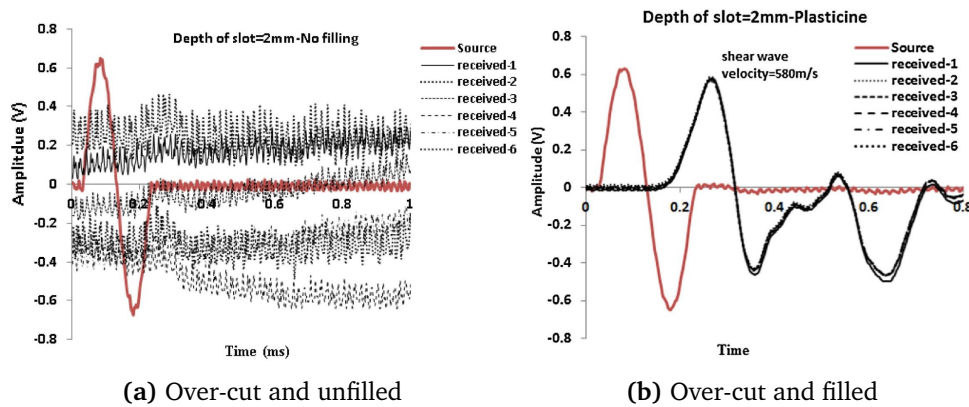


**Figure 4.7:** Effect on using infilling material in over-cut slots (Xiao et al., 2018)

For an over-cut slot with no filling, Figure 4.7a, the signals are way too degraded to be interpreted, while an over-cut slot with a filling, Figure 4.7b, gives significantly clearer results. Xiao et al. (2018) concluded that enhancing the contact with an infilling material improved both the consistency and stability, and reduced the sensitivity of the measurements.



## Chapter 5

# Electrical Resistivity

In this chapter electrical resistivity is described. The resistivity behavior in stabilized soils is then described, and lastly, the methods of measuring electrical resistivity are presented.

### 5.1 Resistivity Theory

Electrical resistivity testing in soil is a method that has been gaining importance in geotechnical engineering in recent years. The electrical resistivity of soil measures how strongly the soil resists electrical currents. The resistivity of soils depends among others on the porosity, density, degree of saturation, mineral composition, temperature, and particle shape and orientation, (Vincent et al., 2017). Electrical resistivity for a specimen,  $\rho$  [ $\Omega\text{m}$ ] is defined as in Equation 5.1:

$$\rho = \frac{\Delta U A}{I L} \quad (5.1)$$

The electrical conductivity,  $\sigma$  is the reciprocal of the electrical resistivity, calculated as in Equation 5.2:

$$\sigma = \frac{1}{\rho} \quad (5.2)$$

### 5.2 Resistivity for Soil Materials

For soils, resistivity measurements can be used to classify the type of soil. Different types of soils usually lie within certain ranges of resistivity, based on for instance soil type-specific mineralogy. Figure 5.1 shows typical resistivity ranges for different earth materials.

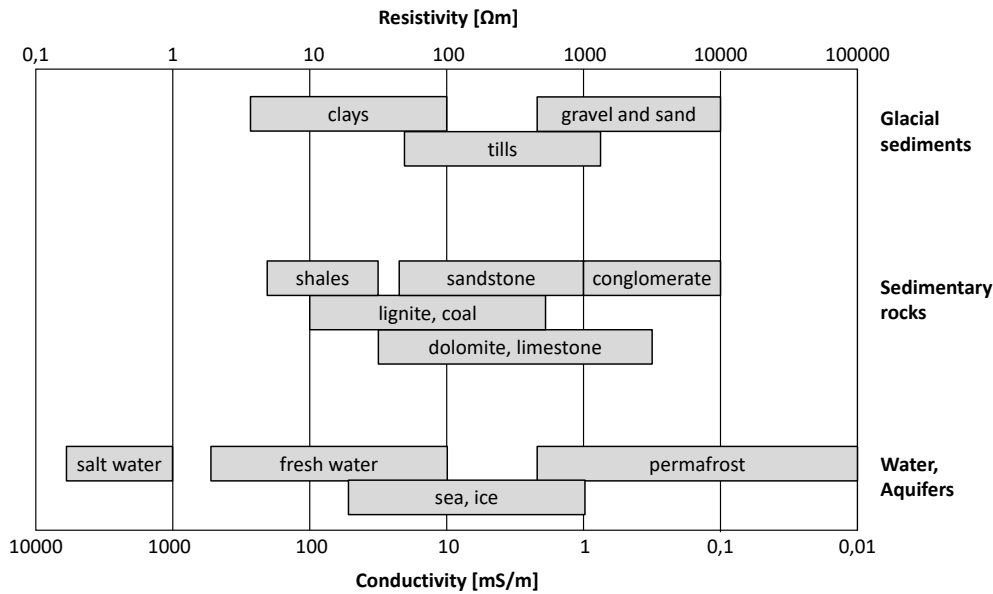


**Figure 5.1:** Typical resistivity for earth materials, modified after (Samouëlian et al., 2005)

For clays, the measured electrical resistivity and salt content of pore fluid is strongly influenced by each other (L'Heureux et al., 2019). Electrical resistivity measurements can be used to determine whether clay has been leached and has the potential of being a sensitive clay. Studies by Solberg et al. (2008) proposed the following classification of clay deposits:

- Dry crust clay:  $> 80 \Omega\text{m}$
- Leached, possible quick clay:  $10\text{-}80 \Omega\text{m}$
- Non-leached marine clay:  $1\text{-}10 \Omega\text{m}$

Typical electrical resistivity values for Norwegian peat are in the range of  $50 - 350 \Omega\text{m}$  according to Paniagua et al. (2021).

### 5.3 Resistivity for Stabilized Soil

Stabilization of soils changes the structure of the soil and will affect the resistivity as well. Added binders react with water in the soil and fill the pores with hydration products instead of water. This will decrease the electrical conductivity of the material and thus increase the resistivity. Ng et al. (2022) showed that for a limited curing period, the changes in conductivity and thus resistivity can be correlated to the strength of stabilized soil. Studies by Liu et al. (2008), Vincent et al. (2017), Zhang et al. (2012) and Zhou et al. (2015), show that the factors in Table 5.1 have an influence on the resistivity in soils and stabilized soils:

**Table 5.1:** Parameters affecting the resistivity for stabilized soil

Parameters	Explanation
Cement content	An increase in cement content will lead to more formation of hydration products. As a result, the resistivity will increase.
Curing time	When the curing time increases, more water will react and form hydration products, and therefore the resistivity increases.
Water content	A decrease in water content will increase the tortuosity of the conduction path for electrical current. This means that the resistivity will increase.
Saturation	Water-filled pores have better conduction than pores filled with air. An increase in saturation is therefore related to a decrease in resistivity.
Porosity	For cement-treated soils the increase in porosity generally correlates with a decrease in resistivity.
Temperature	Temperature has a significant effect on the resistivity measurements. An increase in temperature will decrease the resistivity of soil materials.

## 5.4 Measurement of Resistivity

### 5.4.1 Field Measurements

Measurements of electrical resistivity are non-destructive. The measurements can be performed in the laboratory and in the field. In situ measurements can be done with a Resistivity Piezocone Penetration Test (RCPTU), Airborne Geoscanning (AG), Electrical Resistivity Tomography (ERT) or a multi-electrode borehole cable.

### 5.4.2 Laboratory Measurements

Resistivity measurements can be performed in the laboratory as well as in situ. The electrical resistivity is measured in the laboratory by placing electrodes on each side of a soil sample, applying a voltage, and then measuring the current. Using the same principles as described above, the electrical resistivity is calculated with Equation 5.1.

Laboratory measurements of electrical resistivity can have several different setups. The test setup can consist of two or four electrodes, (Zhou et al., 2015). For the electrical source, either Alternating Current (AC) or Direct Current (DC) can be used (Ng et al., 2022). Different frequencies can also be used when measuring resistivity. The electrodes can be in contact

with the sample on the surface or they can be inserted into the sample for better contact. In order to achieve good results it is important to have proper contact between the electrodes and the sample. Otherwise, the measured current that travels through the sample may be affected by the electrodes not being able to properly transfer the current into the sample, giving measurements not representative of the sample's actual resistivity. This is described as contact resistance (Zhou et al., 2015). Measurement of electrical resistivity in the laboratory is fairly easy and fast to perform. Figure 5.2 shows a simple setup where two electrodes are put on the surface of a sample.

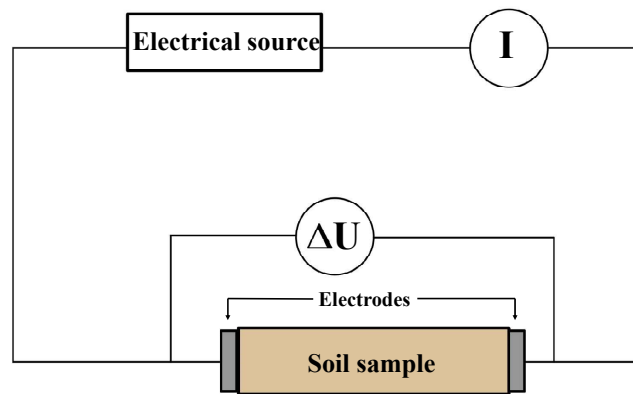


**Figure 5.2:** Schematic of two-electrode probe method, modified after Liu et al. (2008)

Zhou et al. (2015) studied both the effect of using a two-electrode method versus a four-electrode method for resistivity measurements and the effect of used frequency. The study showed that using two electrodes resulted in contact resistance between the electrodes and the soil which caused measurement errors. The study also tested frequencies between 50 Hz to 200 kHz. The resistivity measurements slightly decreased as the frequency increased. Typically, low frequencies are used for resistivity measurements, and the study highlighted that frequencies below 1 kHz did not show any obvious effect on the resistivity measurements.

## Chapter 6

# Test Sites

This chapter aims to give a brief summary of the soil used in this study and the test sites where the soil samples are gathered from. All of the quick clay, soft clay, and peat is collected from Norwegian Geo-Test Sites (NGTS). The characteristic properties of the materials used in this study are presented, and a special focus is aimed at the shear wave velocity and resistivity properties.

### 6.1 Norwegian Geo-Test Sites

Norwegian Geo-Test Sites (NGTS) is a research consortium, which is led by NGI. Other members are NTNU, SINTEF and Statens Vegvesen. The goal was to establish five national geo-test sites used as field laboratories for testing both well-documented and innovative soil investigations and methods. In total, there are five test sites, where each is meant to be representative of a different soil type. This includes; quick clay, soft clay, silt, sand, and permafrost (SINTEF, 2017). An overview of the different NGTS is shown in Figure 6.1. The material used in this thesis is from Tiller-Flotten (quick clay and peat) and Onsøy (soft clay).



Figure 6.1: NGTS locations (SINTEF, 2017)

## 6.2 Tiller-Flotten Testing Site

L'Heureux et al. (2019) presents a detailed characterization of the soils in the Tiller-Flotten area based on an integrated study of geotechnical, geophysical, and geological data acquired from both the field and the laboratory. It aims to form a useful reference for future engineering work on sensitive soils.

### 6.2.1 Location and Quaternary Geology

Approximate 10 km south of Trondheim, the Tiller-Flotten testing site is located, shown in Figure 6.2. The testing site is located at an elevation of ca. 125 m.a.s.l. with drainage down towards Nidelva. Nidelva is located at an elevation of 72 m.a.s.l. and ca. 700 m southeast of the Tiller-Flotten testing site. An area of 150x300 meters has been granted for geotechnical studies (L'Heureux et al., 2019).



Figure 6.2: Location of Tiller-Flotten testing site (Kartverket, 2023)

Maps of the quaternary geology in the area show that the site mainly consists of marine and glaciomarine sediments, which emerged from the much higher sea levels after the last ice age. Surrounding areas also contain thick layers of marine clay, with an omnipresence of ravines and landslide scars. The southwestern part of the site has a ca. 2 m thick peat deposit above the clay. The quaternary geology is shown in Figure 6.3

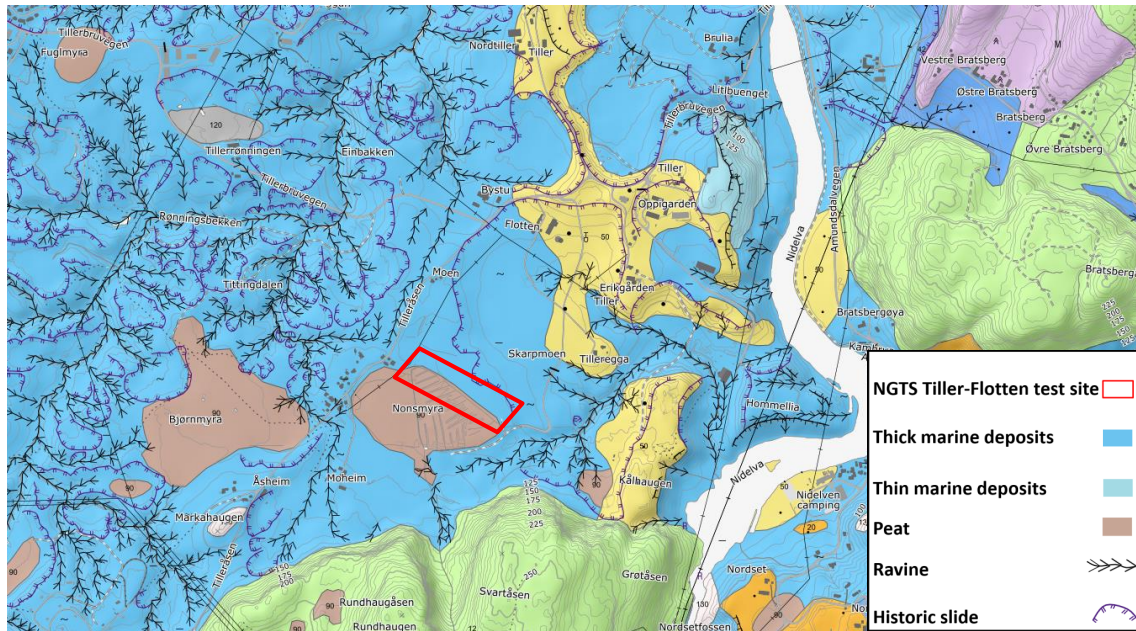


**Figure 6.3:** Map of quaternary geology at the Tiller-Flotten testing site, modified from (NGU, 2023b)

### 6.2.2 Stratigraphy

Based on the results from laboratory- and in situ testing the stratigraphy of the site has been interpreted as in Figure 6.4, and is divided into two main parts. The top layer (I) is assumed to be a ca. 2 m thick desiccated and weathered clay. Layer II is divided into an "A" and "B" section, which is separated due to differences in soil sensitivity. Layer IIa is found to be at 2 - 7,5 meters in depth and is characterized as low to medium-sensitive clay. Further down, layer IIb, from 7,5 meters the clay shows sensitivity often above 100 and is extremely sensitive. Water content varies from 40-50 % near the surface, before decreasing some with depth (to around 30-35 %). The overall bulk density for the profile is around  $18 \text{ kN/m}^3$  (L'Heureux et al., 2019).

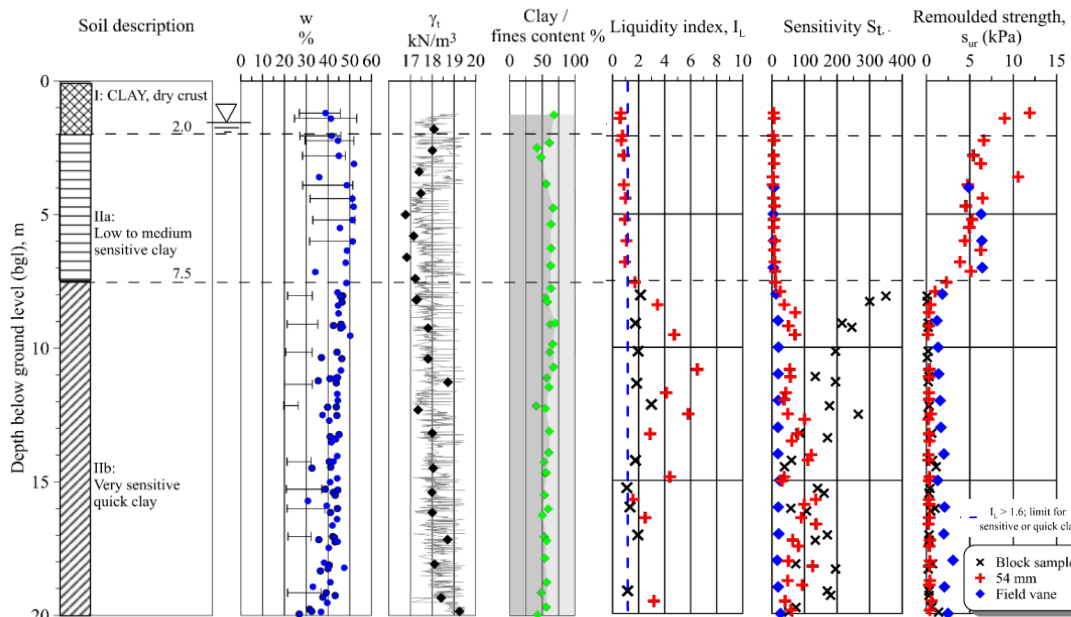


**Figure 6.4:** Interpreted soil profile from Tiller-Flotten testing site, modified from (L’Heureux et al., 2019)

### 6.2.3 Shear Wave Velocity and Stiffness

Shear wave velocities were obtained in situ with the use of a Seismic Dilatometer (SDMT), Seismic Cone Penetration Test (SCPTU), and Multichannel Analysis of Surface Waves (MASW). Shear wave velocities were also measured in the laboratory using bender elements, both unconfined and confined in a triaxial cell. The measured shear wave velocities for in situ ( $V_s$ ), unconfined ( $V_{s,0}$ ) and confined ( $V_{s,1}$ ) are plotted in Figure 6.5. The in situ tests show that the shear wave velocities vary from approximately 120 m/s below the dry crust to around 225 m/s at 20m depth (L’Heureux et al., 2019). It is worth noting that the laboratory tests consistently gave lower values than the in situ tests, whereas the unconfined bender element tests gave lower velocities than the confined tests.



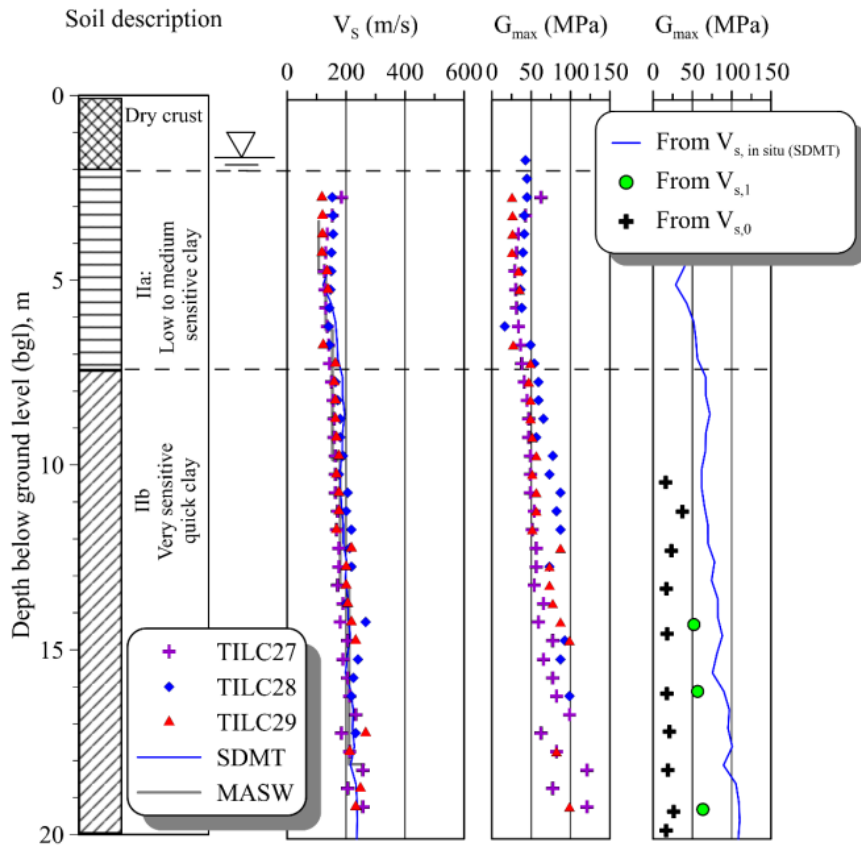


Figure 6.5:  $V_s$  and  $G_{max}$  with depth (L'Heureux et al., 2019)

### 6.2.4 Electrical Resistivity

Electrical resistivity in Tiller-Flotten has been measured using Electrical Resistivity Tomography (ERT) and with a Resistivity Piezocone Penetration Test (RCPTU). The results from both methods showed similar results. In total six ERT profiles were made, where two examples are shown in Figure 6.6 (L'Heureux et al., 2019). The results show that below the dry crust, the resistivity values are fairly constant and range from 30 - 40  $\Omega\text{m}$  down to approximately 35 m below the surface. Below 35 m depth, there is a more conductive layer with a resistivity of less than 10  $\Omega\text{m}$ .

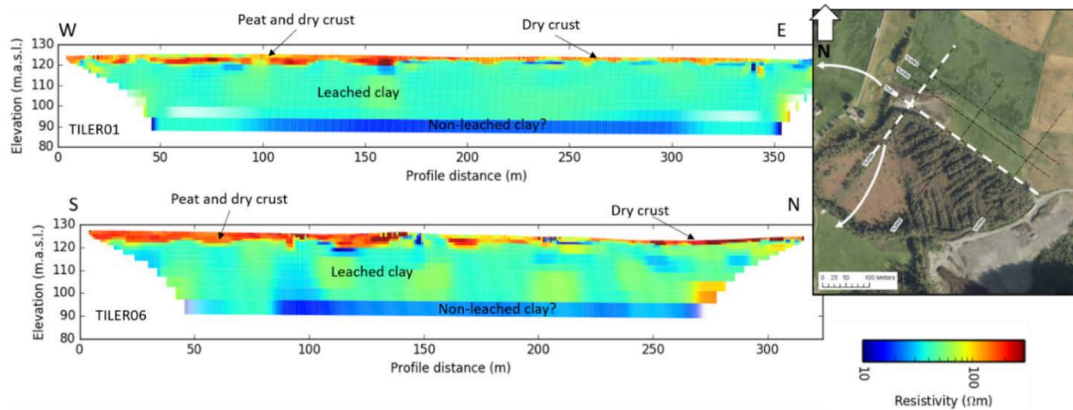


Figure 6.6: Electrical resistivity tomography of Tiller-Flotten (L’Heureux et al., 2019)

### 6.2.5 Tiller-Flotten Peat

The bog/swamp area in the southwestern corner of the Tiller-Flotten testing site is also an area of interest. Here the thickness of the peat layer varies between 1,8 and 2,5 m. A study of Tiller-Flotten peat by Ritter et al. (2022) mapped several peat-relevant parameters, which have been summarized in Figure 6.7. The water content of the peat is around 1000 %. The Von Post scale of the Tiller-Flotten peat is between H1 and H5, whereas most of the peat is in the H2-H3 area. The undrained shear strength ( $c_u$ ) was found to be between 4-6 kPa.

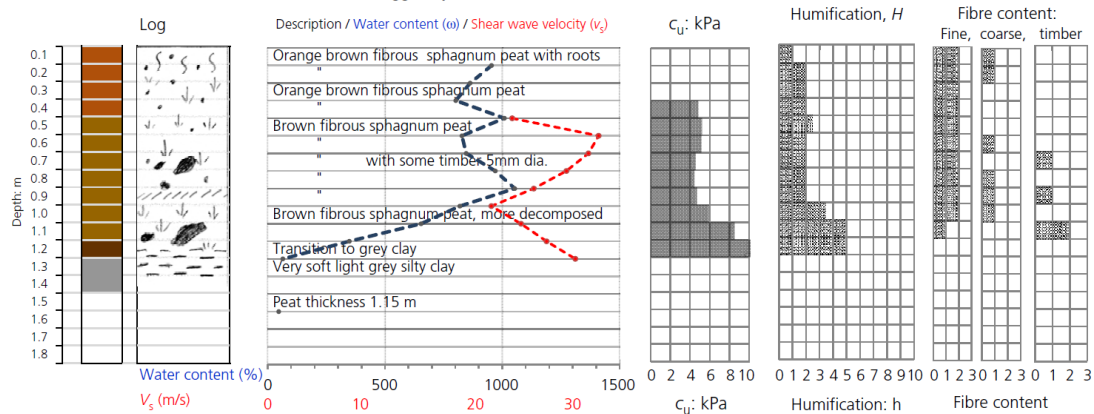


Figure 6.7: Tiller-Flotten peat characterized with Von Post log (Ritter et al., 2022)

Figure 6.7 shows shear wave velocities ranging between 20 - 30 m/s. Another study by Long et al. (2022) showed similar results, with an average shear wave velocity for the entire sampling depth of 23,6 m/s. Previous studies on geotechnical values representing peats from all over Norway indicated shear wave velocities could be expected between 16-24 m/s (Paniagua et al., 2019). Paniagua et al. (2019) also showed values for the electrical resistivity of Norwegian

peat, ranging between 50 - 350  $\Omega$ m. These values are in the same size order as the top layer (Tiller-Flotten peat) of the ERT in Figure 6.6.

### 6.3 Onsøy Testing Site

Initial tests of sediments from the Onsøy area showed potential for being very suitable for research purposes, due to its thickness and uniformity of deposits. Ever since its establishment, the Onsøy area has extensively been used for large-scale field testing and development of new tools (Gundersen et al., 2019a).

#### 6.3.1 Location and Quaternary Geology

Just north of Fredrikstad, in the southeastern part of Norway, the Onsøy testing site is located. The testing site has been relocated multiple times since its original placement due to industrial development. The two locations prior to the newest site from 2016 are usually referred to as Historic Onsøy test sites. The current site is approximately 1,3 km southwest of the historic sites and is limited to an area of approximately 80x75 meters. An overview map of the area is shown in Figure 6.8.



Figure 6.8: Location of Onsøy testing site (Kartverket, 2023)

Maps of the quaternary geology in the area show that the site mainly consists of some thick and less thick deposits of marine sediments, which emerged from the much higher sea levels

after the last ice age. Surrounding areas also contain some larger boulders and rock outcrops. The quaternary geology is shown in Figure 6.9

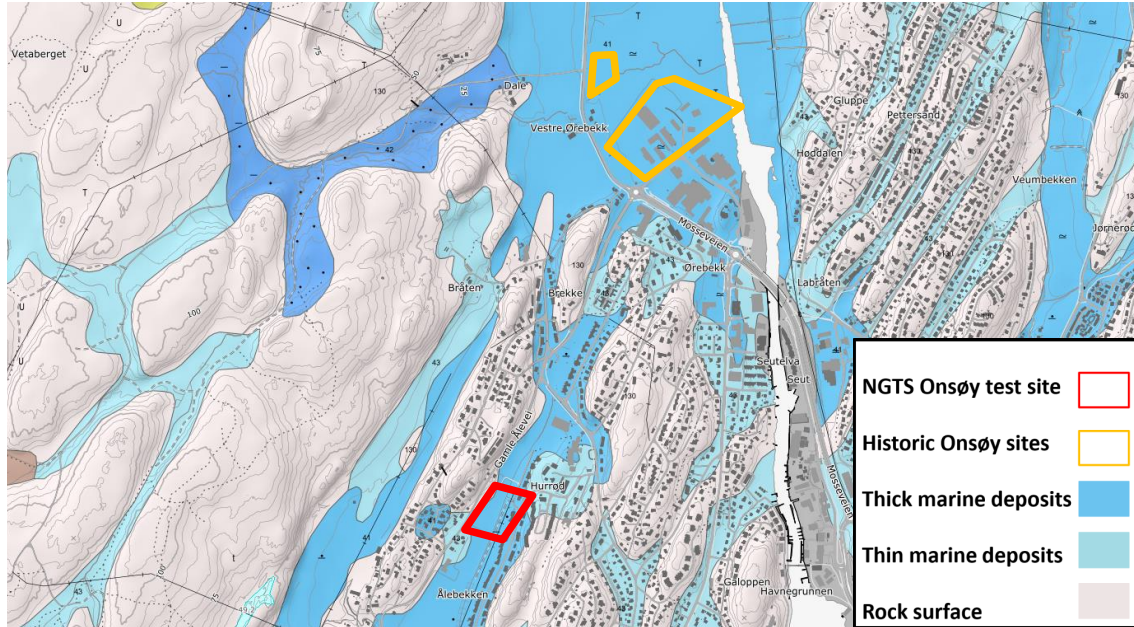
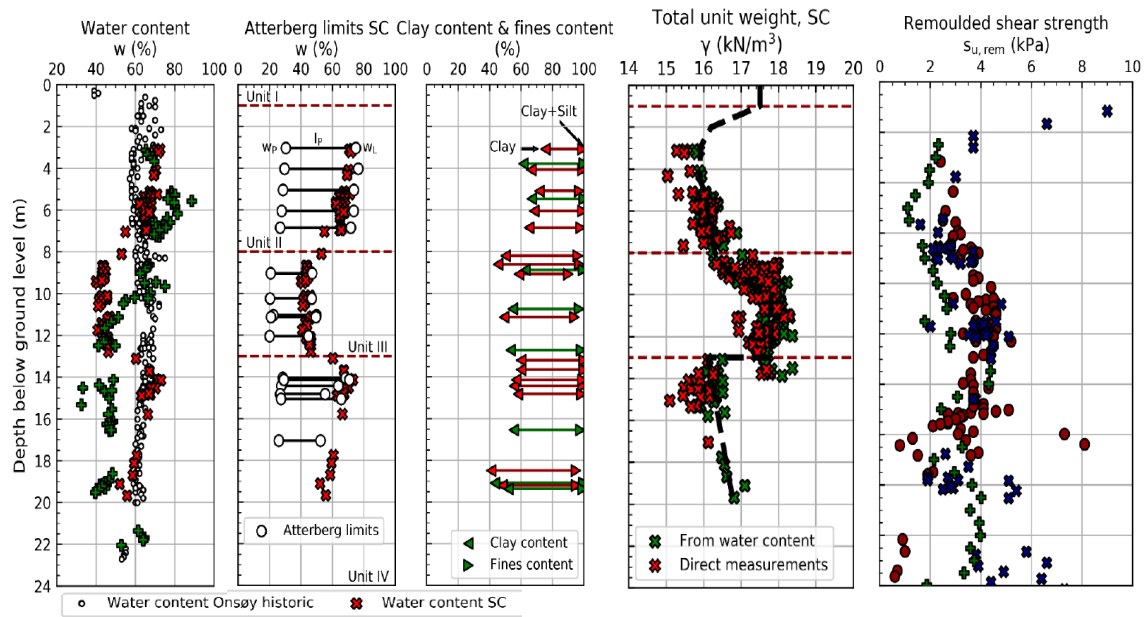


Figure 6.9: Map of quaternary geology at the Onsøy testing site, modified from (NGU, 2023b)

### 6.3.2 Stratigraphy

Based on the results from laboratory- and in situ testing the stratigraphy of the site has been interpreted as in Figure 6.10, and is divided into three different main parts. The top layer (I) is assumed to be a ca. 1 m thick weathered clay crust. Layer II is a clay with high to very high plasticity index and high water content. This layer also contains shells and shell fragments. The layer stretches from ca. 8 - 10,5 m below ground level. Layer III is characterized as clay with medium-high plasticity and water content of around 45 %. At the base of layer III, a 3 cm thick sand layer is identified in a transition to layer IV (Gundersen et al., 2019a).

The typical unit weight for layer I, II, and III is respectively 17,5, 16,2, and 17,8 kN/m<sup>3</sup>. Fall cone tests and field vane tests have been used to find the remoulded shear strength and sensitivity of the material. The plots in Figure 6.10 show that between 2 - 6 m depth the remoulded shear strength (1-3 kPa) is generally lower than between 8 - 12 meters depth (3-5 kPa) (Gundersen et al., 2019a).



**Figure 6.10:** Interpreted soil profile from Onsøy testing site, modified from (Gundersen et al., 2019a)

### 6.3.3 Shear Wave Velocity and Stiffness

Shear wave velocities were obtained in situ with the use of a Seismic Dilatometer (SDMT) and Seismic Cone Penetration Test (SCPTU). Shear wave velocities were also measured in the laboratory using bender elements, with samples confined in a triaxial cell to simulate in situ stresses. The measured shear wave velocities for in situ and laboratory testing are plotted in Figure 6.11 (Gundersen et al., 2019a). The measured shear wave velocities vary from around 75 m/s at 2 m depth to around 150 m/s at 20 m depth.



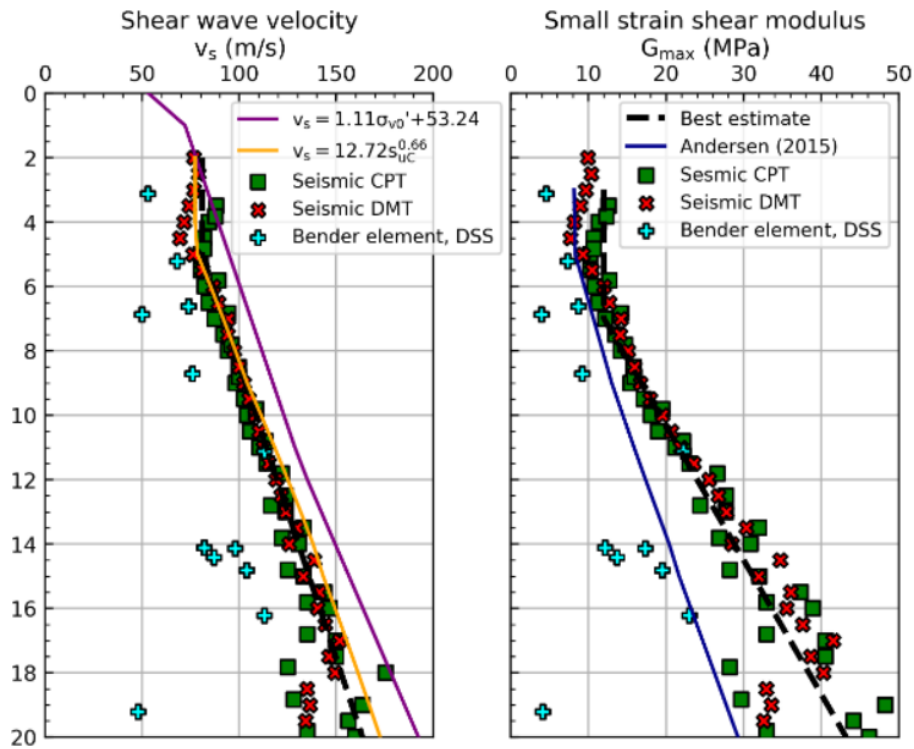


Figure 6.11:  $V_s$  and  $G_{max}$  with depth (Gundersen et al., 2019a)

### 6.3.4 Electrical Resistivity

Electrical resistivity for the Onsøy testing site has been measured using Electrical Resistivity Tomography (ERT). In total two ERT profiles, divided into eight length intervals were performed. An example is shown in Figure 6.12 (Gundersen et al., 2019b). The results show values mainly ranging between 1 - 10  $\Omega\text{m}$ , which are expected results for non-leached clay, as described in Chapter 5 (Solberg et al., 2008).

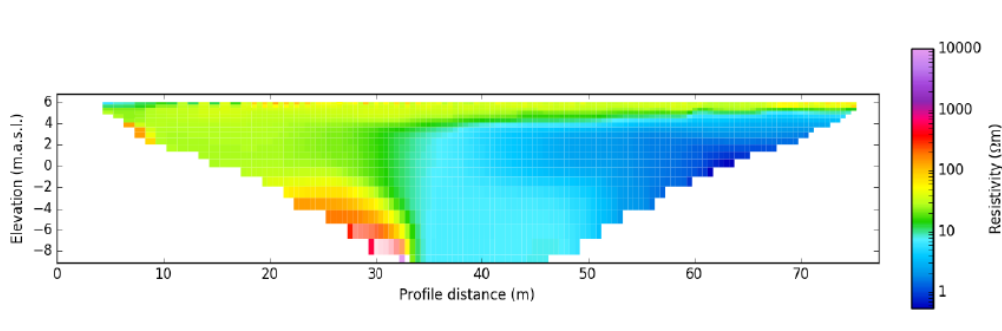


Figure 6.12: Electrical resistivity tomography of Onsøy (Gundersen et al., 2019b)

## **Part II**

# **Lab and Results**





## Chapter 7

# Laboratory Work

This chapter describes the laboratory work that was performed in this study. The procedures, equipment, and tests used in this study are described. The following work was done:

- Preparation of stabilized soil samples
- Pundit testing to measure P-wave and S-wave velocity
- Measurement of electrical resistivity
- Bender element tests to measure S-wave velocity
- Unconfined compression tests
- Index testing

### 7.1 Preparation of Samples

For this study, a total of 108 samples of stabilized soil were prepared. The material used for the samples were Tiller-Flotten quick clay, Onsøy soft clay, and Tiller-Flotten peat. The material arrived remoulded and homogenized and it was sampled from the following depths:

- Quick clay (Tiller-Flotten): 8 - 15 m depth
- Peat (Tiller-Flotten): around 1 m depth
- Soft clay (Onsøy): 5 - 8 m depth

Table 7.2 gives a complete overview of all laboratory-made samples. The table shows which soil type that was mixed with which by-product and cement, the quantity of binders being used and the number of samples made in each batch. The table shows in total 36 different batches, and with 3 samples in each batch, a total of 108 samples were made.

The used binders are mentioned in Section 2.3, and are; Cement (CEM), Ladle Slag 1 (LS1), Bottom Ash (BA), Paper Sludge Ash (PSA), Biochar 1 (BC1) and Biochar 4 (BC4). The quantity of binders is given in kilograms per  $m^3$  of soil to be stabilized.

Due to the large amount of different samples and soil types, it was decided to color code the different soil types, with each by-product given its own shape. These plot IDs are present throughout the whole study and give a more intuitive understanding while presenting results. They are also given in Table 7.2.

Also to help keep track of all the samples, each sample was labeled based on soil type, sample nr., mixture ratio, and used by-product. How this is done, is illustrated below:

<b>Soil type</b>	<b>Sample nr.</b>	<b>Binder ratio*</b>	<b>By-product</b>
<u>Quick clay</u>	<u>1</u>	<u>20/20</u>	<u>LS1</u>

⇒ Q.1.20/20.LS1

\* Binder ratio is given as cement [ $kg/m^3$ ] / by-product [ $kg/m^3$ ]

The sample number indicates which one out of the 3 samples from the specific batch it represents. Only one sample (the one named sample nr. 1) of each batch was tested after 3, 7, 14, 21, and 28 days of curing. The other two samples from each batch were only tested after 28 days of curing and left undisturbed unless it became necessary to replace a broken number 1 sample.

**Table 7.2:** Complete overview of prepared stabilized samples, including which type of soil, binder- combinations and ratios that are used, number of samples made, and belonging plot ID

Type of Soil	Type of By-product	CEM1 [kg/m <sup>3</sup> ]	By-product [kg/m <sup>3</sup> ]	Made samples	Plot ID
Quick clay	LS1	20	20	3	△
Quick clay	LS1	40	40	3	△
Quick clay	LS1	60	60	3	△
Quick clay	BA	20	20	3	■
Quick clay	BA	40	40	3	■
Quick clay	BA	60	60	3	■
Quick clay	PSA	20	20	3	◇
Quick clay	PSA	40	40	3	◇
Quick clay	PSA	60	60	3	◇
Quick clay	BC1	50	50	3	●
Quick clay	BC1	50	100	3	●
Quick clay	BC1	50	200	3	●
Soft clay	LS1	20	20	3	△
Soft clay	LS1	40	40	3	△
Soft clay	LS1	60	60	3	△
Soft clay	BA	20	20	3	■
Soft clay	BA	40	40	3	■
Soft clay	BA	60	60	3	■
Soft clay	PSA	20	20	3	◇
Soft clay	PSA	40	40	3	◇
Soft clay	PSA	60	60	3	◇
Soft clay	BC1	50	50	3	●
Soft clay	BC1	50	100	3	●
Soft clay	BC1	50	200	3	●
Peat	LS1	100	50	3	△
Peat	LS1	100	100	3	△
Peat	LS1	100	200	3	△
Peat	BA	100	50	3	■
Peat	BA	100	100	3	■
Peat	BA	100	200	3	■
Peat	PSA	100	50	3	◇
Peat	PSA	100	100	3	◇
Peat	PSA	100	200	3	◇
Peat	BC4	100	200	3	●
Peat	BC4	100	300	3	●
Peat	BC4	100	400	3	●

For mixing, the corresponding amount of grams from the ratios was calculated from the material's unit weight and weighed amount of material. For the Tiller-Flotten quick clay and Onsøy clay, it was found that 1500 grams of material was sufficient for one batch (3 samples). The Tiller-Flotten peat only needed around 900 grams, due to its significantly lower density. The unstabilized material was first mixed in a standard Kenwood mixer for around 1 minute. The cement and by-product were then added and mixed until it was clearly a homogeneous mix. This process is shown in Figure 7.1

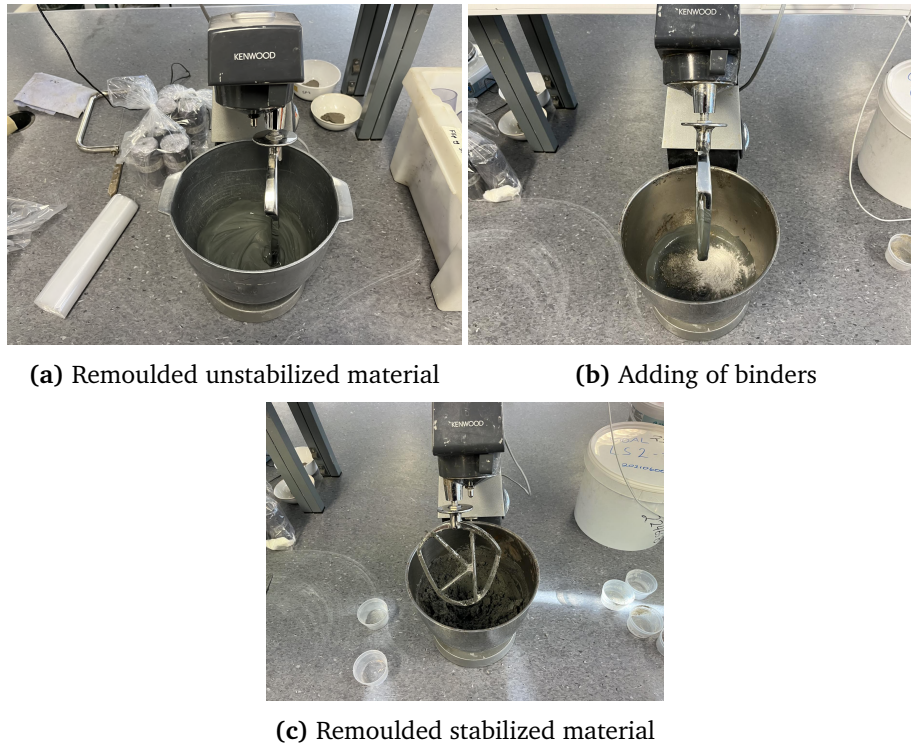


**Figure 7.1:** Process of mixing unstabilized material with binders

The stabilized samples were cast in 108 x 54 mm cylinders using an impact compaction rodding method. This is a method NGI developed by slightly adjusting an older impact compaction method from NGF (Hov & Paniagua, 2022; NGF, 2012). This method is also compared to other commonly used methods by Kitazume et al. (2015), where it was shown to be highly applicable for several conditions. A step-by-step procedure looked like this:

- 1 Homogenize the natural soil using a Kenwood mixer.
- 2 Add the measured cement and by-product.
- 3 Mix until the mixture achieves visual homogeneity.
- 4 Incrementally place the mixture in layers of approximately 20 mm inside the cylinder.
- 5 Perform sequential compaction for each layer by stamping with a 20 mm diameter rod.
- 6 Each layer was deemed compacted when as much air as possible was expelled and no visible separation between layers existed.

### Storage of samples

A prepared sample is shown in Figure 7.2a. Each sample was thereafter systematically labeled and stored in a plastic bag with samples from the same batch, as shown in Figure 7.2b. In order for the samples to not dry out, a piece of wet paper was put in each plastic bag with samples. The samples were stored at room temperature of around  $22 \pm 2$  °C.

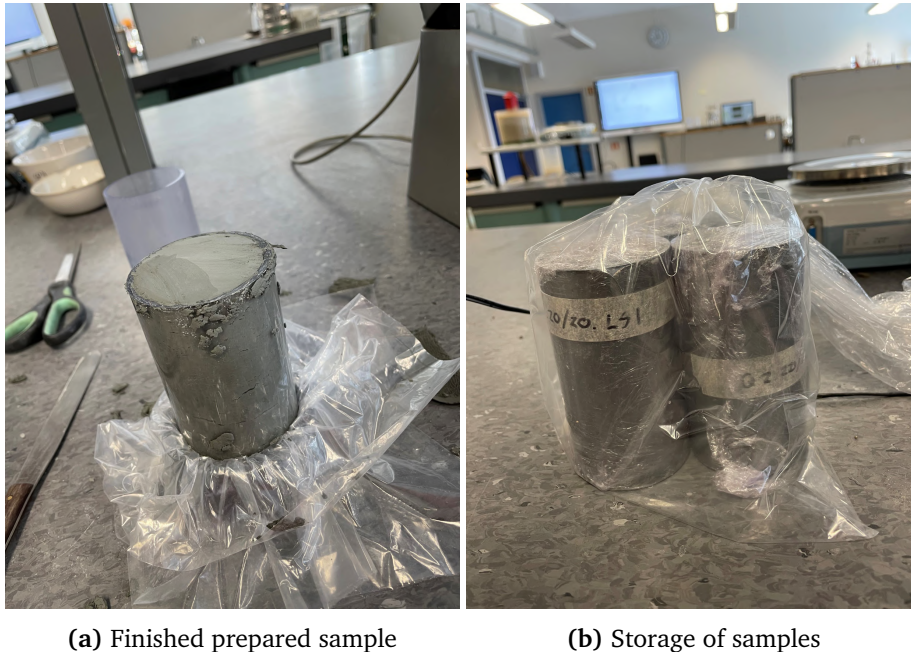


**Figure 7.2:** Illustration of finished moulded sample and how they got stored

### Extrusion of Samples

The need for a fragile extrusion procedure was quickly identified. To ensure optimal further testing, the samples needed to be extruded from the cylinder moulds<sup>1</sup>.

Figure 7.3a shows the specially designed parts to safely extrude the 108 mm samples from the cylinders. The parts ensured evenly distributed pressure on the sample while keeping it steadily mounted. Figure 7.3b shows the setup during extrusion.

<sup>1</sup>Some electrical resistivity tests were performed with the cylinders still around the samples. This was to not risk the sample breaking during extrusion like similar samples earlier had done. Tests with and without cylinders showed similar results for the electrical resistivity



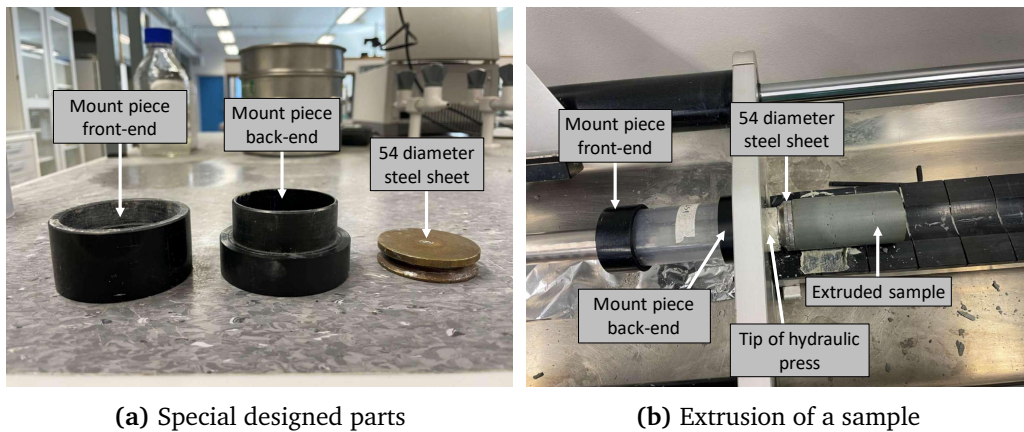


Figure 7.3: Demonstration of sample extrusion with explaining text-boxes

## 7.2 Pundit Test

The Pundit device used in this thesis is the Pundit 200 from Proceq. This apparatus can be connected to several different transducers. In this study, 54 kHz P-wave transducers and 40 kHz dry-point S-wave transducers were used to measure the P-wave and S-wave velocity respectively. An overview of the equipment used in the Pundit test is shown in Figure 7.4.

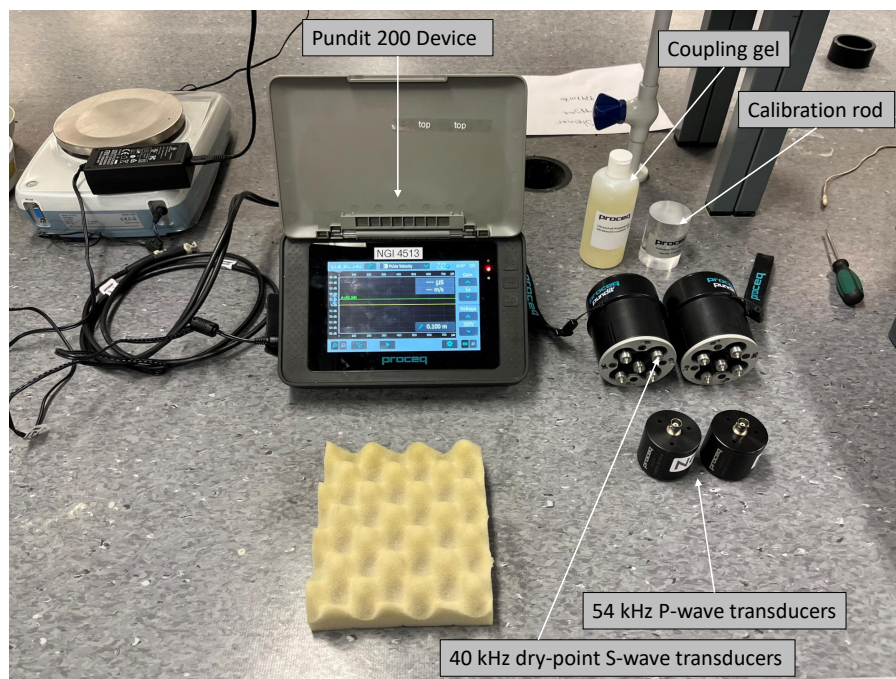


Figure 7.4: Overview of the Pundit setup in this study

The Pundit test itself was performed by placing a stabilized sample on foam in order to avoid disturbance from the surroundings. The transducers were connected to the Pundit 200 device through cables. The transducers were placed on opposite sides of the stabilized sample and ultrasonic pulses were generated at one transducer and detected at the other. The test was controlled by using the touchscreen on the Pundit 200. The transmitter voltage could be adjusted between 100-400 V for the 54 kHz transducers and between 50-100 V for the 40 kHz shear wave transducers. When testing samples the transmitter voltage was set at a low value at first and then adjusted to higher values until a stable signal was achieved. This was to ensure that the best possible signals were measured, and this was also recommended in the manual (Proceq, 2017). The receiver gain was adjustable between 1x and 10000x. This was adjusted during the tests to get the best possible signals.

For most of the samples, the transmitter voltage was set to 200, 250 or 300 V for the 54 kHz P-wave transducers, and 100 V for the 40 kHz S-wave transducers. The receiver gain was most commonly set to either 500x or 1000x. The pulse repetition frequency was set to 10 Hz for all samples.

The P-wave transducers had flat edges with a diameter of 49,7 mm. In order to ensure good contact between transducers and the sample it was essential to use a coupling gel (Proceq, 2017). The coupling gel used was a viscous ultrasound couplant. The arrival of the P-waves was detected by using an auto-trigger which automatically located the first wave to arrive and measured the traveling time and calculated the P-wave velocity from this.

The shear wave transducers had a diameter of 84 mm, which made them too large for the 54 mm samples. However, since the transducers had five contact points it was not necessary for all of the points to be in contact with the sample. The shear wave transducers were in contact with the samples through three points. In order to detect the shear waves it was important that the two transducers were orientated parallel to each other. Otherwise, the shear waves would be rotated, which would make them harder to detect. For the dry-point shear wave transducers, no coupling gel was required. According to Corbett (2016) there seems to be no detectable P-wave component when using dry point shear wave transducers. This means that the arrival of the shear wave could be detected as the first wave to arrive using automatic triggering, which was done in this thesis.

The length of the sample was entered on the touchscreen of the Pundit 200 before testing. That way the apparatus could calculate the velocity as output instantly in addition to measuring the travel time of the pulses. After starting the test the received waves were immediately shown on the Pundit screen. The results could also be saved on the device and transferred to a computer. Figure 7.5 shows an example of a file that was stored and later displayed on a computer.

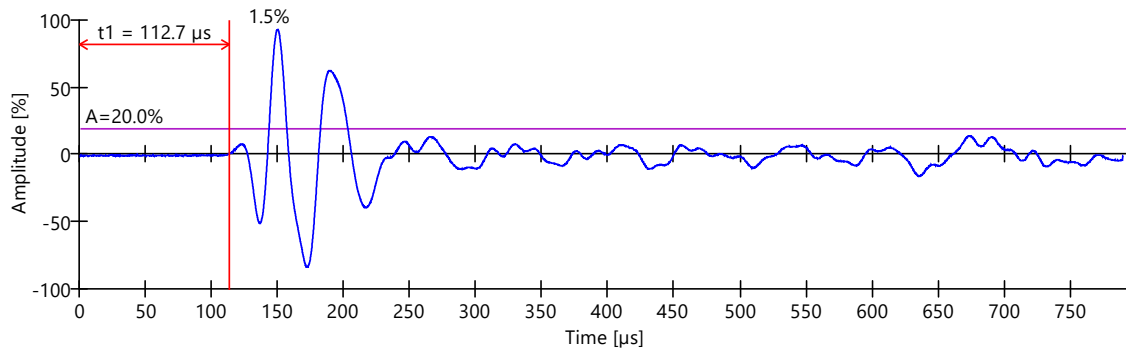


Figure 7.5: Example of a Pundit Proceq 200 file

### 7.3 Bender Element Testing

The bender element equipment used in this study consisted of GDS bender elements, a Data Acquisition (DAQ) device, a power supply, an amplifier, and a computer with software to control the testing. The bender elements had a width of around 2mm, a length of 12 mm, and a height of around 2,5 mm. The bender elements were integrated into a triaxial cell. For this study, however, the bender element tests were performed unconfined. This is usually what is done for stabilized soils (Di Sante et al., 2022).

The DAQ unit had a sampling rate of 200 kHz, which corresponds to a sampling interval of 5  $\mu$ s. The bender elements could generate sinusoidal pulses with a maximum amplitude of  $\pm 10$  V. The input frequency was limited by an amplifier at around 50 kHz. However, when the frequency increased fewer data points could be generated and the signals became weaker. The LabVIEW software was used to control the test and visualize the results while testing. In the LabVIEW software, the input frequency and amplitude could be controlled while testing. When performing the bender element tests, the received signal was immediately shown in the LabVIEW software, and the peak-to-peak travel time [ms] and shear wave velocity [m/s] were calculated. The output data could also be stored as text files in order to analyze it in other softwares such as Microsoft Excel or Python.

#### 7.3.1 Preparation of Samples for the Bender Element Test

The stabilized Tiller-Flotten peat and Onsøy soft clay samples with lower binder contents were soft enough to be directly placed onto the bender elements in the same way as for regular clay samples. This was not possible for the stiffer stabilized Tiller-Flotten quick clay and Onsøy soft clay samples with a higher binder content. In order to place these samples onto the bender elements, a slot with dimensions 4x14x4 mm in width, length, and height was carved on each side of the sample. These dimensions were slightly larger than the bender element dimensions. The slots were filled with fast-setting gypsum in order to ensure full contact between the bender elements and the samples. This is shown to give similar results as with the use of exact cut slots, as mentioned in section 4.2.5. A crib with dimensions to fit our 108x54 mm samples was made in the lab, together with two metal sheets with cut-out dimensions of 4x14 mm in



width and length. The creation of this crib was inspired by the study by Lindh (2016). The use of this crib ensured that the slots were always cut in the center of the sample and with the proper dimensions. The crib and carving process is shown in Figure 7.6.

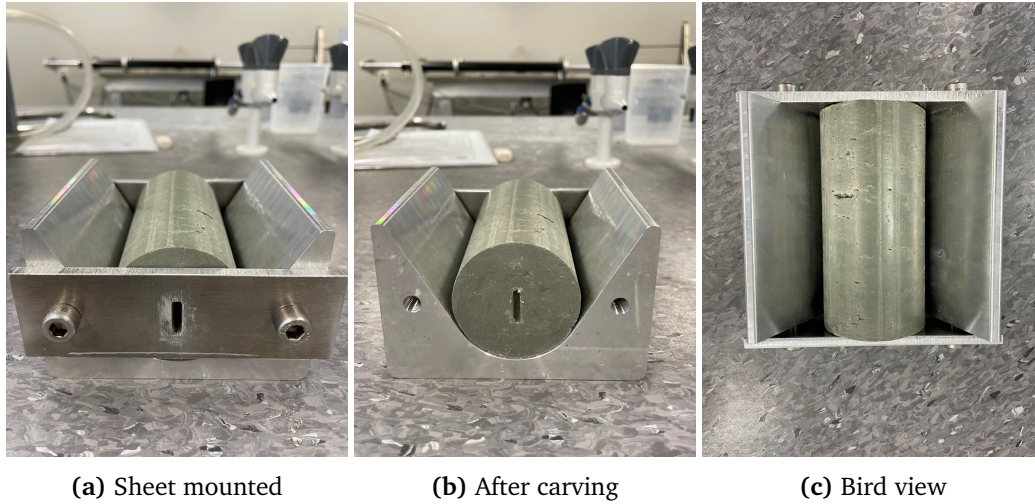


**Figure 7.6:** Used setup for carving slots in samples, made by the laboratory at NTNU

The slots were then filled with fast-setting hobby gypsum, from Panduro<sup>®</sup> (2023), as shown in Figure 7.7. After placing gypsum in the slots, the sample was placed on the bender elements. The gypsum was then left to harden for 5 minutes in order to ensure that the gypsum was stiff enough before testing. After 5 minutes of curing the bender element test was performed.

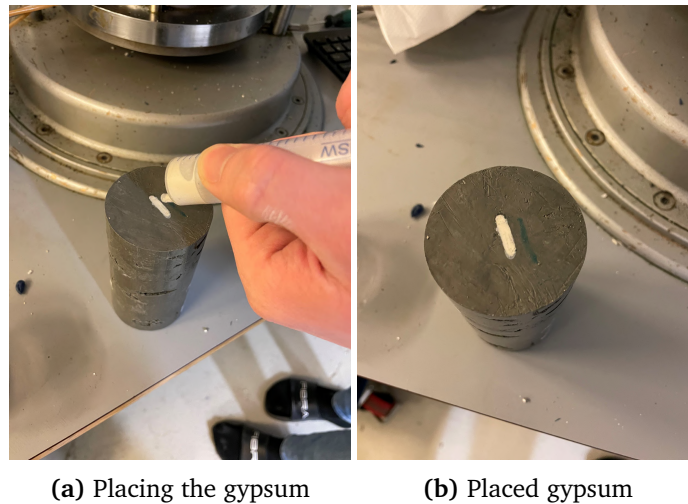


**Figure 7.7:** Process of filling carved slots with gypsum

All of the tests were performed unconfined. An illustration of the different stabilized soil types in the bender element setup is given in Figure 7.8.

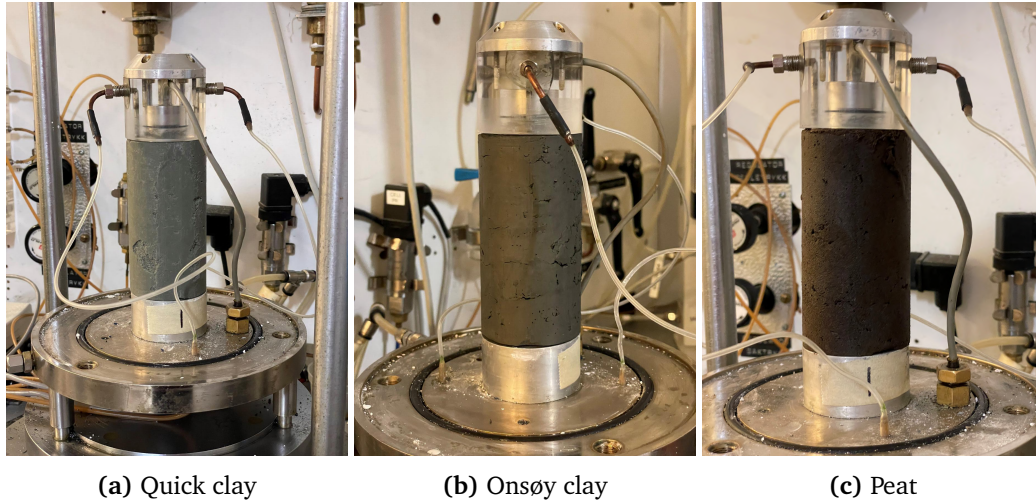


**Figure 7.8:** Setup of bender element testing, with the three different types of stabilized soil

### 7.3.2 Procedure for Testing

After putting a sample on the bender elements, shear waves were transmitted through the sample. The applied voltage was set to either 5 or 10 V for all samples. For each sample, several tests were performed, each with a different frequency. The purpose of doing this was to find the frequency where the received signal had a good match with the sent signal and to see if the measured shear wave velocity was stable for the different frequencies. For each sample, approximately 10 different frequencies were used. The first test was performed with a low frequency, and then the frequency was increased for each test. The data was saved and later analyzed in Python. Figure 7.9 shows the procedure of testing with different frequencies. The tests for the sample in this figure shows that a frequency between 0,5 and 1 kHz seems to give the best match between the sent and received signal. The figure also illustrates how the measured shear wave velocity stabilizes somewhat when the frequency increases. The shear wave velocity,  $v_s$ , was then calculated using the peak-to-peak travel time and the tip-to-tip travel distance with the formula in Equation 7.1:

$$v_s = \frac{L_{tt}}{\Delta t} \quad (7.1)$$

For some of the tests, there was more than just one peak in the received signal. In those cases, the first major peak was chosen. This is further discussed in Chapter 9.

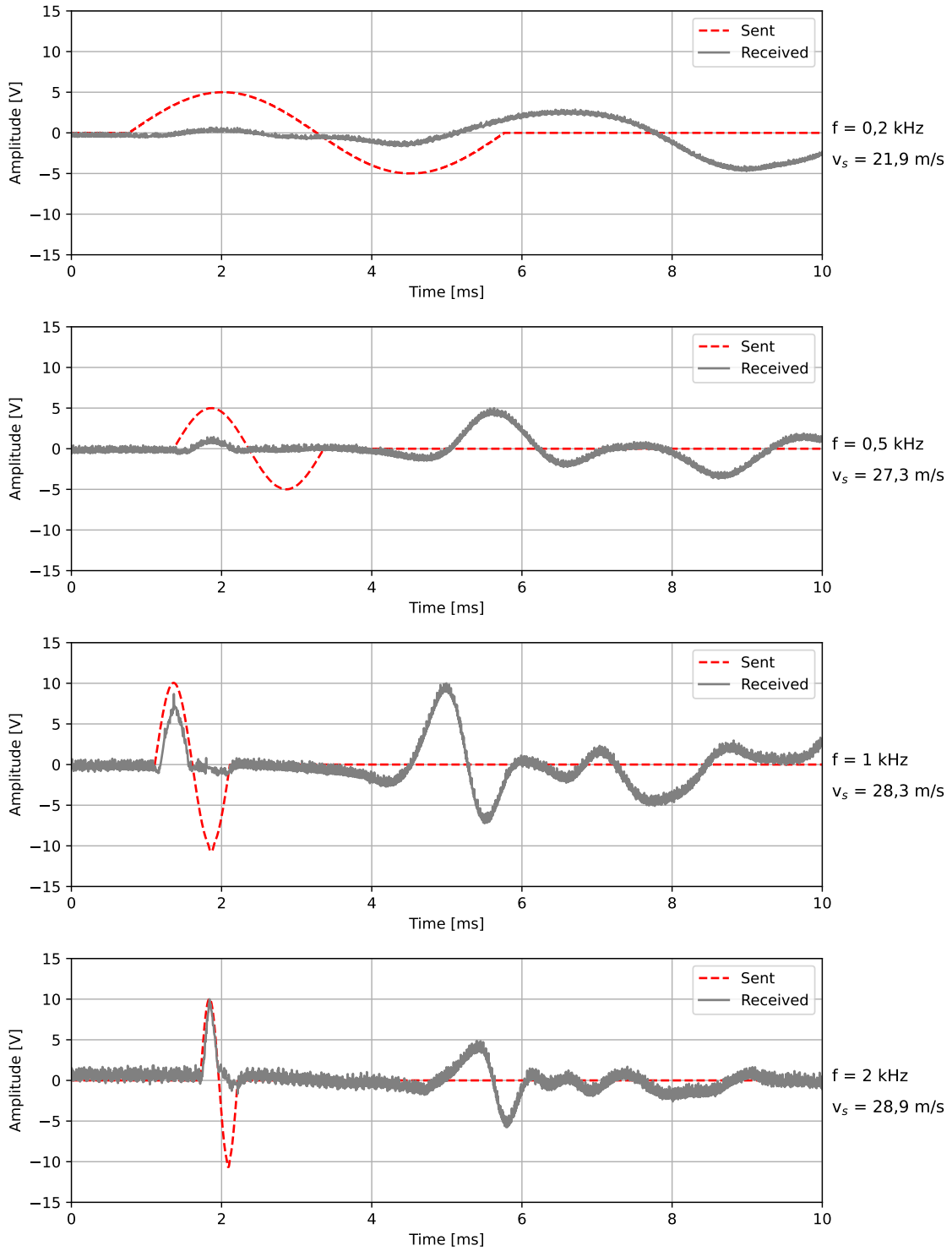


**Figure 7.9:** Procedure of performing bender element tests with several different frequencies in order to calculate the shear wave velocity

## 7.4 Electrical Resistivity Testing

A simple two-electrode setup to measure resistivity was created for this study. An overview of the setup is shown in Figure 7.10. The equipment used was two circular electrodes with 54 mm diameter, two multimeters serving as voltmeter and ammeter, and a conducting gel. AC current and a frequency of 50 Hz were used for the testing. All the tests were performed at room temperature of around  $22 \pm 2$  °C.

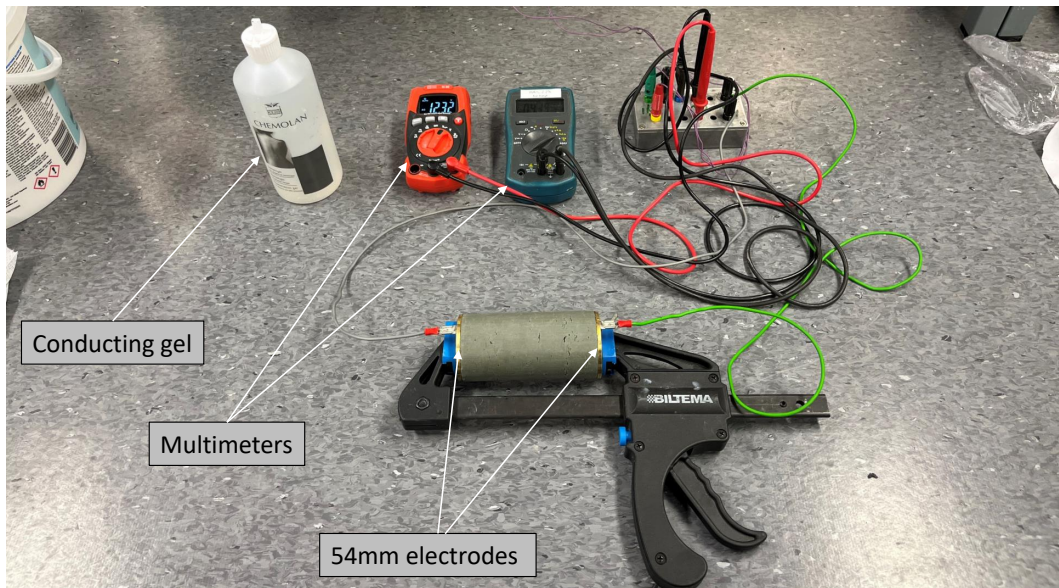


**Figure 7.10:** Overview of the resistivity test setup that was used in this study

The tests were performed by putting a thin layer of conducting gel on both electrodes. The electrodes were then put on each side of the sample and pushed onto the sample with slight pressure. This was done to minimize the contact resistance between the electrodes and the sample. For the resistivity tests in this study, the voltage was not kept constant. The system was connected to a power outlet and the ampere and voltage could be read from the multimeters. The resistivity was then calculated using Equation 7.2:

$$\rho = \frac{\Delta U A}{I L} \quad (7.2)$$

## 7.5 Uniaxial Testing

After completing Pundit-, Resistivity- and for some samples Bender Element-testing, all samples were tested in the uniaxial compression test. All uniaxial tests followed the standardized procedure described in *R210 Laboratorieundersøkelser* from Statens Vegvesen (2016) with some modifications to adapt to the small changes in sample dimensions. Pictures from the uniaxial process are shown in Figure 7.11.



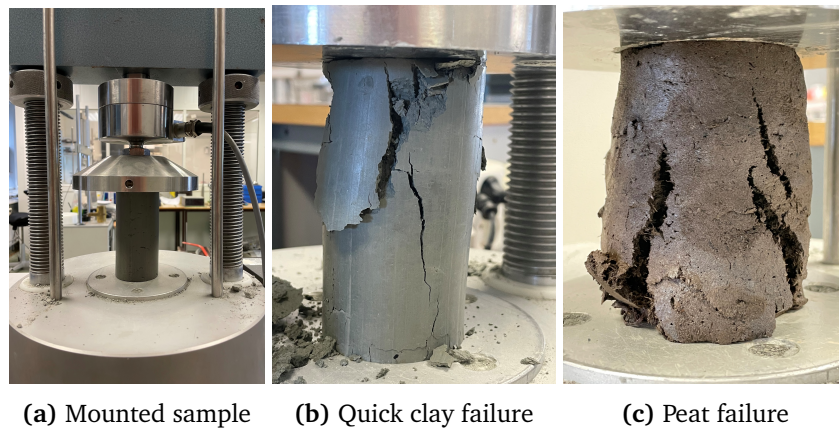


**Figure 7.11:** Setup of the uniaxial test, with sample before test and failure lines after testing

Figures 7.11b and 7.11c show the failure lines for two specific samples following ended uniaxial testing. Raw data from the testing was exported to an Excel sheet to interpret the results. The surface area of the sample [ $\text{mm}^2$ ], force [N], and deformation [mm] from the raw data were used to calculate the axial strain  $\epsilon$  [%], axial stress,  $\sigma_1$  [kPa] and shear stress  $\tau$  [kPa], according to the mentioned standardized procedure (Statens Vegvesen, 2016). Axial- strain and stress were plotted to interpret  $q_{uf}$ ,  $\tau_{max}$  and  $E_{50}$ , as demonstrated in Figure 7.12

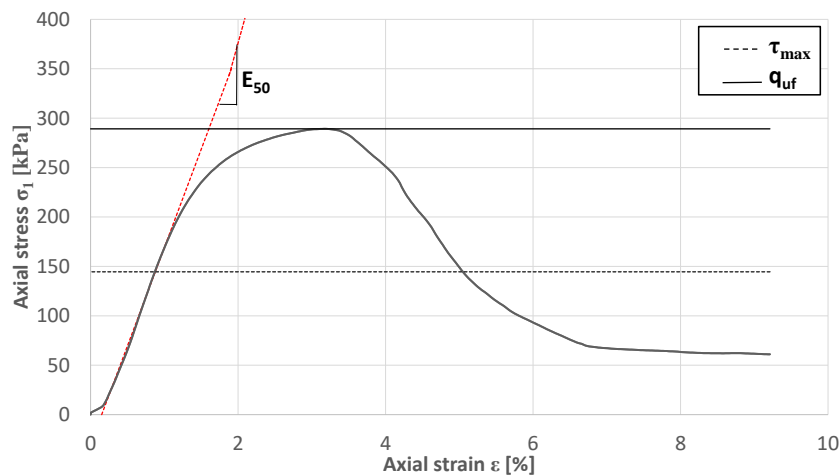


**Figure 7.12:** Example of interpretation from uniaxial test

## 7.6 Index Testing

Index testing is an important part of classifying the soil and its mechanical properties. Only index tests of relevance to the stabilized samples, which did not demand much effort and time, were conducted in this study. These tests were measurements of:

- Density
- Water content

### 7.6.1 Density

To determine the density of the stabilized soil, testing was performed according to the standard ISO 17892-2 (Statens Vegvesen, 2016).

The density for all samples was calculated as given in Equation 7.3.

$$\rho = \frac{m_s}{V} \quad [g/cm^3] \quad (7.3)$$

### 7.6.2 Water Content

To determine the water content of the stabilized soil, testing was performed according to the standard ISO 17892-1 (Statens Vegvesen, 2016).

After performing uniaxial testing, a small portion of the fractured sample was collected and weighed, before being placed in a heating cabinet for 24 hours. The heating cabinet holds a temperature of  $110 \pm 5$  °C. Dry weight was then measured, and the water content was calculated with Equation 7.4:

$$w = \frac{m_1 - m_2}{m_2 - m_c} \cdot 100\% = \frac{m_w}{m_d} \cdot 100\% \quad [\%] \quad (7.4)$$

# Chapter 8

## Results

This chapter gives a presentation of the test results. Discussions and interpretations around the results are given in detail in Chapter 9. All samples with pictures and results from tests conducted after 28 days are given in Appendix A.

### 8.1 Variation of Wave Velocities over Time

The variation of wave velocities over time is presented in this section. The P-wave and S-wave velocities were measured on all samples after 3, 7, 14, 21, and 28 days of curing with the Pundit test. For some samples, however, the measurements started after 7 days of curing instead of 3 days. This was due to the sample not being strong enough on day 3, and therefore not ready for extrusion and testing.

#### 8.1.1 P-wave Velocity Variation over Time

P-wave velocities versus time for the stabilized quick clay samples from Tiller-Flotten and the stabilized soft clay samples from Onsøy are presented in Figure 8.1 and Figure 8.2 respectively. P-wave velocity versus time for the peat samples was not possible to measure with the Pundit apparatus, and results for peat are therefore not shown.

### Quick clay (Tiller-Flotten)

The results from measuring P-wave velocities over time on stabilized Tiller-Flotten quick clay generally show an increasing trend for all binder- combinations and quantities. A rough estimate shows that on average, it is an approximate 40% increase of the P-wave velocity between the first and last measurement, considering all measurements in Figure 8.1.

The results show that for both LS1 and BA samples, the velocity increases as the total binder amount increases, whereas for the BC1 samples, the highest binder amount gave the lowest velocity throughout the entire period.

The results also show that all results vary in the same order of magnitude, except for the samples mixed with PSA, where values are a bit lower. Considering every type of binder combination and quantity, except the ones with PSA, the measurements after 3- and 28 days of curing, respectively, vary from approximately 750 - 1400 m/s to 900 - 1600 m/s. Whereas PSA samples vary from approximately 250 - 450 m/s to 400 - 800 m/s looking at the first and last measurement.

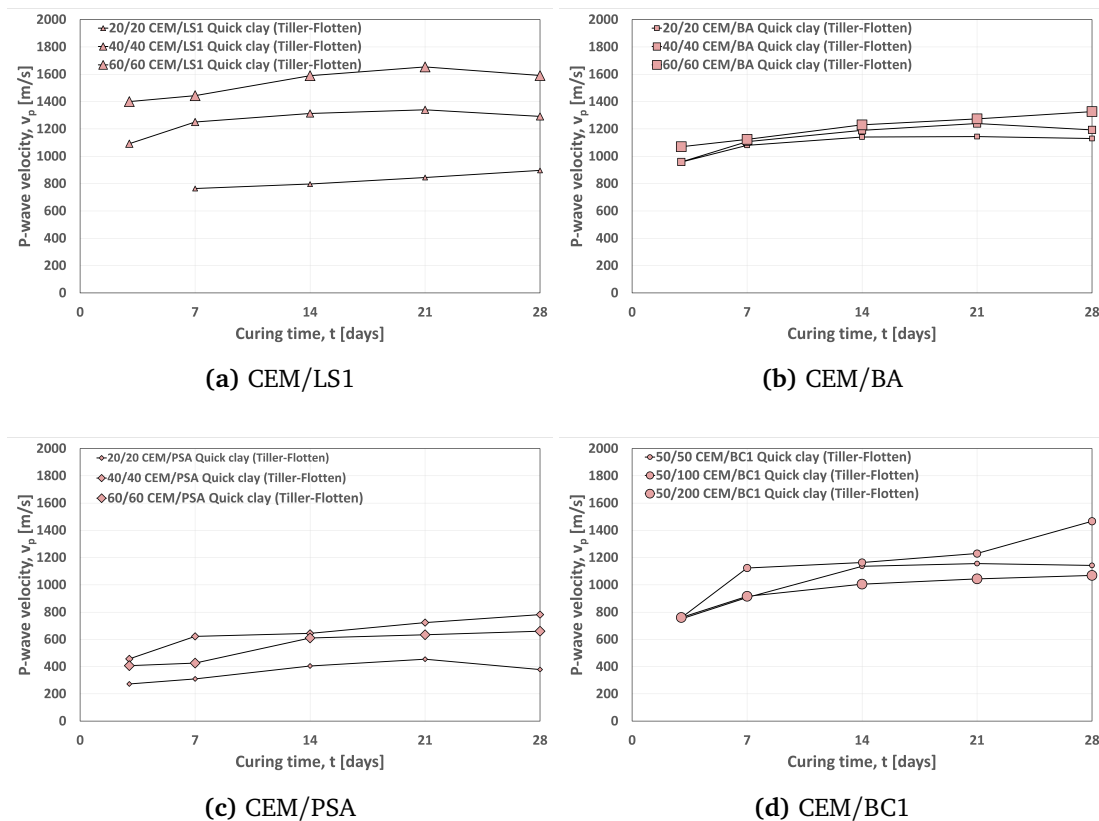


**Figure 8.1:** P-wave velocity variation over time for quick clay (Tiller-Flotten) with binder combinations: (a) CEM/LS1, (b) CEM/BA, (c) CEM/PSA and (d) CEM/BC1



**Soft clay (Onsøy)**

Results of the P-wave velocity of stabilized Onsøy soft clay generally show an increasing trend for all binder- combinations, and quantities between the first and last reading, with scattering tendencies in between. The results are shown in Figure 8.2.

For the majority of the soft clay samples, the use of the Pundit apparatus for measuring P-wave velocity started on day 7. Before this, the apparatus wouldn't give any readings. There are some exceptions, and Figure 8.2 shows all measurements from 3 days give approximately the same velocity, around 300 m/s. The majority of the remaining samples often started around this value for their first reading, and usually increased over time, while some remained around 300 m/s throughout the testing period. A few samples gave readings from around 800 m/s on their first reading but did not further increase as much.

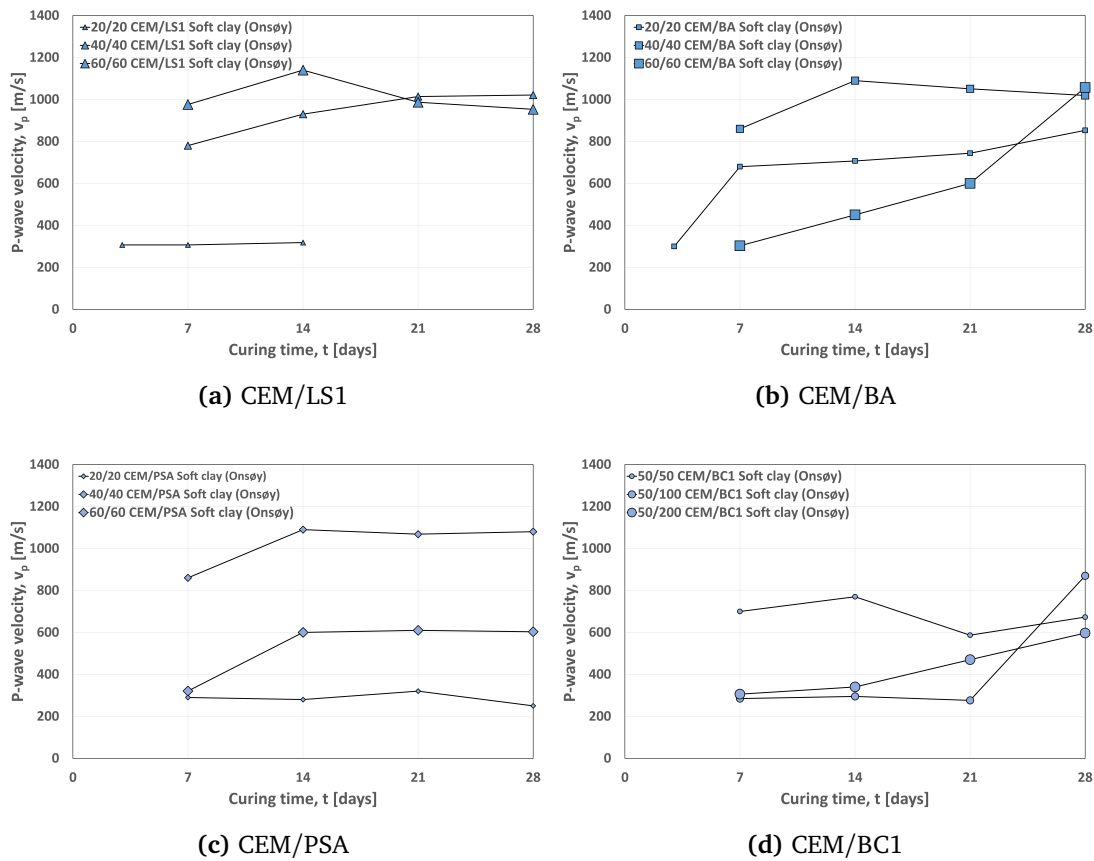


**Figure 8.2:** P-wave velocity variation over time for soft clay (Onsøy) with binder combinations: (a) CEM/LS1, (b) CEM/BA, (c) CEM/PSA and (d) CEM/BC1

### 8.1.2 Shear Wave Velocity Development over Time

Shear wave velocities over time for respectively the quick clay from Tiller-Flotten and the soft clay from Onsøy, are presented in Figure 8.3 and Figure 8.4. For the stabilized Tiller-Flotten peat samples, no shear wave velocities were obtained.

#### Quick clay (Tiller-Flotten)

The results from measuring shear wave velocities over time on stabilized Tiller-Flotten quick clay generally show an increasing trend for all binder- combinations, and total binder quantities. A rough estimate shows that on average, it is an approximate 40% increase of the shear wave velocity between the first and last measurement, considering all measurements in Figure 8.3.

The results in Figure 8.3 show similar variations for the different binder ratios for all binder combinations, except the CEM/LS1 combination. The LS1 samples exhibit larger leaps between their own respective binder ratios.

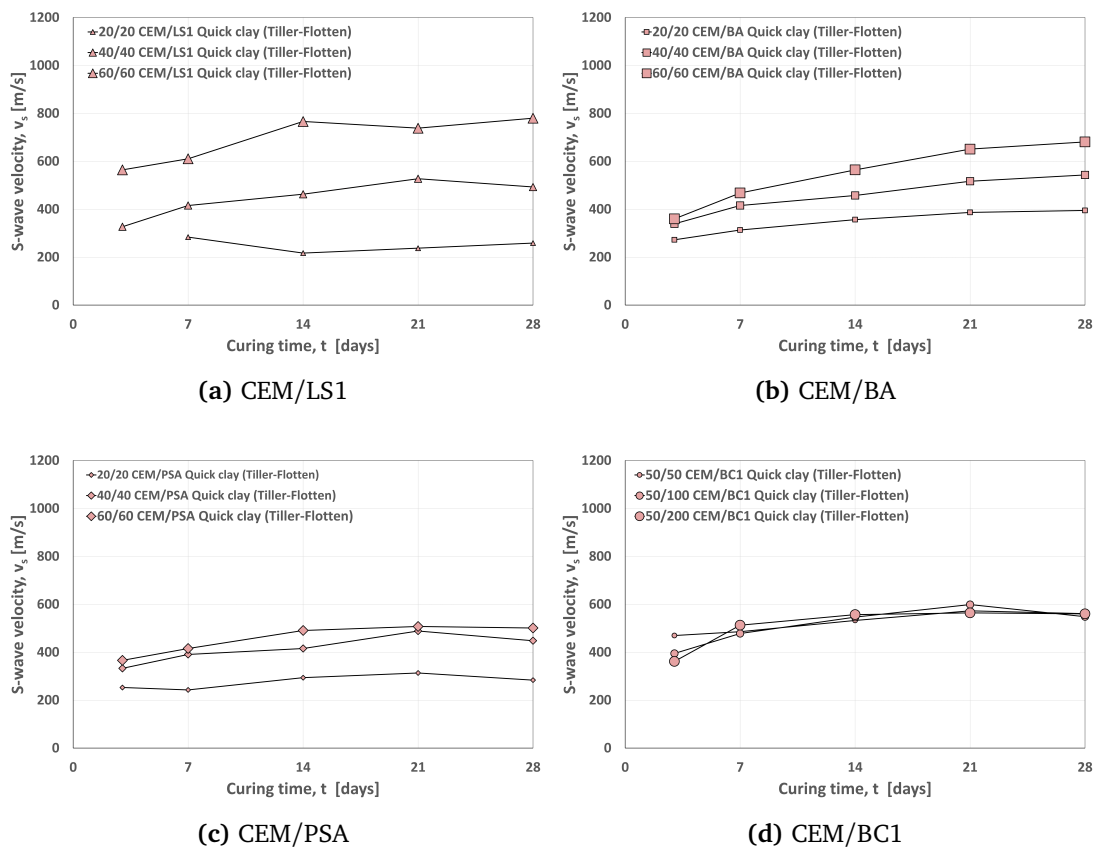


**Figure 8.3:** Shear wave velocity variation over time for quick clay (Tiller-Flotten) with binder combinations: (a) CEM/LS1, (b) CEM/BA, (c) CEM/PSA and (d) CEM/BC1

**Soft clay (Onsøy)**

The results from shear wave velocities for stabilized Onsøy soft clay samples are influenced by the Pundit device’s lack of ability to give readings for shear wave velocities below 200 m/s, which is discussed further in Chapter 9. Nevertheless, the gathered results are shown in Figure 8.4 generally show an increasing trend over time, with a single exception in the 50/100 CEM/BC1 sample.

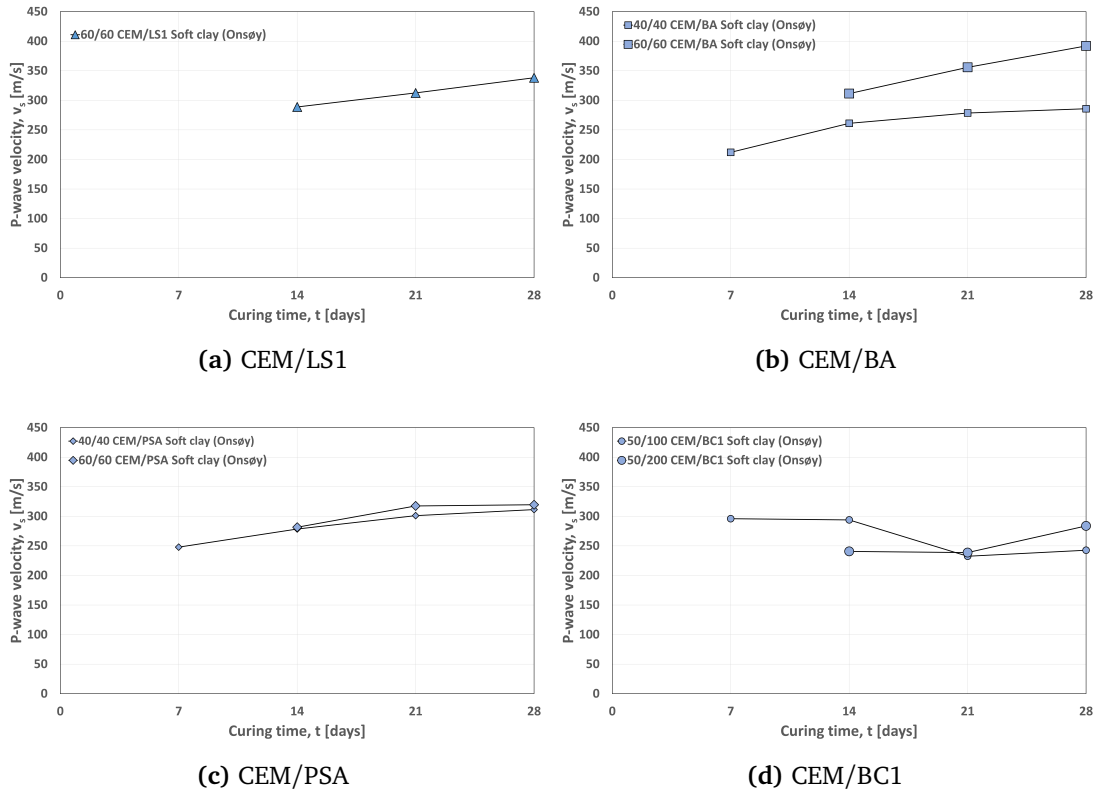


**Figure 8.4:** Shear wave velocity variation over time for soft clay (Onsøy) with binder combinations: (a) CEM/LS1, (b) CEM/BA, (c) CEM/PSA and (d) CEM/BC1

## 8.2 Development of Electrical Resistivity over Time

This section presents the results of the electrical resistivity variations over time for the samples. The measured variations over time for the quick clay from Tiller-Flotten, soft clay from Onsøy, and the peat from Tiller-Flotten are shown in respectively Figure 8.5, Figure 8.6 and Figure 8.7.

### Quick clay (Tiller-Flotten)

The results from measuring electrical resistivity over time on stabilized Tiller-Flotten quick clay generally show an increasing trend for all binder- combinations, and quantities. A rough estimate shows that on average, it is an approximate 75% increase of the electrical resistivity between the first and last measurement, considering all measurements in Figure 8.5. However, the resistivity did not consistently increase for each time increment. Some results show that some of the time increment readings gave a drop in electrical resistivity. Some of the results show that samples with the largest amount of binders are the ones with the lowest resistivity. Overall, after 3 days the electrical resistivity ranges approximately between 4 - 10  $\Omega\text{m}$ , while after 28 days of curing it ranges approximately between 13-24  $\Omega\text{m}$ . The exception is the CEM/BA combination, which gave lower values throughout.

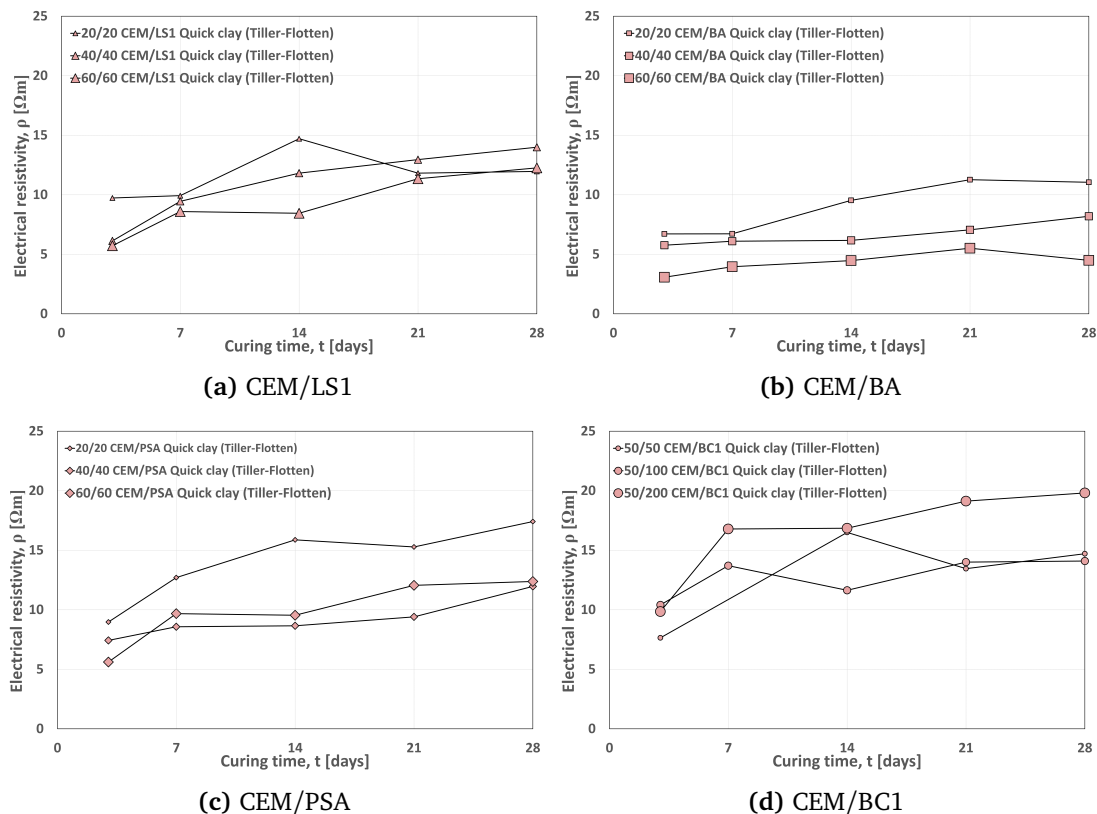


**Figure 8.5:** Electrical resistivity variation over time for quick clay (Tiller-Flotten) with binder combinations: (a) CEM/LS1, (b) CEM/BA, (c) CEM/PSA and (d) CEM/BC1

### Soft clay (Onsøy)

Figure 8.6 indicates that the majority of results from measuring electrical resistivity over time on stabilized Onsøy soft clay shows a general increase for all samples, including all different binder- combinations, and quantities, between day 3 and day 21. All results dip between day 21 to day 28.

The results in Figure 8.6 show that in almost every case, the samples with the highest amount of binder, have the highest electrical resistivity, except the samples mixed with BC1.

Overall, after 3 days the electrical resistivity ranges approximately between 1 - 1,5  $\Omega\text{m}$ , while after 28 days of curing it ranges approximately between 1,2 - 2,4  $\Omega\text{m}$ . The highest measured value are around 3,5  $\Omega\text{m}$  on day 21 of curing for the CEM/PSA combination, before dropping significantly to below 2,5  $\Omega\text{m}$  on day 28 of curing.

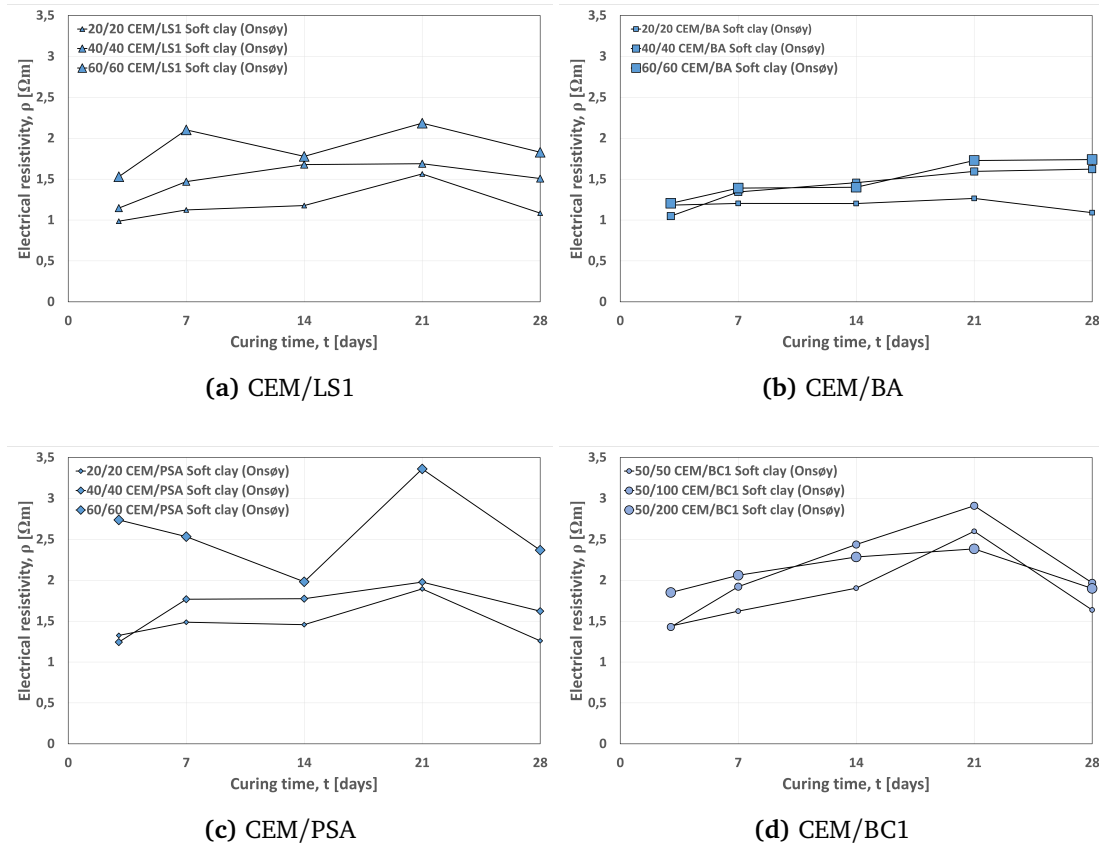


**Figure 8.6:** Electrical resistivity variation over time for soft clay (Onsøy) with binder combinations: (a) CEM/LS1, (b) CEM/BA, (c) CEM/PSA and (d) CEM/BC1

### Peat (Tiller-Flotten)

Figure 8.7 indicates that the majority of results in electrical resistivity over time on stabilized Tiller-Flotten peat shows no clear either increase or decrease in measured electrical resistivity. The only tendency of an increasing electrical resistivity is for the high binder amount imprinted CEM/BC4 samples.

The results show that for the CEM/BA and CEM/PSA samples, there is no significant difference in regard to binder ratios. These sorts of differences are some degree present in the CEM/LS1 and CEM/BC4 samples.

Overall, after 3 days the electrical resistivity ranges approximately between 1,5 - 3,5  $\Omega\text{m}$ , while after 28 days of curing it ranges approximately between 2 - 6  $\Omega\text{m}$ . The exception is the CEM/BA combination, which gave lower values throughout.

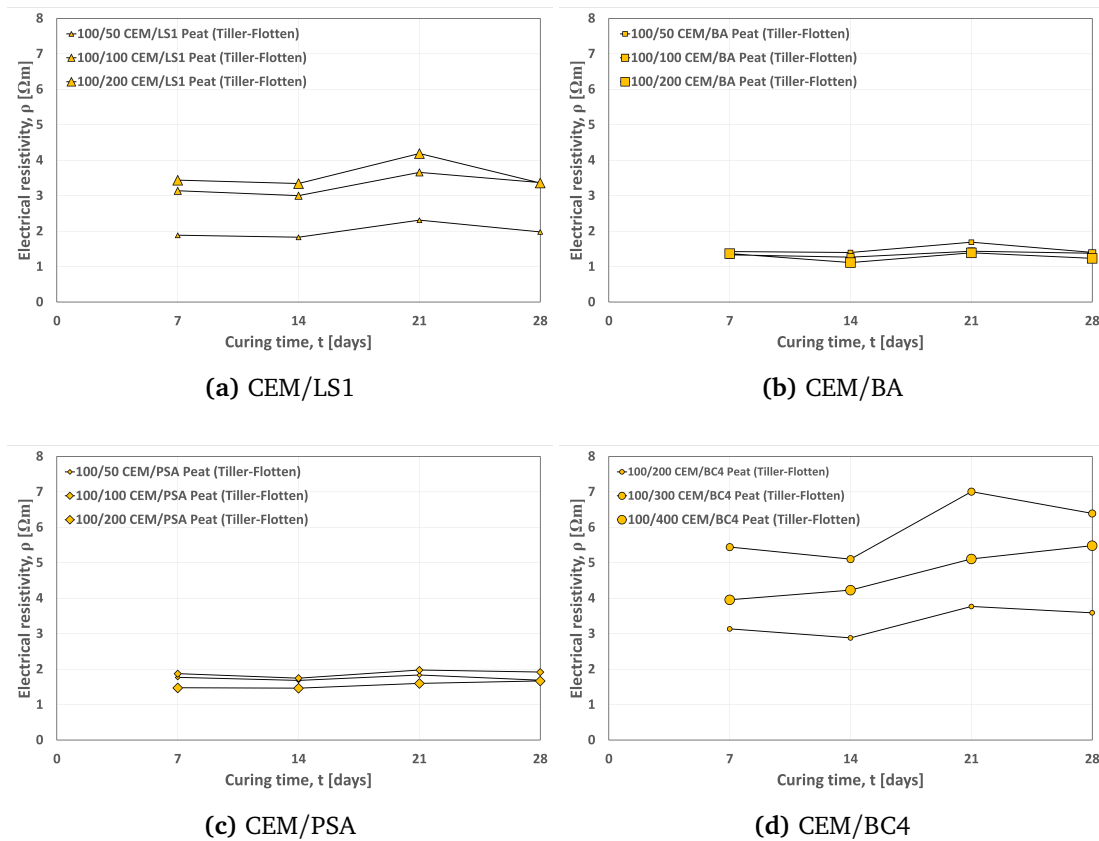


**Figure 8.7:** Electrical resistivity variation over time for peat (Tiller-Flotten) with binder combinations: (a) CEM/LS1, (b) CEM/BA, (c) CEM/PSA and (d) CEM/BC4

### 8.3 Wave Velocities vs. Strength and Stiffness

After 28 days of curing the P-wave and S-wave velocities were measured for all samples. These velocities are plotted against the unconfined compressive strength,  $q_{uf}$ , and secant stiffness,  $E_{50}$  in order to study potential correlations.

#### 8.3.1 P-wave Velocity vs. Strength and Stiffness

Figure 8.8 shows the P-wave velocity from the Pundit test versus the unconfined compressive strength,  $q_{uf}$  and secant stiffness,  $E_{50}$  for the Tiller-Flotten quick clay and Onsøy soft clay samples. Not all the samples are shown in this plot as it was chosen to filter out some values where it was obvious during testing that the results were not reliable.

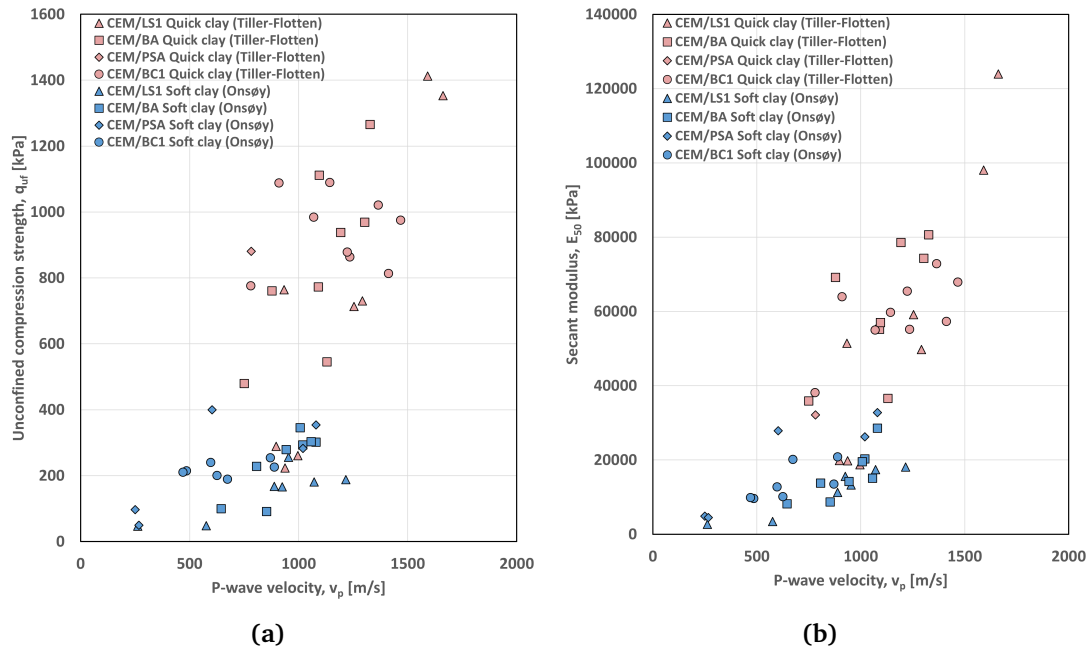


**Figure 8.8:** P-wave velocity versus: (a) unconfined compressive strength,  $q_{uf}$  and (b) secant modulus,  $E_{50}$

In general, the results in Figure 8.8 show a correlation between increasing P-wave velocity with an increasing unconfined compressive strength and increasing secant modulus for both the stabilized quick- and soft clay samples. The stabilized Tiller-Flotten quick clay samples have in general higher strength and stiffness compared to the stabilized Onsøy soft clay samples. The differences in the range of P-wave velocities between the two soil types are less significant.

The P-wave velocity for the stabilized peat samples was relatively large compared to the stabilized quick- and soft clay samples and therefore the peat values are shown in a separate plot in Figure 8.9. The results show no clear correlation between  $v_p$  and  $q_{uf}$  for stabilized Tiller-Flotten peat. All measured P-wave velocities are approximately around 1500 m/s.

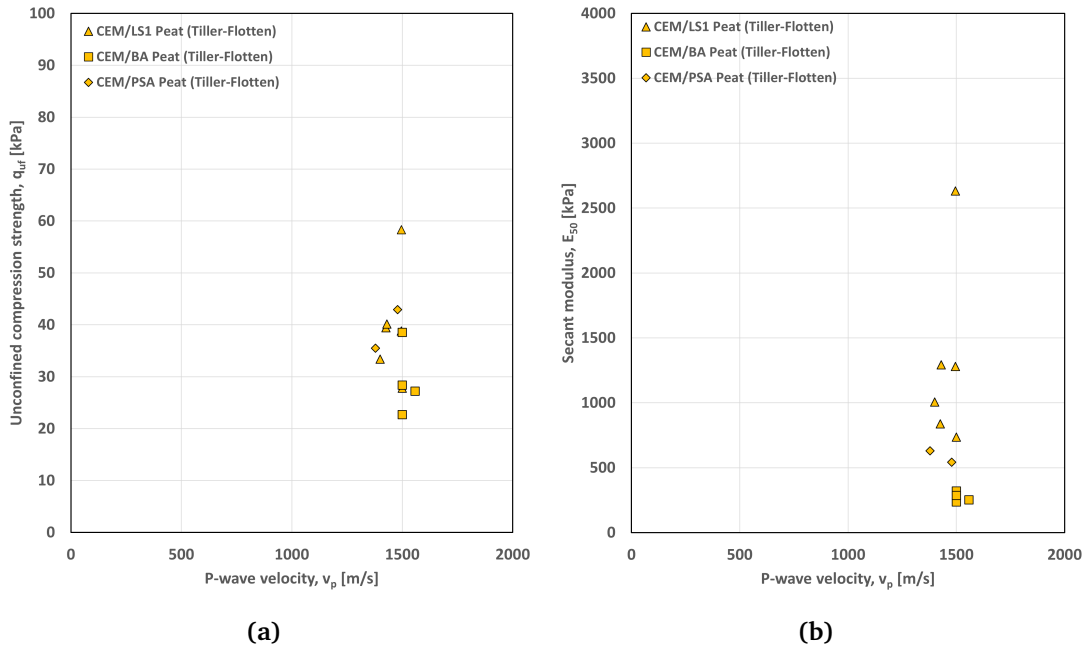


**Figure 8.9:** P-wave velocity versus: **(a)** unconfined compressive strength,  $q_{uf}$  and **(b)** secant modulus,  $E_{50}$

In general, the results of the measured unconfined compressive strength,  $q_{uf}$ , and secant modulus,  $E_{50}$ , in Figure 8.9 shows that it is the CEM/LS1 binder combination often having the highest strength and stiffness. It was the CEM/BA binder combination that often gave the lowest strength and stiffness.



### 8.3.2 Shear Wave Velocity vs. Strength and Stiffness

#### Pundit Measurements

The shear wave velocities measured with the Pundit test after 28 days of curing are shown in Figure 8.10 versus unconfined compressive strength,  $q_{uf}$  and secant stiffness,  $E_{50}$ . Shear wave velocity measurements with the Pundit device were only obtained for the quick clay samples and most of the Onsøy clay samples. The peat samples gave no results using this method. Shear wave velocities below around 200 m/s could not be measured with the Pundit device and the reason for this is discussed in Chapter 9.

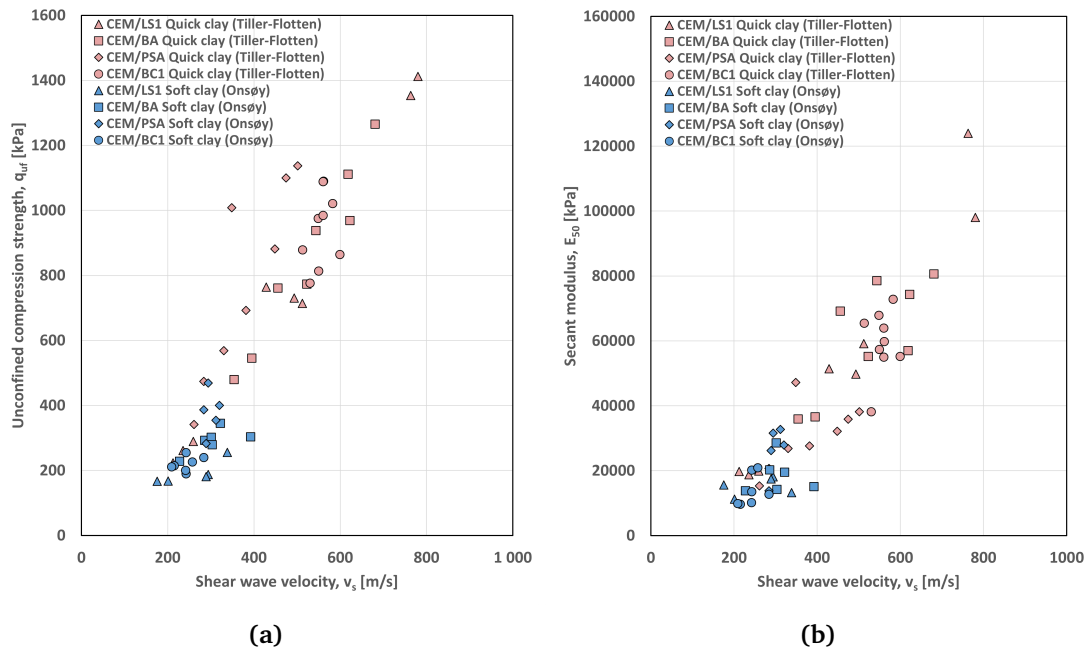


**Figure 8.10:** Shear wave velocity from Pundit tests versus: **(a)** unconfined compressive strength,  $q_{uf}$  and **(b)** secant modulus,  $E_{50}$

In general, the results in Figure 8.10 show a correlation between increasing shear wave velocity with an increasing unconfined compressive strength and increasing secant modulus for both the stabilized quick- and soft clay samples. The stabilized Tiller-Flotten quick clay samples have in general higher strength and stiffness compared to the stabilized Onsøy soft clay samples. The stabilized quick clay samples have a wider range of shear wave velocities compared to the stabilized soft clay samples.

### Bender Element Measurements

The results from the bender element tests are shown in Figure 8.11, where shear wave velocity is plotted versus unconfined compressive strength,  $q_{uf}$  and secant stiffness,  $E_{50}$ . The bender element equipment at the NTNU laboratory could not get proper measurements for the samples with larger shear wave velocities than around 200 m/s, which is the reason why no measurements for stabilized quick clay samples are presented. This is further discussed in Chapter 9.

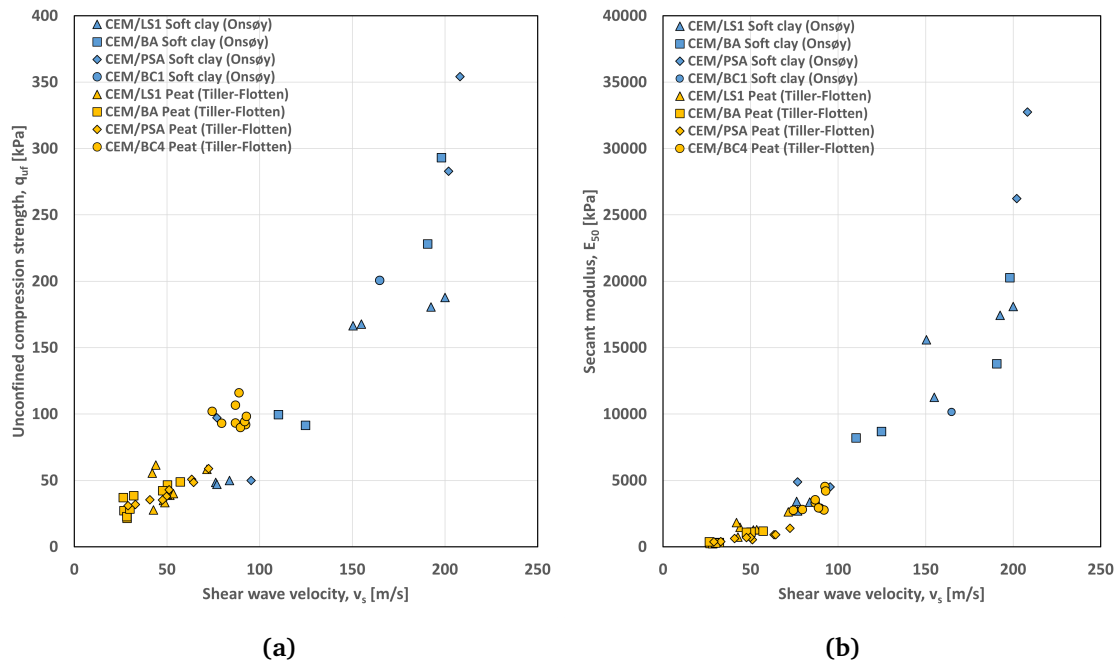
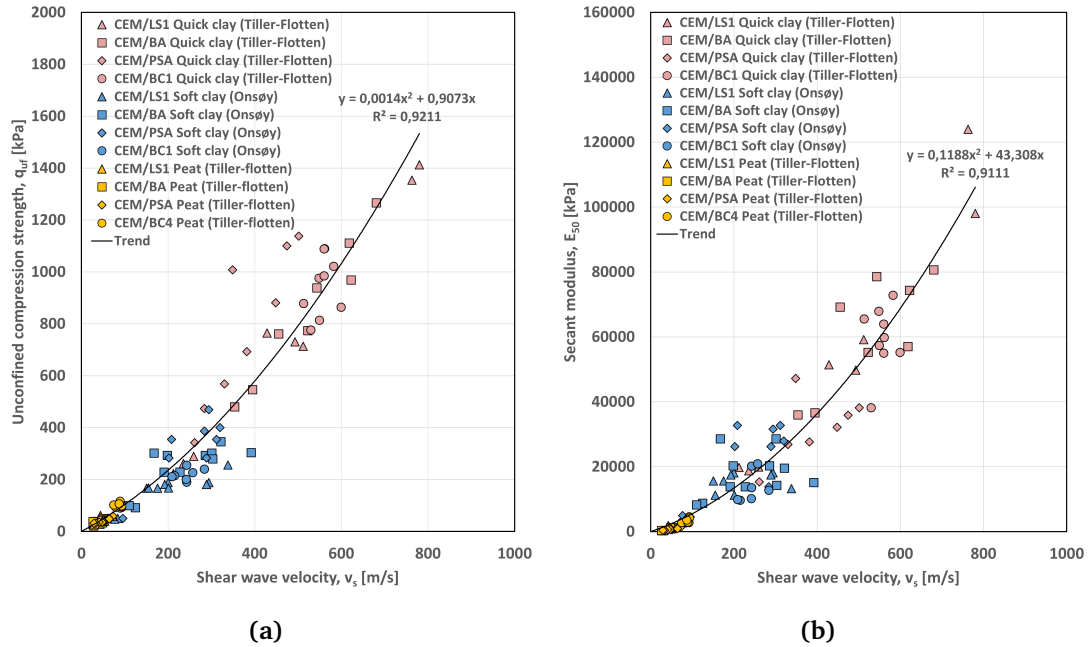


**Figure 8.11:** Shear wave velocity from bender element tests versus: (a) unconfined compressive strength,  $q_{uf}$  and (b) secant modulus,  $E_{50}$

In general, the results in Figure 8.11 show a correlation between increasing shear wave velocity with an increasing unconfined compressive strength and increasing secant modulus for both the stabilized soft clay and peat samples. The stabilized Onsøy soft clay samples have in general higher strength and stiffness compared to the stabilized Tiller-Flotten peat samples. A scattering of results is more apparent for the stabilized soft clay samples compared to the stabilized peat samples.

### Shear Wave Velocities from Bender Elements and Pundit Combined

The results from both the bender element tests and Pundit tests are shown in Figure 8.12. The trendline for all the measurements is plotted to investigate the correlation.



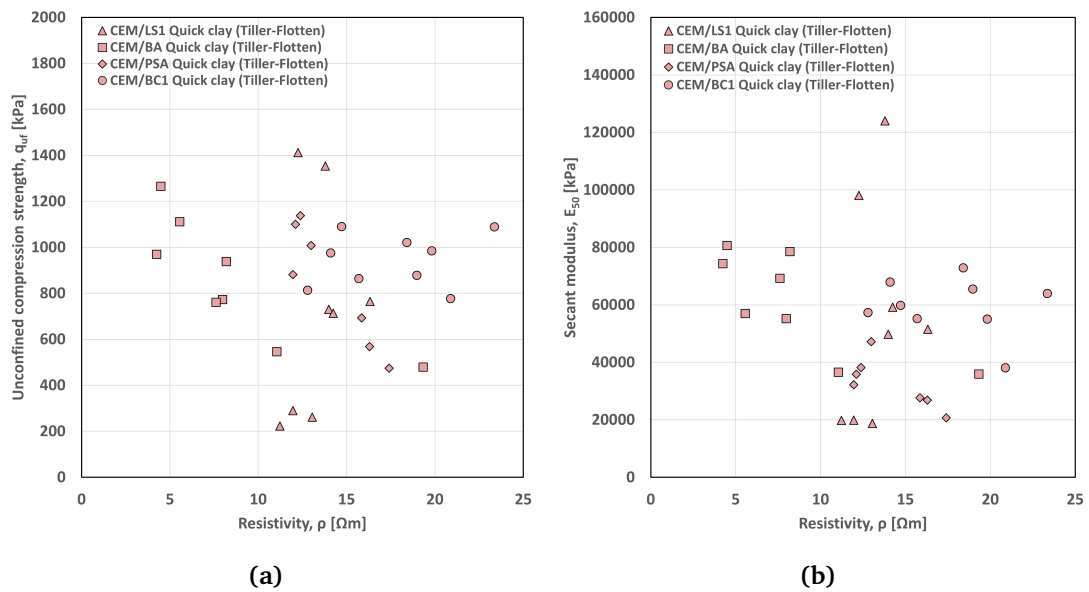
**Figure 8.12:** Shear wave velocity from Pundit and bender element tests versus: **(a)** unconfined compressive strength,  $q_{uf}$  and **(b)** secant modulus,  $E_{50}$

Figure 8.12 shows that all the different soil types follow the same trend. In Figure 8.12a the CEM/PSA binder combinations in stabilized quick clay give the most apparent deviations from the trend.

## 8.4 Electrical Resistivity vs. Strength and Stiffness

After 28 days of curing the electrical resistivity was measured for each sample. These values are plotted against the unconfined compressive strength,  $q_{uf}$ , and secant stiffness,  $E_{50}$  in order to study potential correlations. The results for Tiller-Flotten quick clay, Onsøy clay, and Tiller-Flotten peat are shown in Figure 8.13, Figure 8.14 and Figure 8.15 respectively.

### Quick clay (Tiller-Flotten)



**Figure 8.13:** Electrical resistivity versus: (a) unconfined compressive strength,  $q_{uf}$  and (b) secant modulus,  $E_{50}$

Figure 8.13 shows no indication of correlation between electrical resistivity,  $\rho$ , and neither unconfined compressive strength,  $q_{uf}$ , or secant modulus  $E_{50}$ .

**Soft clay (Onsøy)**

Figure 8.14 shows an increase in resistivity correlates with an increase in both strength and stiffness. Some scatter deviates from this trend.

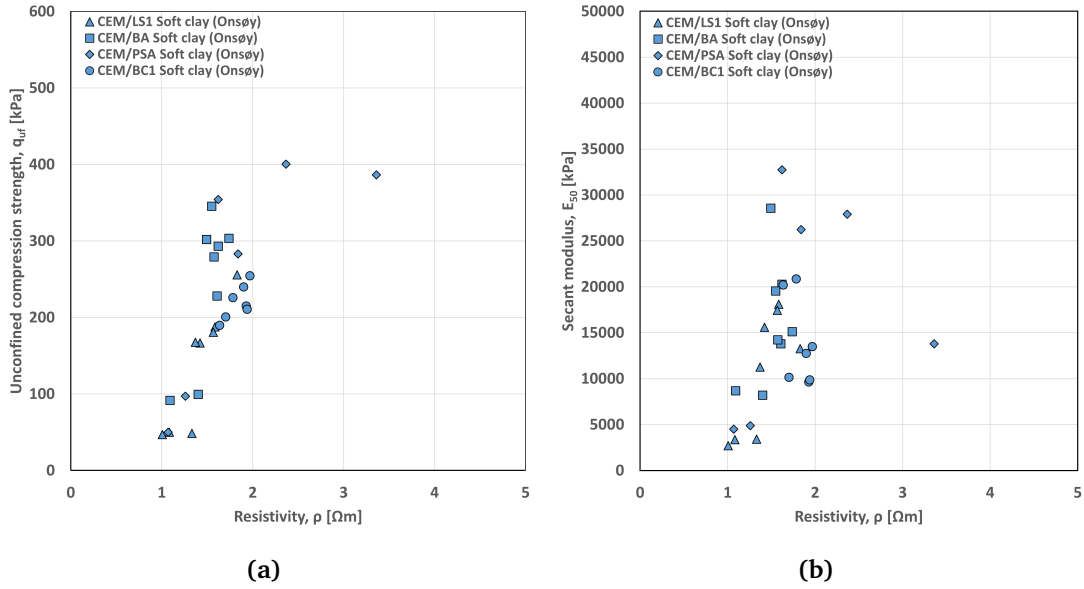


**Figure 8.14:** Electrical resistivity versus: **(a)** unconfined compressive strength,  $q_{uf}$  and **(b)** secant modulus,  $E_{50}$

### Peat (Tiller-Flotten)

Figure 8.15 shows clustering depending on the binder combination. For each specific binder, there is no particular correlation between the resistivity,  $\rho$ , and unconfined compressive strength,  $q_{uf}$ , or secant modulus  $E_{50}$ . For all the samples combined, there is a tendency where an increase in resistivity correlates with increasing strength and stiffness.

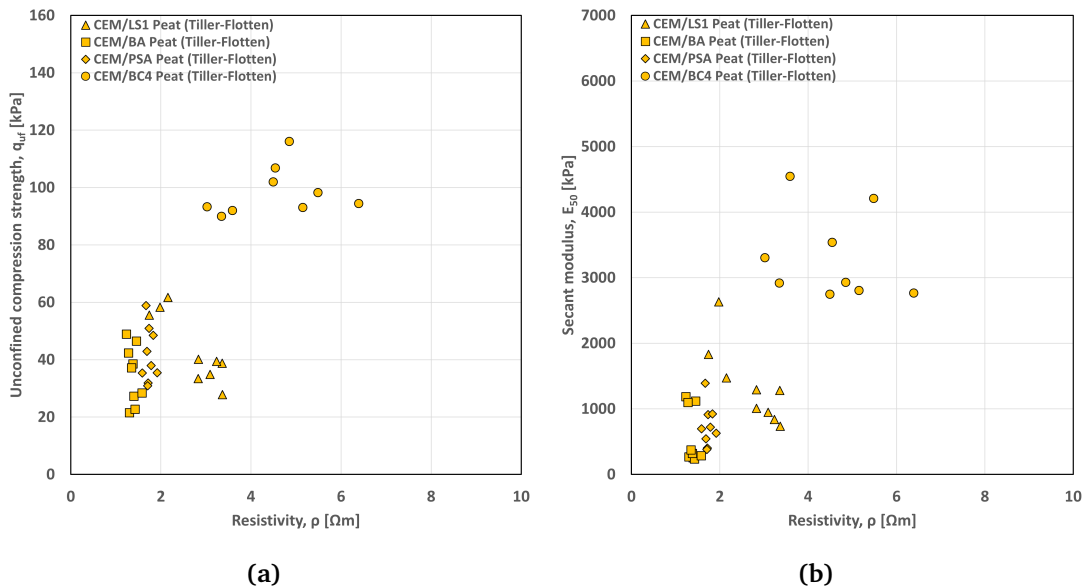


**Figure 8.15:** Electrical resistivity versus: (a) unconfined compressive strength,  $q_{uf}$  and (b) secant modulus,  $E_{50}$

## 8.5 Densities and Water Content of Stabilized Samples

The measured densities of all the stabilized samples are given in Appendix C. The results showed that the average density for stabilized Tiller-Flotten quick clay was  $1,81 \text{ g/cm}^3$ , while for stabilized Onsøy soft clay and Tiller-Flotten the averages were respectively  $1,61 \text{ g/cm}^3$  and  $1,15 \text{ g/cm}^3$ .

The measured water contents are given in Appendix D. In the plots each binder combination is plotted together, to see how the different binder ratios affect the water content. For the stabilized Tiller-Flotten quick clay, Onsøy soft clay, and Tiller-Flotten peat the average water content was respectively 36,9 %, 58,8%, and 246,7 % after 28 days of curing. The lowest ratios are furthest to the left, and the ratio increase towards the right. The results show that all binder combinations for every soil type vary around the same value, except the biochar ones, which tend to be a little lower.

# Chapter 9

## Discussion

In this chapter, the method and results presented in Chapter 7 and Chapter 8 are discussed. The discussions include the results themselves and also the uncertainties and limitations of the methods used in the laboratory.

### 9.1 Handling and Preparation of Samples

This section discusses noted remarks regarding the sample preparation and handling registered during the laboratory work, and how it has affected different parts of the study. In total 9 out of the total 108 samples broke due to handling during the laboratory work.

#### 9.1.1 Sample Molding and Layer Separation

Multiple typical molding techniques used in Nordic countries to prepare stabilized samples in the laboratory are described in the report on optimizing laboratory molding by Hov and Paniagua (2022). In this study, the rodding technique described in Section 7.1 is used.

Already in the preparation of the very first batch, challenges arose in attempting to minimize layer separation during the sequential compaction with manual rodding. Transparent cylinders were used for preparation. This made it possible to see if the layers were compacted properly and helped to easier avoid layer separation. Nevertheless, in certain cases, the presence of layer separation still proved to be hard to identify and extinguish.

The main concern regarding this issue was the potential damage to the samples during the extrusion process, as described in Section 7.1. Samples with significant layering were prone to fracture between the layers while being extruded from the cylinder. 7 of the total 9 broken samples, broke during the extrusion. Figure 9.1 demonstrates a sample that broke during extrusion, clearly displaying two distinct layers at the fracture point.

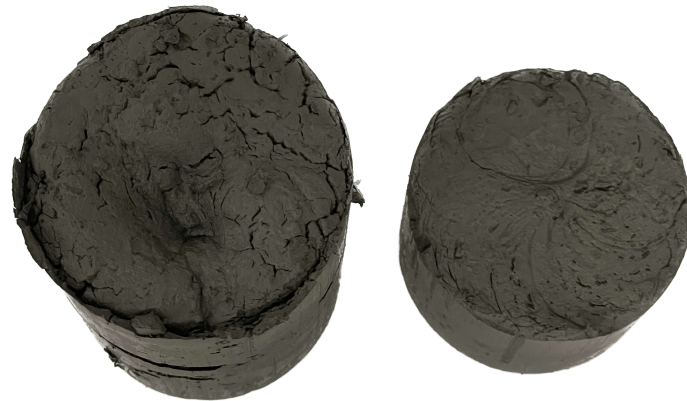


**Figure 9.1:** Fracture between two compaction layers in a sample. Fracture happened between to separate compacted layers

The rodding technique is highly dependent on the individual performing the compaction. Kitazume et al. (2015) tried using a standardized method, which consisted of slowly tamping down 30 times, with the handheld rod. Results showed that the method is applicable and efficient for removing entrapped air in the samples. However, in this study, keeping the applied force constant for every sample showed to be difficult, and some variations in sample moulding must be expected.

Each prepared sample got weighed. In theory, if the moulding was done identically for all samples, all samples in the same batch should weigh the same. The difference in weight is in some way an identification of the subjectivity in the moulding process and could be affecting factors like the porosity in the sample. The difference in weight can be compared to the differences in density since all cylinders have the same volume. Calculated densities for all samples are shown in Appendix C. Results from measured densities show that the maximum deviations between densities in the same batch are 2,9%, and the average is 1,2%. This is believed to show that the moulding has been completed in an acceptable and objectively matter.

## 9.2 P-wave Velocity for Stabilized Soil

The P-wave velocity generally increased with the curing time for most samples that gave proper measurements. This can indicate that the variation of P-wave velocities with curing time, in some way follows the strength development over the same time. The measurements for the stabilized Tiller-Flotten quick clay samples seem to give a somewhat stable increase. The stabilized Onsøy clay samples did however not show a stable trend, and the P-wave velocities had large leaps for some time intervals. For some time intervals, the P-wave velocity also decreased between measurements. The P-wave velocities below 300 m/s are believed to be affected by noise which is discussed further below.

The plots in Figure 8.8 show a trend where increasing P-wave velocity,  $v_p$  is correlated with increasing strength,  $q_{uf}$  and stiffness,  $E_{50}$ . However, the plots have a lot of scatter and the correlation is slightly less significant compared to previous studies by Åhnberg and Holmén



(2011) and Barrett et al. (2013) where  $v_p$  was measured using the resonant column technique. The possible reasons for this scatter are discussed below.

### 9.2.1 Limitations and Noise with the Pundit Device

#### Noise in Measurements

The measured P-wave velocities below 300 m/s are suspected to be influenced by noise. The reason for this is that all the weakest samples got the exact same wave pattern which gave a velocity of around 200-300 m/s. The wave pattern seems more like the sample is vibrating instead of an actual P-wave arriving. Figure 9.2 shows measurements for two different samples where one has a clear wave arrival, while the other one seems to be noise. For the noisy wave, it may seem like a wave is arriving at  $t = 387,5 \mu\text{s}$ . However, the dashed line shows that after around this time both tests show a very similar pattern. This is believed to be noise. Almost all the weakest samples got a similar wave pattern to this noisy wave, and every measurement looking like this got deemed to not being a valid wave. Most of the samples that gave a P-wave velocity below 300 m/s are not shown in the plots in Figure 8.8 because they are believed to be noise. They are, however, given in Appendix A

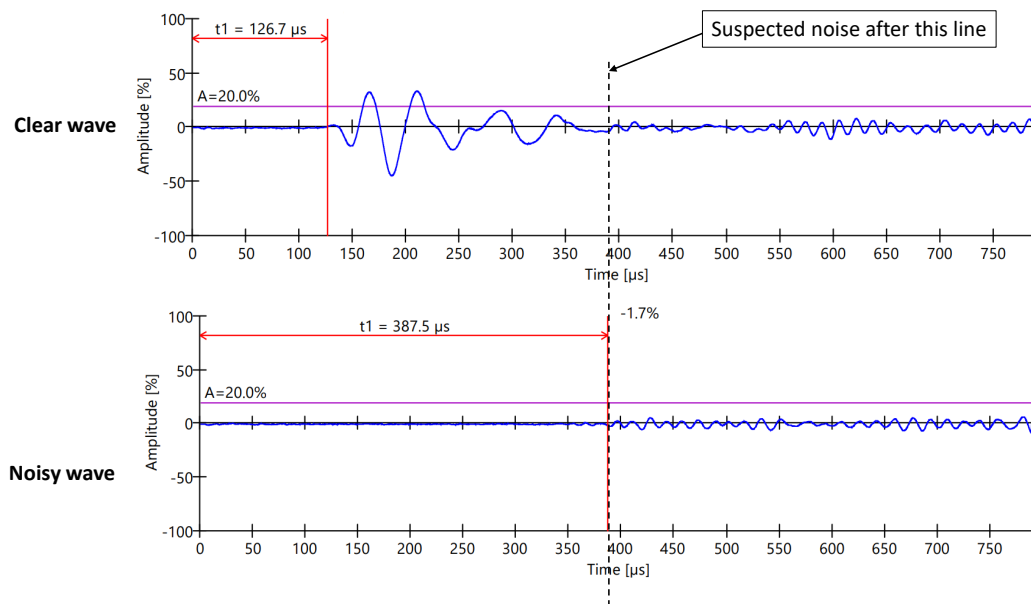


**Figure 9.2:** Comparison between a clear wave arrival and what is suspected to be noise

The reason for the noise could be explained by attenuation due to the large frequency of the transducers (54 kHz). For samples with a low P-wave velocity, the wave may experience more attenuation (energy loss) so that it can't propagate through the whole sample. The results in this study indicate that measuring the P-wave velocity with the Pundit test and 54 kHz

transducers has a lower limit of around 300 m/s. P-wave velocities below this gave no clear wave arrivals.

In the results from measuring the P-wave velocity of stabilized Onsøy soft clay in Figure 8.2 it was pointed out how many readings gave low values, typically around 300 m/s. An example to demonstrate this lower limit is the results from the 20/20 CEM/LS1 Soft clay (Onsøy) in Figure 8.2a. Its results are more or less constant around 300 m/s for all readings. This is assumed to be noise, and that no real P-wave velocities were measured for this sample, which may explain its large deviation from the other two samples in the same plot. From Figure 8.2 it seems like soft clay samples are also affected by noise in the results. For some of the soft clay samples, the P-wave velocity suddenly increases drastically over a time interval. This is believed to be caused by the samples developing enough stiffness for the P-wave to finally properly propagate without the effect of noise.

### Effect of Using Coupling Gel

The P-wave velocity measurements depended on using coupling gel to get good contact between the transducers and the sample. Testing the same sample with and without gel resulted in a large difference in the measured P-wave velocity. The amount of gel used for all the different samples was not kept at the exact same amount all the time, as this would be hard to keep track of. Therefore some deviations could be caused by not enough gel being applied at all tests.

### Effect of Water Content

The P-wave velocity seems to be largely affected by the water content of the samples. All water contents are given in Appendix D. The peat samples where the water content was above 200% showed a P-wave velocity between 1400 and 1600 m/s, which is what the speed of sound in water is at room temperature. For the samples of Onsøy clay, the unconfined compressive strength,  $q_{uf}$ , and secant stiffness,  $E_{50}$  are much lower than for the quick clay samples. However, the P-wave velocities are almost the same. The P-wave velocity was expected to be lower for the samples with lower stiffness. The water content in the Onsøy clay samples was larger than in the quick clay samples, which could lead to the P-waves traveling faster in the pores filled with water. There is a lack of studies on the effect of water content on the P-wave velocity in soils and stabilized soils. However, G. Wang et al. (2022) studied the effect of water content on the P-wave velocity for coal. The study showed a clear trend where  $v_p$  increased gradually as the water content increased.

The plots in Figure 9.3 were made in order to investigate the effect of water content. In Figure 9.3a the measured values of  $v_p$  are plotted versus the stiffness,  $E_{50}$ . In Figure 9.3b the  $v_p$  values are adjusted according to Equation 9.1:

$$v_{p,adjusted} = v_p \frac{w_{avg}}{w} \quad (9.1)$$

where  $v_{p,adjusted}$  is an artificial P-wave velocity adjusted for water content,  $v_p$  is the measured

P-wave velocity,  $w_{avg}$  is the average water content for all the samples in the plot and  $w$  is the measured water content for each sample.

It is important to notice that the adjusted values for  $v_p$  are not meant to be real values for the P-wave velocity and are only constructed to exemplify an idea that came up during the study. They are adjusted only to study if the water content might have some effect on the P-wave velocity. The equation is such that samples with high water content will get a lower adjusted P-wave velocity and samples with a low water content compared to the average will get a higher adjusted P-wave velocity. The plot with adjusted P-wave velocities in Figure 9.3b shows a much better correlation between the P-wave velocity and the secant stiffness than the plot with the actual measured values in Figure 9.3a. The increase of the  $R^2$  value from 0,6755 to 0,8607 verifies that the correlation gets stronger. This artificially constructed scenario shows that P-wave velocities measured with the Pundit device might actually have a decent correlation with stiffness and strength if the problem with water content can be sorted out.

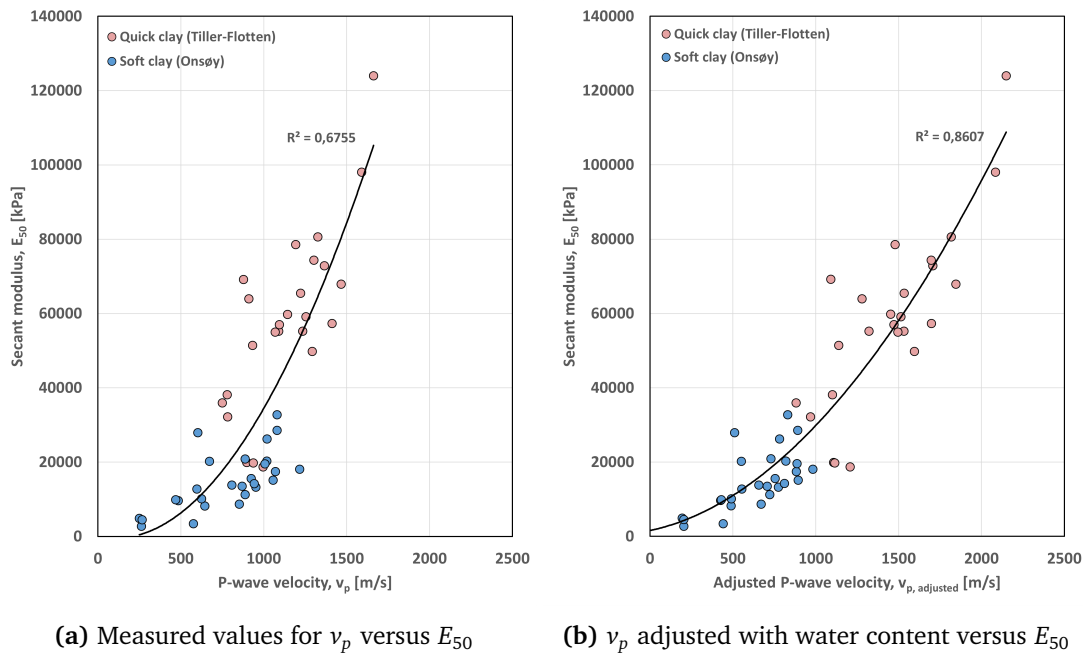


Figure 9.3: Illustration of how the water content might affect the correlation

### 9.2.2 Dynamic Poisson's Ratio

The dynamic Poisson's ratio for the samples was calculated using the P-wave and S-wave velocities measured with the Pundit device after 28 days of curing. This was done to investigate if the measured P-wave and S-wave velocities were reliable, as the Poisson's ratio is expected to be in a certain range for stabilized soil. Previous studies on stabilized soil show Poisson's ratios in between 0,1 and 0,5, (Åhnberg & Holmén, 2011; Barrett et al., 2013; Toohey & Mooney, 2012). The Poisson's ratio was calculated as in Equation 9.2:

$$\nu = \frac{1 - \frac{1}{2} \left( \frac{v_p}{v_s} \right)^2}{1 - \left( \frac{v_p}{v_s} \right)^2} \quad (9.2)$$

Some Poisson's ratios below -1 were calculated, which is theoretically impossible. The samples with negative Poisson's ratios were excluded in the plots of P-wave velocity as it was believed that measurement errors for the P-wave velocity caused this. The Poisson's ratios for all the samples that were positive are shown versus the unconfined compression strength in Figure 9.4. The study by Simmons (1955) showed that an increase in compressive strength for concrete relates to a decrease in the Poisson's ratio and it is possible to assume that there is a similar relation for cement-treated soils. Figure 9.4 shows that the Poisson's ratio generally decreases when the unconfined compression strength increases. Except for one outlier, the positive Poisson's ratio for the samples is between 0,2 and 0,5 which is similar to other studies on stabilized soil. This indicates that the relationship between the P-wave and shear wave velocities seems to be in a decent range.

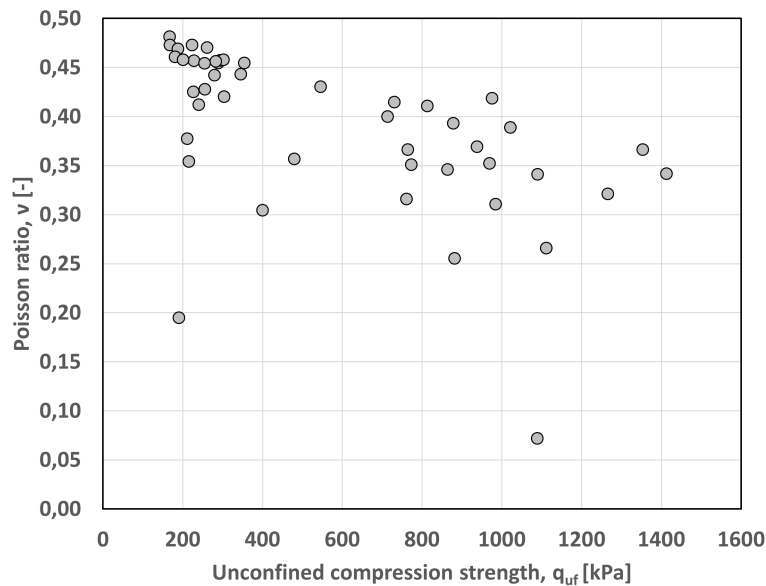


Figure 9.4: Unconfined compression strength versus Poisson's ratio

## 9.3 Shear Wave Velocity for Stabilized soil

### 9.3.1 Shear Wave Velocity versus Curing Time

Using the Pundit apparatus for measuring shear wave variations over time for stabilized samples showed to be an efficient method that gave clear results. This is believed based on the plots in Figure 8.3 clearly showing similar trends for all the different sample combinations. It was shown a 40% increase in shear wave velocity as an average for all samples, between day 3 and

28 of curing. This indicates that in general, the Pundit apparatus can be used for measuring shear wave velocity variations over time and that the shear wave velocity increases with curing time.

### 9.3.2 Shear Wave Velocity versus Strength

Figure 9.5 shows all the shear wave velocity measurements from both the Pundit test and the bender element test versus unconfined compression strength. The results of this study are compared to results from previous studies by Åhnberg and Holmén (2011) and Dannewitz et al. (2005). The trendline shows that this study has a very similar correlation compared to the two other studies for all soil samples and binders. The relationship between the S-wave velocity and the strength in this study also correlates well with the results by Helle et al. (2022). The fact that the correlation in this study is similar to these previous studies increases the reliability of using shear wave velocity to predict strength in stabilized soil. Stabilized peat, soft clay, and quick clay with several different binders all follow the same correlation. This indicates that shear wave velocity can be used as a strength-indicator for stabilized soils independent of the type of soil and binders being used. The shear wave velocities also increased with the curing time for most samples, indicating that it may be related to the strength development. This indicates that the shear wave velocity can be used to estimate strength at any given time, and can be used to study the strength development over time for stabilized soil.

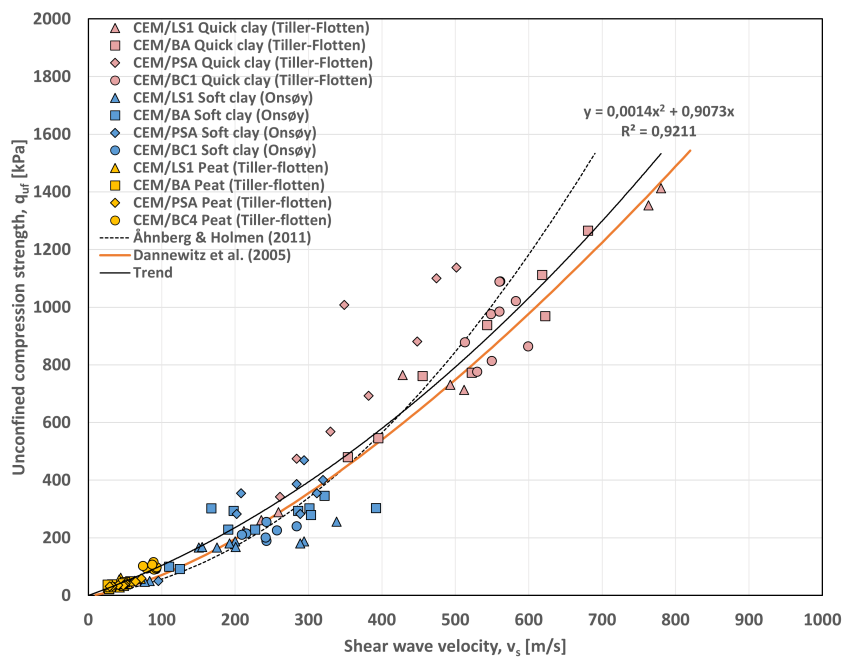


**Figure 9.5:** Shear wave velocity vs. strength for stabilized soil found in this study compared to previous studies by both Åhnberg and Holmén (2011) and Dannewitz et al. (2005)

### 9.3.3 Shear Wave Velocity versus Strength and Stiffness from Pundit Test

Most of the presented shear wave velocity measurements in this study larger than 200 m/s were done with the Pundit test since the bender elements used in this study are believed to work insufficiently for velocities above ca. 200 m/s, which is discussed later in Section 9.3.7. As shown in Figure 9.5 the measured shear wave velocities above 200 m/s that are measured with the Pundit device are very similar to previous studies by Åhnberg and Holmén (2011) and Dannewitz et al. (2005) where the measurements were done by bender elements and the resonant column technique. This indicates that measuring S-wave velocities on stabilized soil with a Pundit device can give reliable measurements for velocities larger than 200 m/s.

### 9.3.4 Limitation of Shear Wave Velocity Measurements with the Pundit Device

Results from the Pundit device equipped with 40 kHz dry-point shear wave transducers used in this study indicate that the device has a lower measuring limit of approximately 200 m/s. It is believed that the reason for the ultrasonic waves not propagating through the samples with lower velocities than 200 m/s is caused by the attenuation (energy loss) of the waves. Attenuation is frequency dependent, and the ultrasonic waves with this test have a very high frequency of 40 kHz. For samples with a low shear wave velocity, the waves will spend more time propagating through the sample, and thus more energy loss will occur in the contact points between particles. When the bender element tests were performed on the samples with shear wave velocities below 200 m/s a frequency between 0,6 kHz and 10 kHz was used. Therefore it seems like a frequency of 40 kHz is very large for some of these samples.

As mentioned in Section 4.2.2, the determination of the actual first arrival of the shear wave can be complex. This was illustrated in Figure 4.5. When doing measurements with the Pundit device on samples with low shear wave velocities the received signal was often very weak. This made it hard to properly identify the exact same first arrival point, which could have caused some deviation in the measurements of different samples. However, these differences were very small.

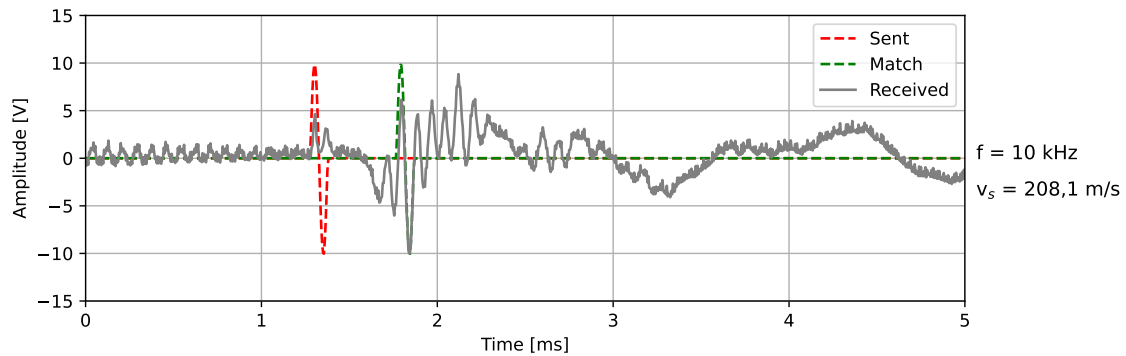
### 9.3.5 Shear Wave Velocity from Bender Element Testing

The bender element tests were performed after 28 days of curing. The results plotted in Figure 8.11 show a correlation between the S-wave velocity from bender elements,  $v_s$  and strength,  $q_{uf}$  and stiffness,  $E_{50}$ . The bender element test provided clear results for the peat samples and the weakest Onsøy clay samples. However, for the samples with higher shear wave velocity than around 200 m/s, testing with bender elements was very difficult. For these samples, the received signals were very poor and it was impossible to identify the arriving shear waves, and therefore no results were obtained. The reasons for these poor results are discussed below.

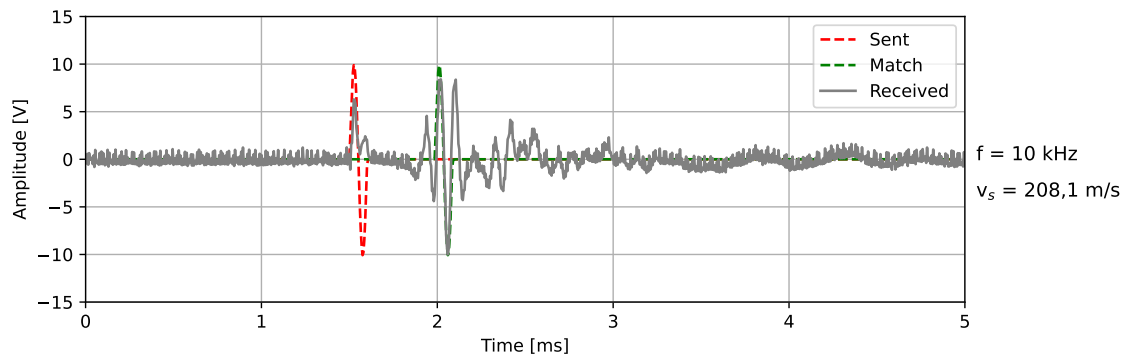
### 9.3.6 Effect of the Carved Slots Filled with gypsum

The samples that were soft enough for the bender elements to be pushed into directly gave good results with the bender element test. The stiffer samples with S-wave velocities above 200 m/s, however, gave very poor results. One reason for this could be that these samples

were not pushed directly into the samples. Instead, a slot was cut in advance and filled with gypsum to ensure contact, as described in Section 7.3.1. To investigate the effect of the carved slots, two of the soft samples were first pushed directly onto the bender elements in order to do the bender element test. After doing this, slots were carved in these samples and filled with gypsum. Then the bender element test was performed on these samples again. The result for this comparison is shown in Figure 9.6. The results show that the arrived waves are very similar, and in this case, the exact same shear wave velocities were measured. For the other test, there was a deviation of around 1%. This shows that the technique of carving a slot filled with gypsum should provide reliable results. Therefore the effect of carving slots filled with gypsum does not seem to be the cause of the poor results for the quick clay samples. Previous studies also show that this method of using carved slots filled with gypsum gives reliable results (Åhnberg & Holmén, 2011; Lindh, 2019; Xiao et al., 2018).



(a) Bender elements are pushed directly into the sample



(b) A slot is cut and filled with gypsum before pushing in bender elements

**Figure 9.6:** Comparison of received signals by: (a) pushing bender elements directly into the sample and (b) cutting a slot filled with gypsum

### 9.3.7 Effect of Frequency

In order to obtain proper measurements of the shear wave velocity with the bender element test it is important that the frequency isn't too low. Figure 9.7 shows how the calculated shear wave velocity for three different samples varied with the input frequency in the bender element test. Low frequencies usually gave very low shear wave velocities. When the frequency increases the measured shear wave velocity also increases. Above a certain frequency, the shear wave velocity stabilizes somewhat. For all interpretations from the bender elements in this study, the stabilized frequency ranges were found before determining shear wave velocities. The plot illustrates that using too low frequencies may severely affect the value of the measured shear wave velocity. This shows similar behavior to the study by Xiao et al. (2018) where low frequencies gave low velocities and then the velocity stabilized as the frequency increased.

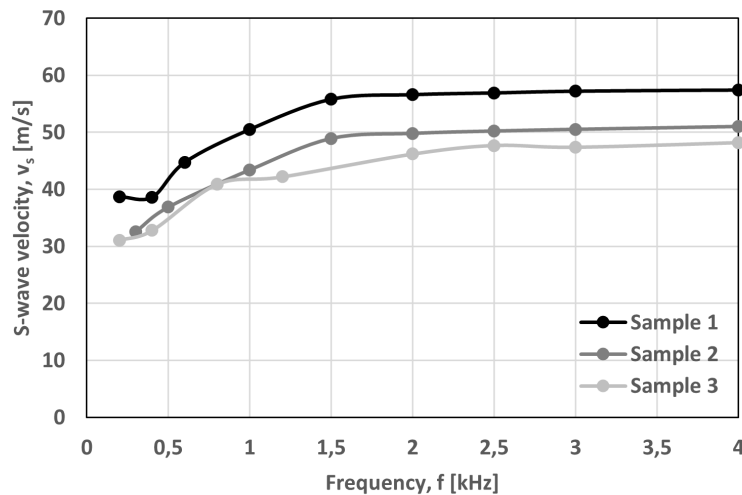


Figure 9.7: Variation of S-wave velocity with frequency for three different samples

As reported by Lee and Santamarina (2005) the input frequency should ideally match the resonant frequency of the BE-soil-system. Equation 4.6 shows that the resonant frequency of the BE-soil-system is dependent on the shear wave velocity in the numerator of the equation. This means that for larger shear wave velocities the resonant frequency of the system increases, and therefore the input frequency should ideally increase.

Figure 9.8 shows the input frequency and the respective calculated shear wave velocity for all the samples in this study. A clear trend is shown where the samples with larger shear wave velocities require higher input frequencies. The plot also shows how the largest measured shear wave velocity with the bender element test in this study is around 200 m/s. This upper limit is believed to be caused by the limitation of the DAQ unit in the NTNU laboratory. The DAQ unit had a sampling rate of 200 kHz. The tests with frequencies larger than 12 kHz usually gave very poor readability of the received signal and it was heavily influenced by noise. As mentioned in Chapter 7 the number of data points was reduced when the frequency increased.



Shear wave velocities measured with the Pundit device gave values up to around 800 m/s for the samples in this study. According to the trendline in Figure 9.8 the frequency would need to be much larger than 12 kHz in order to get the optimal frequency<sup>1</sup> for samples with a shear wave velocity of up to 800 m/s. Therefore almost no results were obtained for samples that had larger shear wave velocities than 200 m/s using the bender elements.

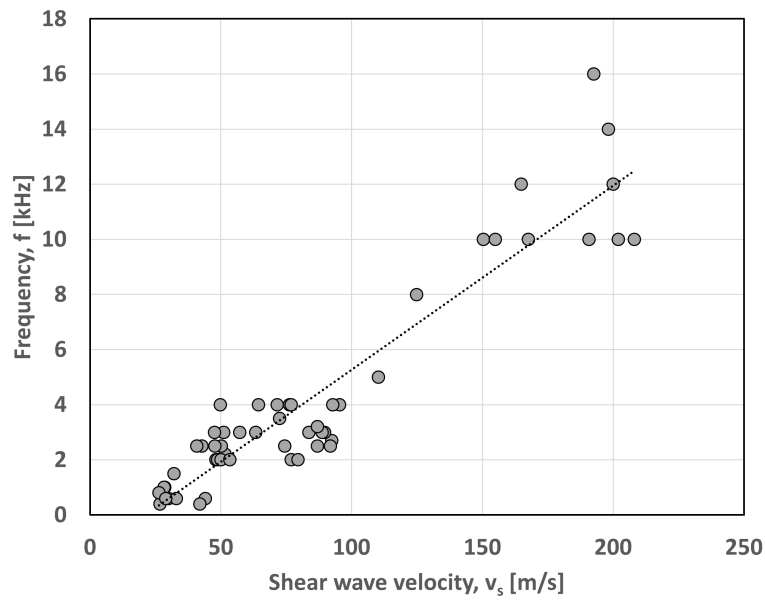


**Figure 9.8:** Presentation of each input frequency and the respective calculated shear wave velocity for all samples in this study, and the belonging trendline

### 9.3.8 Near-field Effect

As discussed in Chapter 4 it is important to avoid the near-field effect when performing bender element tests. Otherwise, the near-field effect can mask the arrival of the shear wave which makes it difficult to calculate the proper shear wave velocity. The near-field effect is dependent on the tip-to-tip length,  $L_{tt}$  and the wavelength,  $\lambda$ . The wavelength is calculated as given by Equation 9.3:

$$\lambda = \frac{v_s}{f} \quad (9.3)$$

The tip-to-tip length,  $L_{tt}$ , and the shear wave velocity,  $v_s$ , are already determined. The only way to prevent the near-field effect is therefore to adjust the frequency. Figure 9.9 shows how the samples may be affected by the near-field effect. Almost all samples are within the discussed requirement to prevail the near-field effect: of  $2 < L_{tt}/\lambda < 9$ . This shows that for almost all of the samples, the near-field effect should be prevented. It is possible that the calculated shear

<sup>1</sup>A frequency that matches the resonant frequency of the BE-soil-system

wave velocities are affected by the near-field effect for the three points in Figure 9.9 that have  $L_{tt}/\lambda < 2$ . However, for most of the bender element tests the near-field effect seems to be avoided. This strengthens the validity of the bender element results<sup>2</sup>.

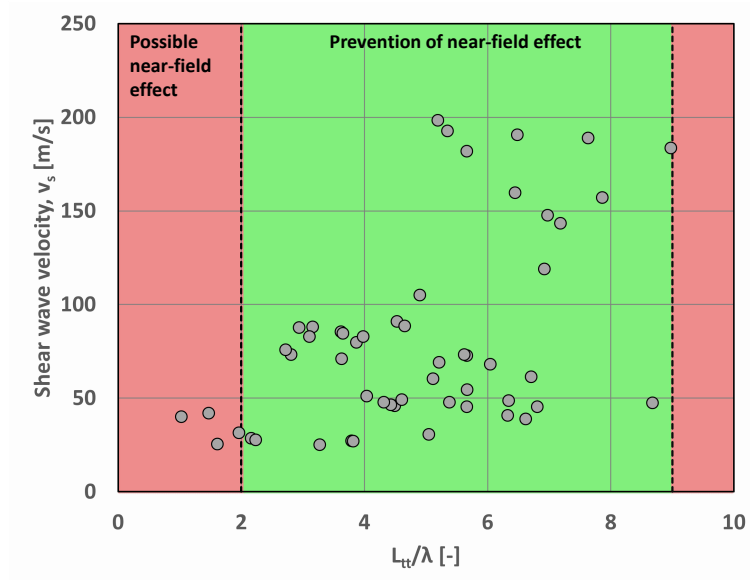


**Figure 9.9:** Plot of the  $L_{tt}/\lambda$  ratio for all the samples that were tested with bender elements to see if the requirement to prevail the near-field effect is fulfilled. Values within the green zone are considered sufficient

### 9.3.9 Peak-to-Peak method

The method used to calculate the shear wave velocity with bender elements was the peak-to-peak method. The disadvantage of this method is that it is somewhat subjective, as discussed in Section 4.2.2. It is not always straightforward to locate the shear wave arrival. Some of the tests resulted in several peaks arriving. This makes it hard to know which peak to choose in the receiving signal. Figure 9.10 shows how such a received signal looked like. The difference in using the first and second peaks usually gave a difference of around 20 % on the calculated shear wave velocity. In this study, the first major peak was used to calculate the shear wave velocity despite the second peak often having a better match with the sent signal. This was done because the first major peak usually had such a large amplitude that it was believed that it had to be the shear wave.

<sup>2</sup>This does not apply to the bender element tests performed on the quick clay samples, since these tests gave no results

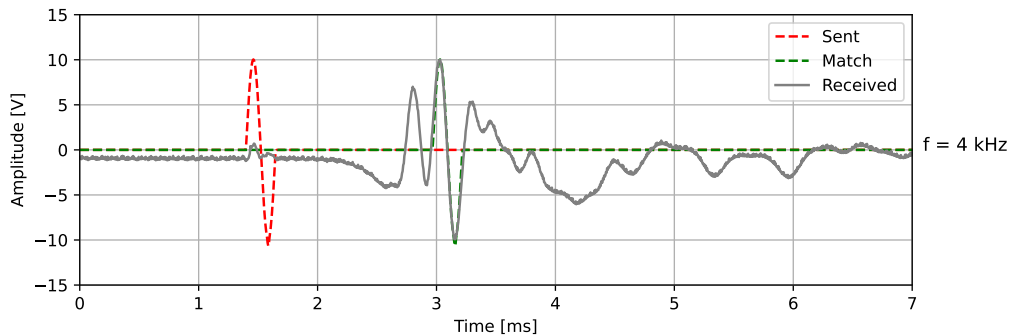
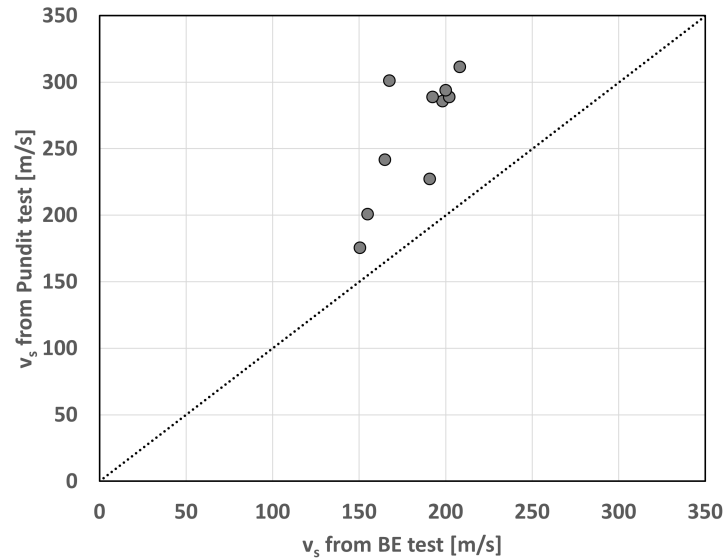


Figure 9.10: Illustration of several peaks arriving in the received signal

## 9.4 Comparison of bender element and Pundit results

Part of this thesis is to evaluate and compare the validity and applicability of using the less known Pundit device for measuring shear wave velocity on stabilized soil, compared to the more common bender element method. The measured shear wave velocities from the Pundit test are compared to the ones obtained by doing bender element tests. For the tests where it was possible to measure shear wave velocity using both bender elements and the Pundit device, the results are plotted in Figure 9.11. This was not possible for many of the samples, as bender element testing had an upper limit around 200 m/s and the Pundit test had a lower limit around 200 m/s. If the two tests gave exactly the same values, all points would lie on the dashed line. However, the results from the Pundit test are consistently larger than those from bender elements. One reason for this could be that for the Pundit test the method of first arrival was used to calculate the shear wave velocity, while for bender elements the peak-to-peak method was used. Corbett (2016) studied the use of a Pundit device with dry-point shear wave transducers and concluded with there not seeming to be a P-wave component. Therefore the method of first arrival should be valid for the Pundit measurements. However, not many studies have been done on this subject and it is possible that there actually is a P-wave component that might arrive earlier than the shear waves.



**Figure 9.11:** Shear wave velocities from the bender element test versus shear wave velocities from the Pundit test. The dashed line illustrates where the values from both method are equal

Another factor that might influence the results obtained from the Pundit test compared to the bender element test is that very different frequencies were used. The Pundit test always used a frequency of 40 kHz. When using the bender element test, lower frequencies were used. For the compared values in Figure 9.11 the input frequency for the bender element tests was around 10 kHz. It is possible that the bender element measurements would have given larger shear wave velocities if the input frequency was 40 kHz. However, as previously mentioned, it was not possible to achieve such high frequencies with the equipment used in this study.

There is a large difference in the simplicity and how time-consuming the two tests are. Doing bender element testing on stabilized soil requires that a slot is cut in the sample and filled with gypsum/plasticine. This is time-consuming, and the slots can be inconvenient if other tests are going to be performed on the sample. The use of a Pundit device equipped with 40 kHz dry-point transducers requires much less time to perform, and in addition, it does not leave a slot in the sample.

## 9.5 Electrical Resistivity

The electrical resistivity did not exhibit consistent behavior and variation with the curing time in the same way as the P-wave and S-wave velocities did for most samples. The correlation between resistivity and strength and stiffness was found to be poor for the stabilized quick clay samples in this study. For the samples of soft clay and to some degree the peat samples, however, there is some tendency where an increase in resistivity correlates with increasing strength and stiffness. The results are believed to be affected by how the tests were performed. This is discussed below.

### 9.5.1 Effect of Contact Resistance

The method used to measure electrical resistivity was the two-electrode method. The study by Zhou et al. (2015) showed that this setup can cause measurement errors due to contact resistance between the electrodes and the sample. In order to prevent this a thin layer of conducting gel was applied to the electrodes. This was done in the hope of ensuring good contact between the electrodes and the samples.

Some preliminary tests were done with and without the use of conducting gel. The tests with conducting gel gave lower resistivity values than the ones without gel which showed that the conducting gel reduced the contact resistance. However, there was no established amount of gel to use for the tests. It was believed that a thin layer of gel would be enough to reduce the contact resistance sufficiently. During testing, it was discovered that increasing the amount of gel more than usual had a large impact on the resistivity measurements. After this was discovered the amount of contact gel was increased for the rest of the testing, which resulted in lower resistivity measurements. This explains why for some of the charts where electrical resistivity is plotted versus curing time there is a sudden drop in resistivity between day 21 and day 28.

The increased amount of conducting gel was used for one-third of the quick clay samples and all the peat samples and soft clay samples on day 28. This means that the plots of quick clay samples with resistivity versus strength and stiffness in Figure 8.13 might be largely affected by contact resistance. The plots of electrical resistivity versus time may also be influenced by varying contact resistance for each measurement. The resistivity for all the peat and soft clay samples on day 28 was measured with the decided increased amount of conducting gel. Therefore the plots in Figure 8.14 and 8.15 are assumed to be less affected by contact resistance.

Due to the larger amount of conducting gel seeming to decrease the contact resistance, it is subsequently believed that if implemented already from day 3, all values of resistivity versus curing time would be scaled down and have a much clearer increasing trend towards the believed correct value after 28 days. Thereby, avoiding a significant dip between before and after applying more conducting gel.

The shape of the samples is also believed to cause some contact resistance. When preparing the samples it was attempted to best effort to get the surfaces as flat as possible. Most of the clay samples had somewhat flat surfaces. For the peat samples, however, it was harder to get flat surfaces due to the fibers in the material. Therefore it was hard to get perfect contact between the electrodes and some of the peat samples due to the fibers and edges not always being flat. This is believed to have caused some contact resistance.

### 9.5.2 Effect of Different Soils and Binders on the Resistivity

It is relevant to investigate if the electrical resistivity is affected by the type of soil and binders being used in the stabilized soil. In order for the resistivity to be a useful parameter to estimate the strength in stabilized soil it should ideally not be dependent on the type of soil and binders being used. In order to study this, all the samples are shown in Figure 9.12 where the resistivity is plotted versus the unconfined strength. The plot shows that there is some clustering

separating the different soil types. However, within the specific soil types, the different binder combinations for quick clay and soft clay show less clustering compared to the peat samples. For the peat samples, there is no particular correlation when looking separately at the cluster of each specific binder combination, but looking at the peat overall, some degree of correlation is apparent between the resistivity and strength. From the plot in Figure 9.12, it seems like there is not a clear correlation between the resistivity and strength that applies to all kinds of stabilized soils, unlike for S-wave velocity where all the soil types followed the same trend. It must be pointed out that the resistivity values for the quick clay are very uncertain because of the contact resistance discussed above.

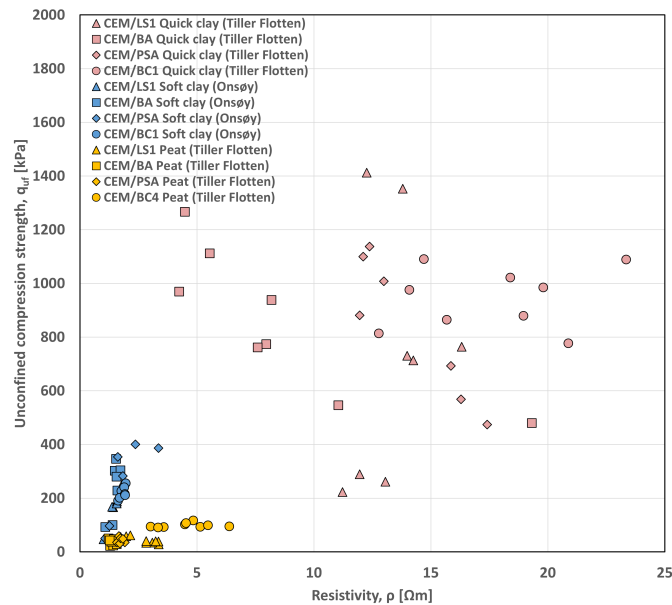


**Figure 9.12:** Electrical resistivity,  $\rho$  versus unconfined compression strength,  $q_{uf}$  for all samples in this study

### 9.5.3 Effect of Voltage

As mentioned in Chapter 7 the voltage was not kept constant when measuring the resistivity. Instead, the system was connected to a power outlet, and the voltage and current were read from multimeters. The voltage measured was very similar for each type of soil. Quick clay samples measured voltages of around 13 V, soft clay measured voltages around 8 V, and peat usually measured around 10 V. According to Ng et al. (2022) the resistivity typically decreases if the voltage is increased. This means that when comparing the different soil types, the resistivity values might also be slightly affected by the voltage that was used.

### 9.5.4 Difference Between Resistivity in Laboratory and In Situ

The measured resistivity for the stabilized soil samples in this study is very different compared to the in situ resistivity measurements for Tiller-Flotten peat- and quick clay and Onsøy clay

presented in Chapter 6. The Tiller-Flotten quick clay in this study is sampled at a depth between 8 - 15 m and the Tiller-Flotten peat is sampled at a depth of 1 m. The soft clay from Onsøy is from 5 - 8 m depth. Since the material used in this thesis arrived remoulded, it was not possible to measure resistivity for the material prior to stabilization. According to L'Heureux et al. (2019) and Gundersen et al. (2019b), the in situ resistivity for the soils at these depths before stabilization is approximate:

- Quick clay (Tiller-Flotten): 30 - 40  $\Omega\text{m}$
- Peat (Tiller-Flotten): 100 - 200  $\Omega\text{m}$
- Soft clay (Onsøy): 1 - 10  $\Omega\text{m}$

When stabilizing the soil by adding binders it is expected that the resistivity will increase since the conductive water in the pores reacts with binders and form hydration products, as discussed in Chapter 5. However, the stabilized samples in this study dropped significantly in resistivity. The electrical resistivity measurements for the stabilized soil samples after 28 days are in the order:

- Stabilized quick clay (Tiller-Flotten): 4 - 24  $\Omega\text{m}$
- Stabilized peat (Tiller-Flotten): 1 - 7  $\Omega\text{m}$
- Stabilized soft clay (Onsøy): 1 - 3,5  $\Omega\text{m}$

The resistivity measurements were much lower for the stabilized soil samples than the in situ measurements of the soils at the Tiller-Flotten and Onsøy sites. The reason for the decrease in resistivity is believed to be caused by the difference in temperature. According to L'Heureux et al. (2019) the temperature in the peat area at 1 m depth is around 11 °C<sup>3</sup>, while the temperature at 8-15 m depth for the quick clay is around 5 °C. The Onsøy clay at 5-8 m depth has a temperature of around 6 °C according to (Gundersen et al., 2019a). The resistivity measurements in this study are done at room temperature, which is around 22 ± 2 °C and is warmer than the temperatures in situ. As mentioned in Section 5.3, an increase in temperature will decrease the resistivity of soil. The low resistivity values for the stabilized soil samples could therefore be caused by the change in temperature.

### 9.5.5 Comparing Stabilized Soil Samples Mixed in the Laboratory and Field

It is known that stabilized soil in the laboratory differs from in situ stabilized soil due to different mixing procedures. Paniagua Lopez et al. (2022) studied the difference in porosity between laboratory-mixed clay samples and clay samples mixed in the field. The study showed that field-mixed samples had lower porosity than the samples mixed with the NGF method, which is similar to the method that is used in this thesis. Electrical resistivity for stabilized soils is dependent on the porosity such that an increase in porosity will decrease the resistivity, according

---

<sup>3</sup>The depth of the peat is so shallow that the temperature will vary with the season. It is not known if the resistivity measurements were performed at the same time of year as the temperature measurements.

to Zhang et al. (2012).

The saturation of the stabilized soil will also affect the electrical resistivity. Zhou et al. (2015) showed that an increase in saturation clearly correlates with a decrease in resistivity. The samples of stabilized soil mixed in the laboratory were not fully saturated in this study. For the clay samples, this is comparable to field-mixed samples, as Paniagua Lopez et al. (2022) showed that field-mixed samples contained trapped air and were not fully saturated after 28 and 70 days. For stabilized peat, however, it is believed that the laboratory saturation differs more from the in situ conditions. As already mentioned the temperature might also be very different in the field than in the laboratory.

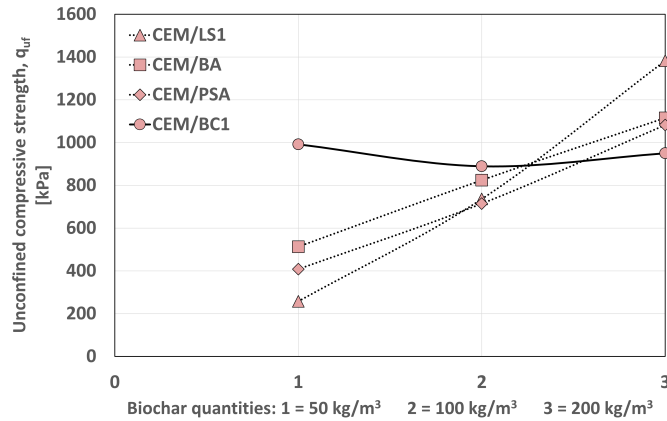
## 9.6 Effect of Different By-products and Binder Ratios

Some remarks on how the different by-products and different binder ratios have affected the results are discussed in this section.

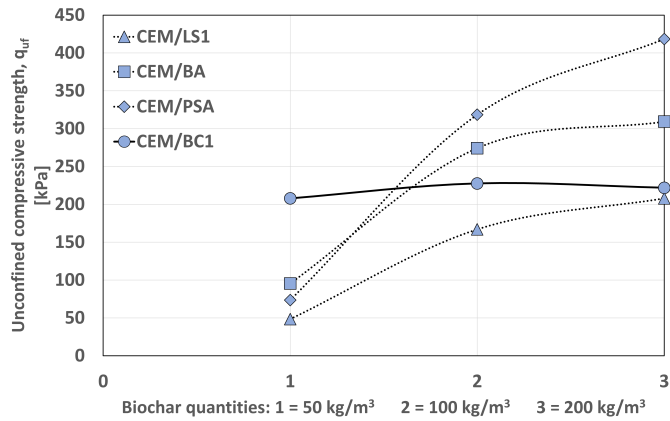
Comparing how the different ratios within one binder combination affect the results, there are some obvious trends. For both P-wave and S-wave velocity, the results from Tiller-Flotten quick clay, with combinations CEM/LS1, CEM/BA and CEM/PSA shows in that, in general, a higher amount of total binder gives higher velocities. This is shown in Figure 8.3 and Figure 8.1. The CEM/BC1 combination deviates from this trend and shows more or less similar S-wave velocities for all ratios. For the P-wave velocities, the two lower ratios gave the highest velocities. It, therefore, seems like the biochar combinations affect the samples differently than the three other by-products.

Also if correlated to the unconfined compressive strength, the biochar combinations show significant deviations compared to the other combinations. For Tiller-Flotten quick clay and Onsøy soft clay, all three other binder combinations show a clear trend of higher binder quantities giving higher strengths, while for the biochar combination, the strength decreases with higher quantities. This is clearly seen in Figure 9.13 where the unconfined compressive strength is plotted with its different binder ratios. This effect on how it may be an optimum quantity of biochar is presented back in Section 2.3.5, where Ritter et al. (2023) showed that surpassing this optimum amount gave decreasing values for strength. Since the total binder quantity in the CEM/BC1 combination is significantly higher than the others, it can be discussed that if these have been mixed with similar total binder quantities, the same decreasing effect would occur.





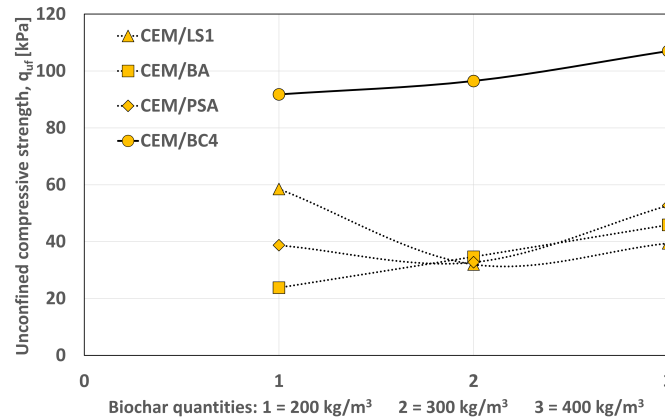
(a) Tiller-Flotten quick clay



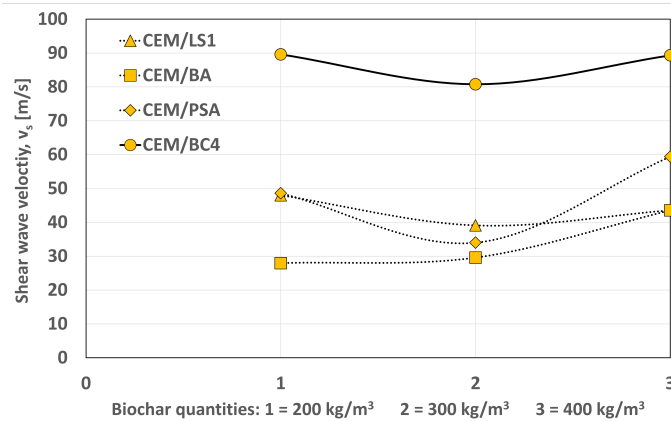
(b) Onsøy soft clay

**Figure 9.13:** Effect on biochar quantity compared to other binder combinations in (a) stabilized Tiller-Flotten quick clay and (b) stabilized Onsøy soft clay

Ritter et al. (2022) showed that for the specific tested biochar quantities on stabilized peat in his study, there was no optimum biochar content, and higher quantities tended to give higher strengths. This is found in the results of this study as well, as shown in Figure 9.14a, where the strength of stabilized peat increases with higher biochar quantities. In Figure 9.14a it is believed the other binder combinations are lower due to their significantly lower total binder quantities. Since testing for wave velocities on peat with the Pundit apparatus gave no clear results, this effect of binder combinations and ratio have been compared to the binder element testing, in Figure 9.14b. The high total binder amount in the CEM/BC4 combinations, clearly give higher velocities than the rest, just as it does with the strength.



(a) UCS vs. binder combinations

(b)  $v_s$  vs. binder combinations

**Figure 9.14:** Comparison of (a) UCS vs. binder combinations and (b)  $v_s$  vs. binder combinations for stabilized Tiller-Flotten peat

Since the two plots are more or less in the same shape, i.e. proportional to each other, Figure 9.14 also illustrates another point; different binders tend to affect the UCS of the sample, but the correlation between measured  $v_s$  and UCS exhibits similar behavior, independent of what binder is used.

The results of the measured water content, see Appendix D, shows that often the biochar combinations have lower water contents, compared to the other combinations. This is believed to be due to the significantly larger amount of binder in this combination. The lower water content will give a lower w/c ratio and in theory higher strengths. This effect could be seen by comparing the relatively high strength of the CEM/BC4 combination in Figure 9.14 and the relatively low water contents for the same combination in Appendix D. For the peat, the total amount of binder in the CEM/BC4 combination is much higher compared to the three other combinations. This is not seen for the biochar combination in Figure 9.13, where the amount of binder in the biochar combination, is much more similar to the three other combinations.

## **Part III**

# **Conclusion and Further Work**



## Chapter 10

# Conclusion and Further Work

### 10.1 Conclusion

The results for the stabilized samples showed that the P-wave velocity generally increased with the curing time. An increase in the P-wave velocity,  $v_p$ , showed to correlate with an increase for both the unconfined compression strength,  $q_{uf}$  and the secant stiffness,  $E_{50}$ . However, the correlation is affected by much scatter. The limitation of measuring the P-wave velocity using a Pundit device is that the large frequency of the apparatus causes much attenuation. Due to the attenuation, there seems to be a lower measurement limit of around 300 m/s for P-wave velocities. The measurements of the P-wave velocities using the Pundit apparatus are believed to be affected by differences in water content.

The shear wave velocity increased with the curing time for the majority of the samples. A good correlation was found where increasing shear wave velocity correlates with an increase in the unconfined compression strength,  $q_{uf}$  and secant stiffness,  $E_{50}$ . The shear wave velocity for peat was measured using bender elements, and for quick clay, the shear wave velocities were measured with a Pundit device. For the soft clay, shear wave velocities were obtained with both bender element- and Pundit testing. The correlation between shear wave velocity and strength and stiffness found in this study applies to stabilized quick clay, soft clay and peat, using several different binders. The correlation is similar to previous studies, which indicates that the shear wave velocity can be used as a parameter to estimate strength and stiffness for stabilized soils independent of what type of soil and binders are being used. The fact that the shear wave velocity increases with the curing time and correlates to the strength, indicates that shear wave velocity can be used to estimate the strength at any given time in the curing period.

The two apparatuses that were used to measure the shear wave velocity were the bender elements and a Pundit device. The bender elements exhibited an upper measurement limit of around 200 m/s, due to limitations with the specific used bender elements setup not being able to properly handle frequencies from 12 kHz and higher. The Pundit device exhibited a lower measurement limit of around 200 m/s, most likely caused by a large amount of attenuation

due to the transducers operating at a frequency of 40 kHz.

Because of these limits, there were not many samples that were measured using both the Pundit device and the bender elements, and therefore there is a lack of values in order to get a good comparison of the apparatuses. For the few samples where both apparatuses got measurements, the Pundit device consistently measured larger velocities than the bender elements. The Pundit transducers operating at higher frequencies are believed to have some impact on the shear wave velocity. Despite the Pundit measurements being larger than the bender elements in this study, they showed strong similarities to several previous studies. This indicates that measurements done with the Pundit device on stabilized soil with shear wave velocity from around 200 m/s and higher are reliable. By comparing the practical usage of the two methods for measuring shear wave velocity, the Pundit apparatus showed to be much more applicable due to its straightforward and quick procedure. Unlike the bender elements, the Pundit apparatus does not leave any disturbance on the sample post-testing. It also eliminates any need for the time- and resource-consuming processes of pre-cutting the samples.

Measurements of electrical resistivity were not found to have any specific correlations to the strength and stiffness of the stabilized quick clay samples. The samples of soft clay and to some degree the peat samples had a tendency where an increase in electrical resistivity correlated with an increase in strength and stiffness. The electrical resistivity did not show a consistent behavior with the curing time. Many of the electrical resistivity measurements over time are believed to be influenced by varying contact resistance. This applies to all the samples between day 3 and 21, and most of the quick clay samples on day 28 as well.

According to this study, the best practice for measuring P-wave velocities with the Pundit device is to ensure enough coupling gel in order to get good contact between the transducers and the sample. In order for the P-wave velocities not to be affected by noise the velocity should be above 300 m/s. When measuring shear wave velocities with a Pundit device equipped with 40 kHz dry-point transducers there is no need for coupling gel. The wave arrival can be detected as the first arrival using the auto-trigger function in the Pundit device. In order to get shear wave velocity measurements using the Pundit device, the velocity must be larger than around 200 m/s. For bender elements, it is very important to not use a frequency that is too low in order to get reliable measurements of the shear wave velocity. This could be done by using several different frequencies to find the frequency ranges giving stabilized results. It was shown that carving slots in stabilized samples and using gypsum as an infilling material, gave the same results as directly pressing the samples onto the bender elements. When measuring the resistivity it is important to avoid contact resistance to the extent that's possible to get good measurements.

## 10.2 Further Work

The correlation between the P-wave velocity and strength and stiffness in this study was affected by much scatter for all the soil types. It was discussed how the water content of the samples possibly could affect the propagation of the P-waves, and thereby affecting the measurements. In any future attempt to try and get a more reliable correlation between the P-wave

velocity and the strength and stiffness of stabilized soil with the Pundit apparatus, the effect of water content should be looked further into.

To study the performance of measuring shear wave velocities with the Pundit device further, other methods of measurement can be used for comparison, such as the resonant column technique. Further comparison with the bender elements using higher frequencies could also be interesting. The measurement of shear wave velocity on stabilized soil in this study showed that using the Pundit device equipped with 40 kHz dry-point shear wave transducers was significantly less time-consuming than using bender elements. This is mainly due to testing with the Pundit device eliminating the need for carving a slot in the sample, compared to the bender elements. Further verification of the Pundit device could result in it becoming a new aid in measuring the shear wave velocity for stabilized soils.

The resistivity in stabilized soil would also be interesting to further investigate since many of the measurements in this study seem to be unreliable due to contact resistance. The measurement method could be improved and perhaps a four-electrode setup can give more reliable results. For the values to be more comparable to in situ resistivity, in terms of porosity, temperature, and saturation, it can be interesting to check if stabilized soil samples stored, cured, and tested closer to actual in situ conditions would have any effect.





# Bibliography

- Ahmad, S., et al. (2013). Study of concrete involving use of waste paper sludge ash as partial replacement of cement. *IOSR Journal of Engineering (IOSRJEN)*.
- Åhnberg, H., & Holmén, M. (2011). Assessment of stabilised soil strength with geophysical methods. *Proceedings of the Institution of Civil Engineers-Ground Improvement*, 164(3), 109–116.
- Andi, M., et al. (2019). Correlation of reinforcement concrete quality based on variations in upv testing methods. 673(1), 012043. %5Curl%7Bhttps://iopscience.iop.org/article/10.1088/1757-899X/673/1/012043/meta%7D
- Arroyo, M., Muir Wood, D., & Greening, P. D. (2003). Source near-field effects and pulse tests in soil samples. *Géotechnique*, 53(3), 337–345.
- Aziman, M., Hazreek, Z., Azhar, A., & Haimi, D. (2016). Compressive and shear wave velocity profiles using seismic refraction technique. 710(1), 012011.
- Barrett, A. G., Nauleau, E., Le Kouby, A., Pantet, A., Reiffsteck, P., & Martineau, F. (2013). Free-free resonance testing of in situ deep mixed soils. *Geotechnical Testing Journal*, 2(36), 9p.
- Baustad, P. (2022). En laboratoriestudie av styrke og stivhet i kalksementstabilisert leire. *Masteroppgave NTNU*.
- Bell, F. (1996). Lime stabilization of clay minerals and soils. *Engineering Geology*, 42(4), 223–237.
- Berbar, O. (2020). Deformation of norwegian peat. *Master's thesis in Geotechnics and Geohazards, NTNU*.
- Blackland Centre. (2015). *Von post humification scale*. Retrieved May 28, 2023, from <https://www.blacklandcentre.org/the-science/von-post-humification-scale/>
- Brattli, B. (2015). *Pensumhefte - ingeniørgeologi løsmasser*. NTNU-Trondheim, Institutt for geovitenskap og petroleum.
- Carlsten, P. (1988). Torv-geotekniska egenskaper och byggmetoder. *Statens geotekniska institut*.

- Corbett, D. (2016). Advances in ultrasonic testing-research into the application of dry point contact transducers, 1–7.
- Dannewitz, N., AB, H. G., & Eriksson, H. (2005). Utvecklingsprojekt 11357 seismisk kontrollmetod för kc-pelare.
- Di Sante, M., Bernardo, D., Bellezza, I., Fratolocchi, E., & Mazzieri, F. (2022). Linking small-strain stiffness to development of chemical reactions in lime-treated soils. *Transportation Geotechnics*, 34, 100742.
- Gu, X., Yang, J., & Huang, M. (2013). Laboratory measurements of small strain properties of dry sands by bender element. *Soils and Foundations*, 53(5), 735–745.
- Gundersen, A., et al. (2019a). Characterization and engineering properties of the ngts on søy soft clay site. *AIMS Geosciences* 5(3):665-703.
- Gundersen, A., et al. (2019b). Field and laboratory test results from ngts soft clay site – on søy. *NGI-rapport;20160154-10-R*.
- Hamid, M., et al. (2021). Incorporation of biochar in cementitious materials: A roadmap of biochar selection. *Construction and Building Materials* 283 (2021): 122757.
- Helle, T. E., et al. (2022). Klimagrunns arbeidsmetodikk for dokumentasjon og prediksjon av skjærfasthet og stivhet i bindemiddelstabiliserte pelar.
- Hov, F. F., & Paniagua, P. (2022). Optimization of laboratory molding techniques for nordic dry deep mixing. *Geotechnical Testing Journal*, 45(4).
- Hwang, Y.-I., Sung, D., Kim, H.-J., Song, S.-J., Kim, K.-B., & Kang, S.-S. (2020). Propagation and attenuation characteristics of an ultrasonic beam in dissimilar-metal welds. *Sensors*, 20(21), 6259.
- I.Vegas et al. (2006). Obtaining a pozzolanic addition from the controlled calcination of paper mill sludge. performance in cement matrices. *Materiales de Construcción* 56.283: 49-60.
- Jacobsen, S., et al. (2023). Concrete technology. *Kompendium i TKT4215 - Concrete Technology* 1.
- Janz, M., & Johansson, S.-E. (2002). The function of different binding agents in deep stabilization. *Swedish Deep Stabilization Research Centre*.
- Jordan, A. (2014). Lightening the clay. *EGU BLOGS*.
- Karlsen, F., & Sund-Olsen, S. (2022). A laboratory study on the use of non-destructive testing for evaluation of the strength and deformation properties of stabilized soils. *TBM4500 - Bygg og miljøteknikk, fordypningsprosjekt*.
- Kartverket. (2023). Norgeskart.
- Kitazume, M., et al. (2015). Applicability of molding procedures in laboratory mix tests for quality control and assurance of the deep mixing method. *Soils and Foundations*, 55(4), 761–777.

- Lee, J.-S., & Santamarina, J. (2005). Bender elements: Performance and signal interpretation. *Journal of Geotechnical and Geoenvironmental Engineering*, 131, 1063–1188.
- L'Heureux, J.-S., et al. (2019). The tiller-flotten research site: Geotechnical characterization of a very sensitive clay deposit. *AIMS Geosciences* 5(4):831-867.
- L'Heureux, J.-S., & Long, M. (2017). Relationship between shear-wave velocity and geotechnical parameters for norwegian clays. *Journal of geotechnical and Geoenvironmental engineering*, 143(6), 04017013.
- Lindh, P. (2016). *Seismik testning av stabiliserad jord med bender element vid triaxialförsök*. Statens geotekniske institut.
- Lindh, P. (2019). Laboratoriestudie av spänningnivåns och härdningstemperaturens betydelse för hållfasthetstillväxt hos stabiliserad jord. utvärdering av p-och s-vågor vid olika härdningsförfaranden.
- Liu, S. Y., et al. (2008). Experimental study on the electrical resistivity of soil-cement admixtures. *Environmental Geology* 54 (2008): 1227-1233.
- Long, M., et al. (2022). Engineering properties of norwegian peat for calculation of settlements. *Engineering Geology* 308 (2022): 106799.
- Makusa, G. P. (2012). Soil stabilization methods and materials. *Department of Civil, Environmental and Natural resources engineering - Lulea University of Technology*.
- Mohammad, A. B., et al. (2022). Recycled coal bottom ash as sustainable materials for cement replacement in cementitious composites: A review. *Construction and Building Materials* 338 (2022): 127624.
- Morawska, M. (2019). An experimental study of anisotropic stiffness of tiller-flotten quick clay using bender elements. *Master's Thesis. NTNU*.
- Negronk-Mendoza, A. (2020). Clay. *Encyclopedia of Astrobiology*, 480.483.
- Ng, Y. C., Kek, H. Y., Hu, X., Wong, L. N., Teo, S., Ku, T., & Lee, F.-H. (2022). An approach for characterising electrical conductivity of cement-admixed clays. *Soils and Foundations*, 62(2), 101127.
- NGF. (2012). Veiledning for grunnforsterkning med kalksementpeler.
- NGU. (2023a). Kvikkleire.
- NGU. (2023b). Løsmassekart.
- Nordal, S., & Eiksund, G. (2021). Geodynamics.
- Nordal, S., et al. (2020). Introduksjon til geoteknikk. *Kompendium TBA4100*.
- NVE. (2019). Sikkerhet mot kvikkleireskred. 1.
- Panduro®. (2023). Hobbygips 5 kg.

- Paniagua, P., Long, M., & L'Heureux, J. (2021). Geotechnical characterization of norwegian peat: Database. *IOP Conference Series: Earth and Environmental Science*, 710(1), 012016.
- Paniagua, P., et al. (2019). Geotechnical characterization of norwegian peat:database. *IOP Conf. Ser.: Earth Environ. Sci.* 710 012016.
- Paniagua Lopez, A. P., Falle, F., Sølve, H., Tekseth, K. R. B., Mirzaei, F., & Breiby, D. W. (2022). Comparing laboratory and field samples of lime-cement improved norwegian clay.
- PLAXIS. (2023). Material models manual 2d.
- Proceq. (2017). Pundit proceq operating instructions.
- Rankka, K., et al. (2004). Quick clay in sweden.
- Rio, J. F. M. E. (2006). Advances in laboratory geophysics using bender elements.
- Ritter, S., et al. (2022). Biochar amendment for improved and more sustainable peat stabilisation. *Proceedings of the Institution of Civil Engineers - Ground Improvement*.
- Ritter, S., et al. (2023). Biochar in quick clay stabilization: Reducing carbon footprint and improving shear strength.
- Samouëlian, A., Cousin, I., Tabbagh, A., Bruand, A., & Richard, G. (2005). Electrical resistivity survey in soil science: A review. *Soil and Tillage research*, 83(2), 173–193.
- Sanchez-Salinerio, I., Roesset, J. M., Stokoe, I., & Kenneth, H. (1986). Analytical studies of body wave propagation and attenuation.
- Shearer, P. M. (2010). Introduction to seismology: The wave equation and body waves. *unpublished, Institute of Geophysics and Planetary Physics, Scripps Institution of Oceanography, University of California, San Diego*.
- Shi, C. (2002). Characteristics and cementitious properties of ladle slag fines from steel production. *Cement and Concrete Research*.
- Siddique, R. (2007). Waste materials and by-products in concrete. *Springer Science & Business media*.
- Simmons, J. (1955). Poisson's ratio of concrete: A comparison of dynamic and static measurements. *Magazine of Concrete Research*, 7(20), 61–68.
- SINTEF. (2017). Norwegian geo-test sites. *SINTEF.no-prosjekter*.
- Solberg et al. (2008). Resistivity measurements as a tool for outlining quick-clay extent and valley-fill stratigraphy: A feasibility study from buvika, central norway. *Canadian Geotechnical Journal* 45.2 (2008): 210-225.
- SSV. (2018). Håndbok v220 - geoteknikk i vegbygging.
- Statens Vegvesen. (2016). Håndbok r210 - laboratorieundersøkelser.
- Syversen, F. S. G. (2013). En studie av den mineralogiske sammensetningen i norske sensitive leirer: Med et geoteknisk perspektiv. *Masteroppgave, Institutt for geofag ved UiO*.










- Toohy, N., & Mooney, M. (2012). Seismic modulus growth of lime-stabilised soil during curing. *Geotechnique*, 62(2), 161–170.
- Valsson, S. M., Dahl, M., Haugen, E., & Degago, S. A. (2021). Estimating shear wave velocity with the sptu and bender element. *710*(1), 012017.
- Viggiani, G., & Atkinson, J. (1995). Interpretation of bender element tests. *Geotechnique*, 45(1), 149–154.
- Vincent, N. A., et al. (2017). Laboratory electrical resistivity studies on cement stabilized soil. *Hindawi International Scholarly Research Notices*.
- VJTECH. (2020). Bender element testing - an introduction.
- Wang, G., Wang, S., Li, J., Chen, X., Qin, C., & Ju, S. (2022). Experimental research on propagation and attenuation of ultrasonic waves in water-bearing coal. *Fuel*, 324, 124533.
- Wang, Y., et al. (2016). A novel method for determining the small-strain shear modulus of soil using the bender elements technique. *Canadian Geotechnical Journal*, 54(2), 280–289.
- Wang, Y., Lo, K., Yan, W., & Dong, X. (2007). Measurement biases in the bender element test. *Journal of Geotechnical and Geoenvironmental Engineering*, 133(5), 564–574.
- Xiao, H., et al. (2018). Bender element measurement of small strain shear modulus of cement-treated marine clay—effect of test setup and methodology. *Construction and building materials*, 182, 433–447.
- Yesiller, N., et al. (2001). Ultrasonic testing for evaluation of stabilized mixtures. *Transportation research record*, 1757(1), 32–42.
- Zhang, D.-w., Chen, L., & Liu, S.-y. (2012). Key parameters controlling electrical resistivity and strength of cement treated soils. *Journal of Central South University*, 19(10), 2991–2998.
- Zhou, M., Wang, J., Cai, L., Fan, Y., & Zheng, Z. (2015). Laboratory investigations on factors affecting soil electrical resistivity and the measurement. *IEEE Transactions on Industry Applications*, 51(6), 5358–5365.











## **Appendix A**

# **Complete Sample Review**

Appendix A gives a complete overview of every sample made with relevant results. Samples without pictures are due to the sample being fractured, and no pictures were taken.

Q.1.20/20.LS1			Q.2.20/20.LS1			Q.3.20/20.LS1		
								
Height	108	[mm]	Height	108	[mm]	Height	108	[mm]
Diameter	54	[mm]	Diameter	54	[mm]	Diameter	54	[mm]
Electrical Resistivity, $\rho$	11,96	[ $\Omega$ m]	Electrical Resistivity, $\rho$	13,06	[ $\Omega$ m]	Electrical Resistivity, $\rho$	11,22	[ $\Omega$ m]
Pundit: $v_p$	897	[m/s]	Pundit: $v_p$	996	[m/s]	Pundit: $v_p$	937	[m/s]
Pundit: $v_s$	259,1	[m/s]	Pundit: $v_s$	235,5	[m/s]	Pundit: $v_s$	212,1	[m/s]
Bender Element: $v_s$	182	[m/s]	Bender Element: $v_s$	x	[m/s]	Bender Element: $v_s$	x	[m/s]
UCS, $q_{uf}$	289,23	[kPa]	UCS, $q_{uf}$	261,01	[kPa]	UCS, $q_{uf}$	223,23	[kPa]
UCS, $\tau_{max}$	144,62	[kPa]	UCS, $\tau_{max}$	130,51	[kPa]	UCS, $\tau_{max}$	111,62	[kPa]
Secant modulus, $E_{50}$	19886	[kPa]	Secant modulus, $E_{50}$	18717	[kPa]	Secant modulus, $E_{50}$	19774	[kPa]
Failure strain, $\epsilon_f$	3,19	[%]	Failure strain, $\epsilon_f$	3,72	[%]	Failure strain, $\epsilon_f$	3,79	[%]
Q.1.40/40.LS1			Q.2.40/40.LS1			Q.3.40/40.LS1		
								
Height	108	[mm]	Height	108	[mm]	Height	108	[mm]
Diameter	54	[mm]	Diameter	54	[mm]	Diameter	54	[mm]
Electrical Resistivity, $\rho$	13,99	[ $\Omega$ m]	Electrical Resistivity, $\rho$	16,32	[ $\Omega$ m]	Electrical Resistivity, $\rho$	14,24	[ $\Omega$ m]
Pundit: $v_p$	1292	[m/s]	Pundit: $v_p$	933	[m/s]	Pundit: $v_p$	1254	[m/s]
Pundit: $v_s$	493	[m/s]	Pundit: $v_s$	428,3	[m/s]	Pundit: $v_s$	511,8	[m/s]
Bender Element: $v_s$	x	[m/s]	Bender Element: $v_s$	x	[m/s]	Bender Element: $v_s$	x	[m/s]
UCS, $q_{uf}$	730,45	[kPa]	UCS, $q_{uf}$	764,36	[kPa]	UCS, $q_{uf}$	713,53	[kPa]
UCS, $\tau_{max}$	365,23	[kPa]	UCS, $\tau_{max}$	382	[kPa]	UCS, $\tau_{max}$	356,77	[kPa]
Secant modulus, $E_{50}$	49774	[kPa]	Secant modulus, $E_{50}$	51429	[kPa]	Secant modulus, $E_{50}$	59140	[kPa]
Failure strain, $\epsilon_f$	2,15	[%]	Failure strain, $\epsilon_f$	2,4	[%]	Failure strain, $\epsilon_f$	2,05	[%]
Q.1.60/60.LS1			Q.2.60/60.LS1			Q.3.60/60.LS1		
								
Height	108	[mm]	Height	108	[mm]	Height	108	[mm]
Diameter	54	[mm]	Diameter	54	[mm]	Diameter	54	[mm]
Electrical Resistivity, $\rho$	12,26	[ $\Omega$ m]	Electrical Resistivity, $\rho$	13,79	[ $\Omega$ m]	Electrical Resistivity, $\rho$	x	[ $\Omega$ m]
Pundit: $v_p$	1591	[m/s]	Pundit: $v_p$	1662	[m/s]	Pundit: $v_p$	x	[m/s]
Pundit: $v_s$	780,2	[m/s]	Pundit: $v_s$	763	[m/s]	Pundit: $v_s$	x	[m/s]
Bender Element: $v_s$	292	[m/s]	Bender Element: $v_s$	x	[m/s]	Bender Element: $v_s$	x	[m/s]
UCS, $q_{uf}$	1412,46	[kPa]	UCS, $q_{uf}$	1353,12	[kPa]	UCS, $q_{uf}$	x	[kPa]
UCS, $\tau_{max}$	706,23	[kPa]	UCS, $\tau_{max}$	676,56	[kPa]	UCS, $\tau_{max}$	x	[kPa]
Secant modulus, $E_{50}$	98039	[kPa]	Secant modulus, $E_{50}$	123967	[kPa]	Secant modulus, $E_{50}$	x	[kPa]
Failure strain, $\epsilon_f$	1,93	[%]	Failure strain, $\epsilon_f$	1,41	[%]	Failure strain, $\epsilon_f$	x	[%]



Q.1.20/20.BA			Q.2.20/20.BA			Q.3.20/20.BA		
								
Height	108	[mm]	Height	108	[mm]	Height	108	[mm]
Diameter	54	[mm]	Diameter	54	[mm]	Diameter	54	[mm]
Electrical Resistivity, $\rho$	11,05	[ $\Omega$ m]	Electrical Resistivity, $\rho$	19,33	[ $\Omega$ m]	Electrical Resistivity, $\rho$	x	[ $\Omega$ m]
Pundit: $v_p$	1130	[m/s]	Pundit: $v_p$	750	[m/s]	Pundit: $v_p$	x	[m/s]
Pundit: $v_s$	395,1	[m/s]	Pundit: $v_s$	353,7	[m/s]	Pundit: $v_s$	x	[m/s]
Bender Element: $v_s$	245	[m/s]	Bender Element: $v_s$	x	[m/s]	Bender Element: $v_s$	x	[m/s]
UCS, $q_{uf}$	545,69	[kPa]	UCS, $q_{uf}$	479,5	[kPa]	UCS, $q_{uf}$	x	[kPa]
UCS, $\tau_{max}$	272,85	[kPa]	UCS, $\tau_{max}$	239,7	[kPa]	UCS, $\tau_{max}$	x	[kPa]
Secant modulus, $E_{50}$	36585	[kPa]	Secant modulus, $E_{50}$	35928	[kPa]	Secant modulus, $E_{50}$	x	[kPa]
Failure strain, $\epsilon_f$	2,59	[%]	Failure strain, $\epsilon_f$	2,6	[%]	Failure strain, $\epsilon_f$	x	[%]
Q.1.40/40.BA			Q.2.40/40.BA			Q.3.40/40.BA		
								
Height	108	[mm]	Height	108	[mm]	Height	108	[mm]
Diameter	54	[mm]	Diameter	54	[mm]	Diameter	54	[mm]
Electrical Resistivity, $\rho$	8,19	[ $\Omega$ m]	Electrical Resistivity, $\rho$	7,98	[ $\Omega$ m]	Electrical Resistivity, $\rho$	7,61	[ $\Omega$ m]
Pundit: $v_p$	1193	[m/s]	Pundit: $v_p$	1090	[m/s]	Pundit: $v_p$	878	[m/s]
Pundit: $v_s$	543,3	[m/s]	Pundit: $v_s$	522,3	[m/s]	Pundit: $v_s$	455,4	[m/s]
Bender Element: $v_s$	x	[m/s]	Bender Element: $v_s$	x	[m/s]	Bender Element: $v_s$	x	[m/s]
UCS, $q_{uf}$	937,88	[kPa]	UCS, $q_{uf}$	772,97	[kPa]	UCS, $q_{uf}$	760,84	[kPa]
UCS, $\tau_{max}$	468,94	[kPa]	UCS, $\tau_{max}$	386,48	[kPa]	UCS, $\tau_{max}$	380,42	[kPa]
Secant modulus, $E_{50}$	78571	[kPa]	Secant modulus, $E_{50}$	55215	[kPa]	Secant modulus, $E_{50}$	69182	[kPa]
Failure strain, $\epsilon_f$	2,21	[%]	Failure strain, $\epsilon_f$	2,3	[%]	Failure strain, $\epsilon_f$	2	[%]
Q.1.60/60.BA			Q.2.60/60.BA			Q.3.60/60.BA		
								
Height	108	[mm]	Height	108	[mm]	Height	108	[mm]
Diameter	54	[mm]	Diameter	54	[mm]	Diameter	54	[mm]
Electrical Resistivity, $\rho$	4,49	[ $\Omega$ m]	Electrical Resistivity, $\rho$	4,25	[ $\Omega$ m]	Electrical Resistivity, $\rho$	5,56	[ $\Omega$ m]
Pundit: $v_p$	1327	[m/s]	Pundit: $v_p$	1303	[m/s]	Pundit: $v_p$	1095	[m/s]
Pundit: $v_s$	680,8	[m/s]	Pundit: $v_s$	622,4	[m/s]	Pundit: $v_s$	618,2	[m/s]
Bender Element: $v_s$	288	[m/s]	Bender Element: $v_s$	x	[m/s]	Bender Element: $v_s$	x	[m/s]
UCS, $q_{uf}$	1265,62	[kPa]	UCS, $q_{uf}$	968,91	[kPa]	UCS, $q_{uf}$	1111,33	[kPa]
UCS, $\tau_{max}$	632,81	[kPa]	UCS, $\tau_{max}$	484,45	[kPa]	UCS, $\tau_{max}$	555,67	[kPa]
Secant modulus, $E_{50}$	80645	[kPa]	Secant modulus, $E_{50}$	74324	[kPa]	Secant modulus, $E_{50}$	56995	[kPa]
Failure strain, $\epsilon_f$	2,67	[%]	Failure strain, $\epsilon_f$	2,26	[%]	Failure strain, $\epsilon_f$	3,13	[%]

**Q.1.20/20.PSA****Q.2.20/20.PSA****Q.3.20/20.PSA**










Height	108	[mm]	Height	108	[mm]	Height	108	[mm]
Diameter	54	[mm]	Diameter	54	[mm]	Diameter	54	[mm]
Electrical Resistivity, $\rho$	17,4	[ $\Omega$ m]	Electrical Resistivity, $\rho$	x	[ $\Omega$ m]	Electrical Resistivity, $\rho$	17,92	[ $\Omega$ m]
Pundit: $v_p$	379	[m/s]	Pundit: $v_p$	x	[m/s]	Pundit: $v_p$	346	[m/s]
Pundit: $v_s$	283,7	[m/s]	Pundit: $v_s$	x	[m/s]	Pundit: $v_s$	261,1	[m/s]
Bender Element: $v_s$	208	[m/s]	Bender Element: $v_s$	x	[m/s]	Bender Element: $v_s$	x	[m/s]
UCS, $q_{uf}$	473,93	[kPa]	UCS, $q_{uf}$	x	[kPa]	UCS, $q_{uf}$	341,72	[kPa]
UCS, $\tau_{max}$	238,46	[kPa]	UCS, $\tau_{max}$	x	[kPa]	UCS, $\tau_{max}$	170,86	[kPa]
Secant modulus, $E_{50}$	20690	[kPa]	Secant modulus, $E_{50}$	x	[kPa]	Secant modulus, $E_{50}$	15291	[kPa]
Failure strain, $\epsilon_f$	3,62	[%]	Failure strain, $\epsilon_f$	x	[%]	Failure strain, $\epsilon_f$	3,41	[%]










**Q.1.40/40.PSA****Q.2.40/40.PSA****Q.3.40/40.PSA**










Height	108	[mm]	Height	108	[mm]	Height	108	[mm]
Diameter	54	[mm]	Diameter	54	[mm]	Diameter	54	[mm]
Electrical Resistivity, $\rho$	11,96	[ $\Omega$ m]	Electrical Resistivity, $\rho$	15,85	[ $\Omega$ m]	Electrical Resistivity, $\rho$	16,29	[ $\Omega$ m]
Pundit: $v_p$	782	[m/s]	Pundit: $v_p$	430	[m/s]	Pundit: $v_p$	350	[m/s]
Pundit: $v_s$	448,1	[m/s]	Pundit: $v_s$	381,6	[m/s]	Pundit: $v_s$	330	[m/s]
Bender Element: $v_s$	223	[m/s]	Bender Element: $v_s$	x	[m/s]	Bender Element: $v_s$	x	[m/s]
UCS, $q_{uf}$	881,12	[kPa]	UCS, $q_{uf}$	692,61	[kPa]	UCS, $q_{uf}$	568,71	[kPa]
UCS, $\tau_{max}$	440,56	[kPa]	UCS, $\tau_{max}$	346,31	[kPa]	UCS, $\tau_{max}$	284,35	[kPa]
Secant modulus, $E_{50}$	32164	[kPa]	Secant modulus, $E_{50}$	27607	[kPa]	Secant modulus, $E_{50}$	26829	[kPa]
Failure strain, $\epsilon_f$	3,92	[%]	Failure strain, $\epsilon_f$	3,46	[%]	Failure strain, $\epsilon_f$	3,29	[%]

**Q.1.60/60.PSA****Q.2.60/60.PSA****Q.3.60/60.PSA**









Height	108	[mm]	Height	108	[mm]	Height	108	[mm]
Diameter	54	[mm]	Diameter	54	[mm]	Diameter	54	[mm]
Electrical Resistivity, $\rho$	12,38	[ $\Omega$ m]	Electrical Resistivity, $\rho$	12,11	[ $\Omega$ m]	Electrical Resistivity, $\rho$	12,99	[ $\Omega$ m]
Pundit: $v_p$	660	[m/s]	Pundit: $v_p$	650	[m/s]	Pundit: $v_p$	433	[m/s]
Pundit: $v_s$	501,4	[m/s]	Pundit: $v_s$	474,2	[m/s]	Pundit: $v_s$	348,5	[m/s]
Bender Element: $v_s$	243	[m/s]	Bender Element: $v_s$	x	[m/s]	Bender Element: $v_s$	x	[m/s]
UCS, $q_{uf}$	1137,34	[kPa]	UCS, $q_{uf}$	1099,83	[kPa]	UCS, $q_{uf}$	1008,24	[kPa]
UCS, $\tau_{max}$	568,67	[kPa]	UCS, $\tau_{max}$	549,91	[kPa]	UCS, $\tau_{max}$	504,12	[kPa]
Secant modulus, $E_{50}$	38168	[kPa]	Secant modulus, $E_{50}$	35831	[kPa]	Secant modulus, $E_{50}$	47210	[kPa]
Failure strain, $\epsilon_f$	3,6	[%]	Failure strain, $\epsilon_f$	3,65	[%]	Failure strain, $\epsilon_f$	3,26	[%]








<b>Q.1.50/50.BC1</b>			<b>Q.2.50/50.BC1</b>			<b>Q.3.50/50.BC1</b>		
								
Height	108	[mm]	Height	108	[mm]	Height	108	[mm]
Diameter	54	[mm]	Diameter	54	[mm]	Diameter	54	[mm]
Electrical Resistivity, $\rho$	14,7	[ $\Omega$ m]	Electrical Resistivity, $\rho$	15,69	[ $\Omega$ m]	Electrical Resistivity, $\rho$	18,4	[ $\Omega$ m]
Pundit: $v_p$	1143	[m/s]	Pundit: $v_p$	1235	[m/s]	Pundit: $v_p$	1365	[m/s]
Pundit: $v_s$	561,2	[m/s]	Pundit: $v_s$	599,2	[m/s]	Pundit: $v_s$	582,3	[m/s]
Bender Element: $v_s$	330	[m/s]	Bender Element: $v_s$	x	[m/s]	Bender Element: $v_s$	x	[m/s]
UCS, $q_{uf}$	1089,63	[kPa]	UCS, $q_{uf}$	864,17	[kPa]	UCS, $q_{uf}$	1021,15	[kPa]
UCS, $\tau_{max}$	544,8	[kPa]	UCS, $\tau_{max}$	462,1	[kPa]	UCS, $\tau_{max}$	510,57	[kPa]
Secant modulus, $E_{50}$	59783	[kPa]	Secant modulus, $E_{50}$	55215	[kPa]	Secant modulus, $E_{50}$	72848	[kPa]
Failure strain, $\epsilon_f$	4,05	[%]	Failure strain, $\epsilon_f$	2,29	[%]	Failure strain, $\epsilon_f$	2,06	[%]
<b>Q.1.50/100.BC1</b>			<b>Q.2.50/100.BC1</b>			<b>Q.3.50/100.BC1</b>		
								
Height	108	[mm]	Height	108	[mm]	Height	108	[mm]
Diameter	54	[mm]	Diameter	54	[mm]	Diameter	54	[mm]
Electrical Resistivity, $\rho$	14,09	[ $\Omega$ m]	Electrical Resistivity, $\rho$	12,79	[ $\Omega$ m]	Electrical Resistivity, $\rho$	18,97	[ $\Omega$ m]
Pundit: $v_p$	1467	[m/s]	Pundit: $v_p$	1412	[m/s]	Pundit: $v_p$	1223	[m/s]
Pundit: $v_s$	548,6	[m/s]	Pundit: $v_s$	549,6	[m/s]	Pundit: $v_s$	512,9	[m/s]
Bender Element: $v_s$	243	[m/s]	Bender Element: $v_s$	x	[m/s]	Bender Element: $v_s$	x	[m/s]
UCS, $q_{uf}$	975,57	[kPa]	UCS, $q_{uf}$	813,49	[kPa]	UCS, $q_{uf}$	878,32	[kPa]
UCS, $\tau_{max}$	487,78	[kPa]	UCS, $\tau_{max}$	406,75	[kPa]	UCS, $\tau_{max}$	439,16	[kPa]
Secant modulus, $E_{50}$	67901	[kPa]	Secant modulus, $E_{50}$	57325	[kPa]	Secant modulus, $E_{50}$	65476	[kPa]
Failure strain, $\epsilon_f$	2,26	[%]	Failure strain, $\epsilon_f$	2,25	[%]	Failure strain, $\epsilon_f$	2,07	[%]
<b>Q.1.50/200.BC1</b>			<b>Q.2.50/200.BC1</b>			<b>Q.3.50/200.BC1</b>		
								
Height	108	[mm]	Height	108	[mm]	Height	108	[mm]
Diameter	54	[mm]	Diameter	54	[mm]	Diameter	54	[mm]
Electrical Resistivity, $\rho$	19,82	[ $\Omega$ m]	Electrical Resistivity, $\rho$	20,88	[ $\Omega$ m]	Electrical Resistivity, $\rho$	23,36	[ $\Omega$ m]
Pundit: $v_p$	1069	[m/s]	Pundit: $v_p$	780	[m/s]	Pundit: $v_p$	910	[m/s]
Pundit: $v_s$	560,2	[m/s]	Pundit: $v_s$	529,7	[m/s]	Pundit: $v_s$	560,2	[m/s]
Bender Element: $v_s$	292	[m/s]	Bender Element: $v_s$	x	[m/s]	Bender Element: $v_s$	x	[m/s]
UCS, $q_{uf}$	984,63	[kPa]	UCS, $q_{uf}$	776,39	[kPa]	UCS, $q_{uf}$	1088,6	[kPa]
UCS, $\tau_{max}$	492,31	[kPa]	UCS, $\tau_{max}$	388,19	[kPa]	UCS, $\tau_{max}$	544,31	[kPa]
Secant modulus, $E_{50}$	55000	[kPa]	Secant modulus, $E_{50}$	38136	[kPa]	Secant modulus, $E_{50}$	63954	[kPa]
Failure strain, $\epsilon_f$	3,31	[%]	Failure strain, $\epsilon_f$	3,6	[%]	Failure strain, $\epsilon_f$	3,1	[%]

S.1.20/20.LS1			S.2.20/20.LS1			S.3.20/20.LS1		
								
Height	108	[mm]	Height	108	[mm]	Height	108	[mm]
Diameter	54	[mm]	Diameter	54	[mm]	Diameter	54	[mm]
Electrical Resistivity, $\rho$	1,08	[ $\Omega$ m]	Electrical Resistivity, $\rho$	1,33	[ $\Omega$ m]	Electrical Resistivity, $\rho$	1,01	[ $\Omega$ m]
Pundit: $v_p$	x	[m/s]	Pundit: $v_p$	576	[m/s]	Pundit: $v_p$	262	[m/s]
Pundit: $v_s$	x	[m/s]	Pundit: $v_s$	x	[m/s]	Pundit: $v_s$	x	[m/s]
Bender Element: $v_s$	83,7	[m/s]	Bender Element: $v_s$	76,3	[m/s]	Bender Element: $v_s$	76,9	[m/s]
UCS, $q_{uf}$	49,87	[kPa]	UCS, $q_{uf}$	48,53	[kPa]	UCS, $q_{uf}$	47,08	[kPa]
UCS, $\tau_{max}$	24,93	[kPa]	UCS, $\tau_{max}$	24,27	[kPa]	UCS, $\tau_{max}$	23,54	[kPa]
Secant modulus, $E_{50}$	3365	[kPa]	Secant modulus, $E_{50}$	3415	[kPa]	Secant modulus, $E_{50}$	2703	[kPa]
Failure strain, $\epsilon_f$	3,94	[%]	Failure strain, $\epsilon_f$	4,09	[%]	Failure strain, $\epsilon_f$	5,04	[%]
S.1.40/40.LS1			S.2.40/40.LS1			S.3.40/40.LS1		
								
Height	108	[mm]	Height	108	[mm]	Height	108	[mm]
Diameter	54	[mm]	Diameter	54	[mm]	Diameter	54	[mm]
Electrical Resistivity, $\rho$	1,51	[ $\Omega$ m]	Electrical Resistivity, $\rho$	1,41	[ $\Omega$ m]	Electrical Resistivity, $\rho$	1,37	[ $\Omega$ m]
Pundit: $v_p$	x	[m/s]	Pundit: $v_p$	925	[m/s]	Pundit: $v_p$	888	[m/s]
Pundit: $v_s$	x	[m/s]	Pundit: $v_s$	175,4	[m/s]	Pundit: $v_s$	200,9	[m/s]
Bender Element: $v_s$	x	[m/s]	Bender Element: $v_s$	150,4	[m/s]	Bender Element: $v_s$	154,9	[m/s]
UCS, $q_{uf}$	x	[kPa]	UCS, $q_{uf}$	166,53	[kPa]	UCS, $q_{uf}$	167,74	[kPa]
UCS, $\tau_{max}$	x	[kPa]	UCS, $\tau_{max}$	83,26	[kPa]	UCS, $\tau_{max}$	83,87	[kPa]
Secant modulus, $E_{50}$	x	[kPa]	Secant modulus, $E_{50}$	15596	[kPa]	Secant modulus, $E_{50}$	11258	[kPa]
Failure strain, $\epsilon_f$	x	[%]	Failure strain, $\epsilon_f$	2,23	[%]	Failure strain, $\epsilon_f$	4,87	[%]
S.1.60/60.LS1			S.2.60/60.LS1			S.3.60/60.LS1		
								
Height	108	[mm]	Height	108	[mm]	Height	108	[mm]
Diameter	54	[mm]	Diameter	54	[mm]	Diameter	54	[mm]
Electrical Resistivity, $\rho$	1,83	[ $\Omega$ m]	Electrical Resistivity, $\rho$	1,58	[ $\Omega$ m]	Electrical Resistivity, $\rho$	1,57	[ $\Omega$ m]
Pundit: $v_p$	953	[m/s]	Pundit: $v_p$	1216	[m/s]	Pundit: $v_p$	1071	[m/s]
Pundit: $v_s$	338,2	[m/s]	Pundit: $v_s$	293,9	[m/s]	Pundit: $v_s$	288,8	[m/s]
Bender Element: $v_s$	x	[m/s]	Bender Element: $v_s$	200	[m/s]	Bender Element: $v_s$	192,5	[m/s]
UCS, $q_{uf}$	255,65	[kPa]	UCS, $q_{uf}$	187,80	[kPa]	UCS, $q_{uf}$	180,70	[kPa]
UCS, $\tau_{max}$	127,83	[kPa]	UCS, $\tau_{max}$	93,90	[kPa]	UCS, $\tau_{max}$	90,35	[kPa]
Secant modulus, $E_{50}$	13265	[kPa]	Secant modulus, $E_{50}$	18095	[kPa]	Secant modulus, $E_{50}$	17431	[kPa]
Failure strain, $\epsilon_f$	2,41	[%]	Failure strain, $\epsilon_f$	2,00	[%]	Failure strain, $\epsilon_f$	2,07	[%]

S.1.20/20.BA			S.2.20/20.BA			S.3.20/20.BA		
								
Height	108	[mm]	Height	108	[mm]	Height	108	[mm]
Diameter	54	[mm]	Diameter	54	[mm]	Diameter	54	[mm]
Electrical Resistivity, $\rho$	1,09	[ $\Omega$ m]	Electrical Resistivity, $\rho$	1,39	[ $\Omega$ m]	Electrical Resistivity, $\rho$	x	[ $\Omega$ m]
Pundit: $v_p$	853	[m/s]	Pundit: $v_p$	645	[m/s]	Pundit: $v_p$	x	[m/s]
Pundit: $v_s$	x	[m/s]	Pundit: $v_s$	x	[m/s]	Pundit: $v_s$	x	[m/s]
Bender Element: $v_s$	124,8	[m/s]	Bender Element: $v_s$	110,2	[m/s]	Bender Element: $v_s$	x	[m/s]
UCS, $q_{uf}$	91,50	[kPa]	UCS, $q_{uf}$	99,60	[kPa]	UCS, $q_{uf}$	x	[kPa]
UCS, $\tau_{max}$	45,76	[kPa]	UCS, $\tau_{max}$	49,80	[kPa]	UCS, $\tau_{max}$	x	[kPa]
Secant modulus, $E_{50}$	8686	[kPa]	Secant modulus, $E_{50}$	8209	[kPa]	Secant modulus, $E_{50}$	x	[kPa]
Failure strain, $\epsilon_f$	2,51	[%]	Failure strain, $\epsilon_f$	3,16	[%]	Failure strain, $\epsilon_f$	x	[%]
S.1.40/40.BA			S.2.40/40.BA			S.3.40/40.BA		
								
Height	108	[mm]	Height	108	[mm]	Height	108	[mm]
Diameter	54	[mm]	Diameter	54	[mm]	Diameter	54	[mm]
Electrical Resistivity, $\rho$	1,62	[ $\Omega$ m]	Electrical Resistivity, $\rho$	1,61	[ $\Omega$ m]	Electrical Resistivity, $\rho$	1,49	[ $\Omega$ m]
Pundit: $v_p$	1019	[m/s]	Pundit: $v_p$	807	[m/s]	Pundit: $v_p$	1080	[m/s]
Pundit: $v_s$	285,7	[m/s]	Pundit: $v_s$	227,4	[m/s]	Pundit: $v_s$	301,1	[m/s]
Bender Element: $v_s$	198,1	[m/s]	Bender Element: $v_s$	190,7	[m/s]	Bender Element: $v_s$	167,5	[m/s]
UCS, $q_{uf}$	293,10	[kPa]	UCS, $q_{uf}$	228,06	[kPa]	UCS, $q_{uf}$	301,80	[kPa]
UCS, $\tau_{max}$	146,55	[kPa]	UCS, $\tau_{max}$	114,04	[kPa]	UCS, $\tau_{max}$	150,90	[kPa]
Secant modulus, $E_{50}$	20270	[kPa]	Secant modulus, $E_{50}$	13793	[kPa]	Secant modulus, $E_{50}$	28571	[kPa]
Failure strain, $\epsilon_f$	2,51	[%]	Failure strain, $\epsilon_f$	2,52	[%]	Failure strain, $\epsilon_f$	2,21	[%]
S.1.60/60.BA			S.2.60/60.BA			S.3.60/60.BA		
								
Height	108	[mm]	Height	108	[mm]	Height	108	[mm]
Diameter	54	[mm]	Diameter	54	[mm]	Diameter	54	[mm]
Electrical Resistivity, $\rho$	1,74	[ $\Omega$ m]	Electrical Resistivity, $\rho$	1,57	[ $\Omega$ m]	Electrical Resistivity, $\rho$	1,55	[ $\Omega$ m]
Pundit: $v_p$	1057	[m/s]	Pundit: $v_p$	943	[m/s]	Pundit: $v_p$	1007	[m/s]
Pundit: $v_s$	392	[m/s]	Pundit: $v_s$	303,2	[m/s]	Pundit: $v_s$	321,7	[m/s]
Bender Element: $v_s$	x	[m/s]	Bender Element: $v_s$	x	[m/s]	Bender Element: $v_s$	x	[m/s]
UCS, $q_{uf}$	303,35	[kPa]	UCS, $q_{uf}$	279,14	[kPa]	UCS, $q_{uf}$	345,38	[kPa]
UCS, $\tau_{max}$	151,68	[kPa]	UCS, $\tau_{max}$	139,57	[kPa]	UCS, $\tau_{max}$	172,69	[kPa]
Secant modulus, $E_{50}$	15122	[kPa]	Secant modulus, $E_{50}$	14222	[kPa]	Secant modulus, $E_{50}$	19553	[kPa]
Failure strain, $\epsilon_f$	2,56	[%]	Failure strain, $\epsilon_f$	2,99	[%]	Failure strain, $\epsilon_f$	2,73	[%]



S.1.20/20.PSA			S.2.20/20.PSA			S.3.20/20.PSA		
								
Height	108	[mm]	Height	108	[mm]	Height	108	[mm]
Diameter	54	[mm]	Diameter	54	[mm]	Diameter	54	[mm]
Electrical Resistivity, $\rho$	1,26	[ $\Omega$ m]	Electrical Resistivity, $\rho$	x	[ $\Omega$ m]	Electrical Resistivity, $\rho$	1,07	[ $\Omega$ m]
Pundit: $v_p$	250	[m/s]	Pundit: $v_p$	x	[m/s]	Pundit: $v_p$	267	[m/s]
Pundit: $v_s$	x	[m/s]	Pundit: $v_s$	x	[m/s]	Pundit: $v_s$	x	[m/s]
Bender Element: $v_s$	76,9	[m/s]	Bender Element: $v_s$	x	[m/s]	Bender Element: $v_s$	95,4	[m/s]
UCS, $q_{uf}$	97,15	[kPa]	UCS, $q_{uf}$	x	[kPa]	UCS, $q_{uf}$	49,96	[kPa]
UCS, $\tau_{max}$	48,57	[kPa]	UCS, $\tau_{max}$	x	[kPa]	UCS, $\tau_{max}$	24,98	[kPa]
Secant modulus, $E_{50}$	4889	[kPa]	Secant modulus, $E_{50}$	x	[kPa]	Secant modulus, $E_{50}$	4511	[kPa]
Failure strain, $\epsilon_f$	3,31	[%]	Failure strain, $\epsilon_f$	x	[%]	Failure strain, $\epsilon_f$	3,44	[%]
S.1.40/40.PSA			S.2.40/40.PSA			S.3.40/40.PSA		
								
Height	108	[mm]	Height	108	[mm]	Height	108	[mm]
Diameter	54	[mm]	Diameter	54	[mm]	Diameter	54	[mm]
Electrical Resistivity, $\rho$	1,62	[ $\Omega$ m]	Electrical Resistivity, $\rho$	x	[ $\Omega$ m]	Electrical Resistivity, $\rho$	1,84	[ $\Omega$ m]
Pundit: $v_p$	1080	[m/s]	Pundit: $v_p$	x	[m/s]	Pundit: $v_p$	1020	[m/s]
Pundit: $v_s$	311,4	[m/s]	Pundit: $v_s$	x	[m/s]	Pundit: $v_s$	288,8	[m/s]
Bender Element: $v_s$	208,1	[m/s]	Bender Element: $v_s$	x	[m/s]	Bender Element: $v_s$	202	[m/s]
UCS, $q_{uf}$	354,13	[kPa]	UCS, $q_{uf}$	x	[kPa]	UCS, $q_{uf}$	282,96	[kPa]
UCS, $\tau_{max}$	177,07	[kPa]	UCS, $\tau_{max}$	x	[kPa]	UCS, $\tau_{max}$	141,48	[kPa]
Secant modulus, $E_{50}$	32743	[kPa]	Secant modulus, $E_{50}$	x	[kPa]	Secant modulus, $E_{50}$	26230	[kPa]
Failure strain, $\epsilon_f$	2,11	[%]	Failure strain, $\epsilon_f$	x	[%]	Failure strain, $\epsilon_f$	2,16	[%]
S.1.60/60.PSA			S.2.60/60.PSA			S.3.60/60.PSA		
								
Height	108	[mm]	Height	108	[mm]	Height	108	[mm]
Diameter	54	[mm]	Diameter	54	[mm]	Diameter	54	[mm]
Electrical Resistivity, $\rho$	2,37	[ $\Omega$ m]	Electrical Resistivity, $\rho$	3,36	[ $\Omega$ m]	Electrical Resistivity, $\rho$	5,92	[ $\Omega$ m]
Pundit: $v_p$	603	[m/s]	Pundit: $v_p$	306	[m/s]	Pundit: $v_p$	290	[m/s]
Pundit: $v_s$	319,7	[m/s]	Pundit: $v_s$	283,7	[m/s]	Pundit: $v_s$	293,9	[m/s]
Bender Element: $v_s$	x	[m/s]	Bender Element: $v_s$	x	[m/s]	Bender Element: $v_s$	x	[m/s]
UCS, $q_{uf}$	400,26	[kPa]	UCS, $q_{uf}$	386,31	[kPa]	UCS, $q_{uf}$	468,95	[kPa]
UCS, $\tau_{max}$	200,13	[kPa]	UCS, $\tau_{max}$	193,16	[kPa]	UCS, $\tau_{max}$	234,48	[kPa]
Secant modulus, $E_{50}$	27891	[kPa]	Secant modulus, $E_{50}$	13793	[kPa]	Secant modulus, $E_{50}$	31544	[kPa]
Failure strain, $\epsilon_f$	2,00	[%]	Failure strain, $\epsilon_f$	3,10	[%]	Failure strain, $\epsilon_f$	2,62	[%]





S.1.50/50.BC1			S.2.50/50.BC1			S.3.50/50.BC1		
								
Height	108	[mm]	Height	108	[mm]	Height	108	[mm]
Diameter	54	[mm]	Diameter	54	[mm]	Diameter	54	[mm]
Electrical Resistivity, $\rho$	x	[ $\Omega$ m]	Electrical Resistivity, $\rho$	1,64	[ $\Omega$ m]	Electrical Resistivity, $\rho$	1,78	[ $\Omega$ m]
Pundit: $v_p$	x	[m/s]	Pundit: $v_p$	673	[m/s]	Pundit: $v_p$	888	[m/s]
Pundit: $v_s$	x	[m/s]	Pundit: $v_s$	242,7	[m/s]	Pundit: $v_s$	257	[m/s]
Bender Element: $v_s$	x	[m/s]	Bender Element: $v_s$	x	[m/s]	Bender Element: $v_s$	x	[m/s]
UCS, $q_{uf}$	x	[kPa]	UCS, $q_{uf}$	189,75	[kPa]	UCS, $q_{uf}$	225,99	[kPa]
UCS, $\tau_{max}$	x	[kPa]	UCS, $\tau_{max}$	94,87	[kPa]	UCS, $\tau_{max}$	113,00	[kPa]
Secant modulus, $E_{50}$	x	[kPa]	Secant modulus, $E_{50}$	20202	[kPa]	Secant modulus, $E_{50}$	20870	[kPa]
Failure strain, $\epsilon_f$	x	[%]	Failure strain, $\epsilon_f$	2,20	[%]	Failure strain, $\epsilon_f$	2,19	[%]
S.1.50/100.BC1			S.2.50/100.BC1			S.3.50/100.BC1		
								
Height	108	[mm]	Height	108	[mm]	Height	108	[mm]
Diameter	54	[mm]	Diameter	54	[mm]	Diameter	54	[mm]
Electrical Resistivity, $\rho$	1,97	[ $\Omega$ m]	Electrical Resistivity, $\rho$	1,7	[ $\Omega$ m]	Electrical Resistivity, $\rho$	x	[ $\Omega$ m]
Pundit: $v_p$	870	[m/s]	Pundit: $v_p$	625	[m/s]	Pundit: $v_p$	x	[m/s]
Pundit: $v_s$	242,7	[m/s]	Pundit: $v_s$	241,7	[m/s]	Pundit: $v_s$	x	[m/s]
Bender Element: $v_s$	x	[m/s]	Bender Element: $v_s$	164,8	[m/s]	Bender Element: $v_s$	x	[m/s]
UCS, $q_{uf}$	254,65	[kPa]	UCS, $q_{uf}$	200,71	[kPa]	UCS, $q_{uf}$	x	[kPa]
UCS, $\tau_{max}$	127,32	[kPa]	UCS, $\tau_{max}$	100,36	[kPa]	UCS, $\tau_{max}$	x	[kPa]
Secant modulus, $E_{50}$	13500	[kPa]	Secant modulus, $E_{50}$	10145	[kPa]	Secant modulus, $E_{50}$	x	[kPa]
Failure strain, $\epsilon_f$	2,64	[%]	Failure strain, $\epsilon_f$	4,92	[%]	Failure strain, $\epsilon_f$	x	[%]
S.1.50/200.BC1			S.2.50/200.BC1			S.3.50/200.BC1		
								
Height	108	[mm]	Height	108	[mm]	Height	108	[mm]
Diameter	54	[mm]	Diameter	54	[mm]	Diameter	54	[mm]
Electrical Resistivity, $\rho$	1,89	[ $\Omega$ m]	Electrical Resistivity, $\rho$	1,93	[ $\Omega$ m]	Electrical Resistivity, $\rho$	1,94	[ $\Omega$ m]
Pundit: $v_p$	597	[m/s]	Pundit: $v_p$	485	[m/s]	Pundit: $v_p$	469	[m/s]
Pundit: $v_s$	283,7	[m/s]	Pundit: $v_s$	215,1	[m/s]	Pundit: $v_s$	209	[m/s]
Bender Element: $v_s$	x	[m/s]	Bender Element: $v_s$	x	[m/s]	Bender Element: $v_s$	x	[m/s]
UCS, $q_{uf}$	240,02	[kPa]	UCS, $q_{uf}$	215,06	[kPa]	UCS, $q_{uf}$	210,80	[kPa]
UCS, $\tau_{max}$	120,01	[kPa]	UCS, $\tau_{max}$	107,53	[kPa]	UCS, $\tau_{max}$	105,40	[kPa]
Secant modulus, $E_{50}$	12755	[kPa]	Secant modulus, $E_{50}$	9653	[kPa]	Secant modulus, $E_{50}$	9881	[kPa]
Failure strain, $\epsilon_f$	3,74	[%]	Failure strain, $\epsilon_f$	3,49	[%]	Failure strain, $\epsilon_f$	3,85	[%]

P.1.100/50.LS1			P.2.100/50.LS1			P.3.100/50.LS1		
								
Height	108	[mm]	Height	108	[mm]	Height	108	[mm]
Diameter	54	[mm]	Diameter	54	[mm]	Diameter	54	[mm]
Electrical Resistivity, $\rho$	1,98	[ $\Omega$ m]	Electrical Resistivity, $\rho$	2,15	[ $\Omega$ m]	Electrical Resistivity, $\rho$	1,74	[ $\Omega$ m]
Pundit: $v_p$	1496	[m/s]	Pundit: $v_p$	277	[m/s]	Pundit: $v_p$	260	[m/s]
Pundit: $v_s$	x	[m/s]	Pundit: $v_s$	x	[m/s]	Pundit: $v_s$	x	[m/s]
Bender Element: $v_s$	71,5	[m/s]	Bender Element: $v_s$	44	[m/s]	Bender Element: $v_s$	42	[m/s]
UCS, $q_{uf}$	58,30	[kPa]	UCS, $q_{uf}$	61,67	[kPa]	UCS, $q_{uf}$	55,54	[kPa]
UCS, $\tau_{max}$	29,15	[kPa]	UCS, $\tau_{max}$	30,83	[kPa]	UCS, $\tau_{max}$	27,77	[kPa]
Secant modulus, $E_{50}$	2632	[kPa]	Secant modulus, $E_{50}$	1471	[kPa]	Secant modulus, $E_{50}$	1832	[kPa]
Failure strain, $\epsilon_f$	11,91	[%]	Failure strain, $\epsilon_f$	13,53	[%]	Failure strain, $\epsilon_f$	11,79	[%]
P.1.100/100.LS1			P.2.100/100.LS1			P.3.100/100.LS1		
								
Height	108	[mm]	Height	108	[mm]	Height	108	[mm]
Diameter	54	[mm]	Diameter	54	[mm]	Diameter	54	[mm]
Electrical Resistivity, $\rho$	3,37	[ $\Omega$ m]	Electrical Resistivity, $\rho$	3,09	[ $\Omega$ m]	Electrical Resistivity, $\rho$	2,82	[ $\Omega$ m]
Pundit: $v_p$	1500	[m/s]	Pundit: $v_p$	264	[m/s]	Pundit: $v_p$	1400	[m/s]
Pundit: $v_s$	x	[m/s]	Pundit: $v_s$	x	[m/s]	Pundit: $v_s$	x	[m/s]
Bender Element: $v_s$	42,7	[m/s]	Bender Element: $v_s$	48,1	[m/s]	Bender Element: $v_s$	48,8	[m/s]
UCS, $q_{uf}$	27,79	[kPa]	UCS, $q_{uf}$	34,84	[kPa]	UCS, $q_{uf}$	33,37	[kPa]
UCS, $\tau_{max}$	13,89	[kPa]	UCS, $\tau_{max}$	17,42	[kPa]	UCS, $\tau_{max}$	16,68	[kPa]
Secant modulus, $E_{50}$	735	[kPa]	Secant modulus, $E_{50}$	947	[kPa]	Secant modulus, $E_{50}$	1006	[kPa]
Failure strain, $\epsilon_f$	14,31	[%]	Failure strain, $\epsilon_f$	14,39	[%]	Failure strain, $\epsilon_f$	14,29	[%]
P.1.100/200.LS1			P.2.100/200.LS1			P.3.100/200.LS1		
								
Height	108	[mm]	Height	108	[mm]	Height	108	[mm]
Diameter	54	[mm]	Diameter	54	[mm]	Diameter	54	[mm]
Electrical Resistivity, $\rho$	3,36	[ $\Omega$ m]	Electrical Resistivity, $\rho$	3,24	[ $\Omega$ m]	Electrical Resistivity, $\rho$	2,83	[ $\Omega$ m]
Pundit: $v_p$	1496	[m/s]	Pundit: $v_p$	1426	[m/s]	Pundit: $v_p$	1430	[m/s]
Pundit: $v_s$	x	[m/s]	Pundit: $v_s$	x	[m/s]	Pundit: $v_s$	x	[m/s]
Bender Element: $v_s$	51,6	[m/s]	Bender Element: $v_s$	50,1	[m/s]	Bender Element: $v_s$	53,5	[m/s]
UCS, $q_{uf}$	38,78	[kPa]	UCS, $q_{uf}$	39,43	[kPa]	UCS, $q_{uf}$	40,15	[kPa]
UCS, $\tau_{max}$	19,39	[kPa]	UCS, $\tau_{max}$	19,72	[kPa]	UCS, $\tau_{max}$	20,08	[kPa]
Secant modulus, $E_{50}$	1280	[kPa]	Secant modulus, $E_{50}$	838	[kPa]	Secant modulus, $E_{50}$	1292	[kPa]
Failure strain, $\epsilon_f$	14,86	[%]	Failure strain, $\epsilon_f$	13,96	[%]	Failure strain, $\epsilon_f$	13,34	[%]



P.1.100/50.BA			P.2.100/50.BA			P.3.100/50.BA		
								
Height	108	[mm]	Height	108	[mm]	Height	108	[mm]
Diameter	54	[mm]	Diameter	54	[mm]	Diameter	54	[mm]
Electrical Resistivity, $\rho$	1,39	[ $\Omega$ m]	Electrical Resistivity, $\rho$	1,3	[ $\Omega$ m]	Electrical Resistivity, $\rho$	1,43	[ $\Omega$ m]
Pundit: $v_p$	1558	[m/s]	Pundit: $v_p$	262	[m/s]	Pundit: $v_p$	1500	[m/s]
Pundit: $v_s$	x	[m/s]	Pundit: $v_s$	x	[m/s]	Pundit: $v_s$	x	[m/s]
Bender Element: $v_s$	26,8	[m/s]	Bender Element: $v_s$	28,5	[m/s]	Bender Element: $v_s$	28,3	[m/s]
UCS, $q_{uf}$	27,21	[kPa]	UCS, $q_{uf}$	21,47	[kPa]	UCS, $q_{uf}$	22,72	[kPa]
UCS, $\tau_{max}$	13,61	[kPa]	UCS, $\tau_{max}$	10,74	[kPa]	UCS, $\tau_{max}$	11,36	[kPa]
Secant modulus, $E_{50}$	252	[kPa]	Secant modulus, $E_{50}$	267	[kPa]	Secant modulus, $E_{50}$	236	[kPa]
Failure strain, $\epsilon_f$	19,71	[%]	Failure strain, $\epsilon_f$	15,64	[%]	Failure strain, $\epsilon_f$	17,51	[%]
P.1.100/100.BA			P.2.100/100.BA			P.3.100/100.BA		
								
Height	108	[mm]	Height	108	[mm]	Height	108	[mm]
Diameter	54	[mm]	Diameter	54	[mm]	Diameter	54	[mm]
Electrical Resistivity, $\rho$	1,38	[ $\Omega$ m]	Electrical Resistivity, $\rho$	1,59	[ $\Omega$ m]	Electrical Resistivity, $\rho$	1,35	[ $\Omega$ m]
Pundit: $v_p$	1500	[m/s]	Pundit: $v_p$	1500	[m/s]	Pundit: $v_p$	256	[m/s]
Pundit: $v_s$	x	[m/s]	Pundit: $v_s$	x	[m/s]	Pundit: $v_s$	x	[m/s]
Bender Element: $v_s$	32,1	[m/s]	Bender Element: $v_s$	30	[m/s]	Bender Element: $v_s$	26,4	[m/s]
UCS, $q_{uf}$	38,54	[kPa]	UCS, $q_{uf}$	28,39	[kPa]	UCS, $q_{uf}$	37,14	[kPa]
UCS, $\tau_{max}$	19,27	[kPa]	UCS, $\tau_{max}$	14,20	[kPa]	UCS, $\tau_{max}$	18,57	[kPa]
Secant modulus, $E_{50}$	320	[kPa]	Secant modulus, $E_{50}$	286	[kPa]	Secant modulus, $E_{50}$	372	[kPa]
Failure strain, $\epsilon_f$	21,24	[%]	Failure strain, $\epsilon_f$	14,61	[%]	Failure strain, $\epsilon_f$	16,44	[%]
P.1.100/200.BA			P.2.100/200.BA			P.3.100/200.BA		
								
Height	108	[mm]	Height	108	[mm]	Height	108	[mm]
Diameter	54	[mm]	Diameter	54	[mm]	Diameter	54	[mm]
Electrical Resistivity, $\rho$	1,23	[ $\Omega$ m]	Electrical Resistivity, $\rho$	1,46	[ $\Omega$ m]	Electrical Resistivity, $\rho$	1,28	[ $\Omega$ m]
Pundit: $v_p$	302	[m/s]	Pundit: $v_p$	308	[m/s]	Pundit: $v_p$	309	[m/s]
Pundit: $v_s$	x	[m/s]	Pundit: $v_s$	x	[m/s]	Pundit: $v_s$	x	[m/s]
Bender Element: $v_s$	57,2	[m/s]	Bender Element: $v_s$	50,2	[m/s]	Bender Element: $v_s$	47,7	[m/s]
UCS, $q_{uf}$	48,91	[kPa]	UCS, $q_{uf}$	46,48	[kPa]	UCS, $q_{uf}$	42,30	[kPa]
UCS, $\tau_{max}$	24,45	[kPa]	UCS, $\tau_{max}$	23,24	[kPa]	UCS, $\tau_{max}$	21,15	[kPa]
Secant modulus, $E_{50}$	1185	[kPa]	Secant modulus, $E_{50}$	1119	[kPa]	Secant modulus, $E_{50}$	1097	[kPa]
Failure strain, $\epsilon_f$	13,64	[%]	Failure strain, $\epsilon_f$	12,86	[%]	Failure strain, $\epsilon_f$	12,09	[%]

P.1.100/50.PSA			P.2.100/50.PSA			P.3.100/50.PSA		
								
Height	108	[mm]	Height	108	[mm]	Height	108	[mm]
Diameter	54	[mm]	Diameter	54	[mm]	Diameter	54	[mm]
Electrical Resistivity, $\rho$	1,69	[ $\Omega$ m]	Electrical Resistivity, $\rho$	1,79	[ $\Omega$ m]	Electrical Resistivity, $\rho$	1,59	[ $\Omega$ m]
Pundit: $v_p$	1479	[m/s]	Pundit: $v_p$	308	[m/s]	Pundit: $v_p$	253	[m/s]
Pundit: $v_s$	x	[m/s]	Pundit: $v_s$	x	[m/s]	Pundit: $v_s$	x	[m/s]
Bender Element: $v_s$	51,1	[m/s]	Bender Element: $v_s$	49,8	[m/s]	Bender Element: $v_s$	47,6	[m/s]
UCS, $q_{uf}$	42,92	[kPa]	UCS, $q_{uf}$	37,97	[kPa]	UCS, $q_{uf}$	35,32	[kPa]
UCS, $\tau_{max}$	21,46	[kPa]	UCS, $\tau_{max}$	18,99	[kPa]	UCS, $\tau_{max}$	17,66	[kPa]
Secant modulus, $E_{50}$	542	[kPa]	Secant modulus, $E_{50}$	719	[kPa]	Secant modulus, $E_{50}$	695	[kPa]
Failure strain, $\epsilon_f$	20,59	[%]	Failure strain, $\epsilon_f$	15,66	[%]	Failure strain, $\epsilon_f$	12,41	[%]
P.1.100/100.PSA			P.2.100/100.PSA			P.3.100/100.PSA		
								
Height	108	[mm]	Height	108	[mm]	Height	108	[mm]
Diameter	54	[mm]	Diameter	54	[mm]	Diameter	54	[mm]
Electrical Resistivity, $\rho$	1,92	[ $\Omega$ m]	Electrical Resistivity, $\rho$	1,72	[ $\Omega$ m]	Electrical Resistivity, $\rho$	1,71	[ $\Omega$ m]
Pundit: $v_p$	1379	[m/s]	Pundit: $v_p$	272	[m/s]	Pundit: $v_p$	275	[m/s]
Pundit: $v_s$	x	[m/s]	Pundit: $v_s$	x	[m/s]	Pundit: $v_s$	x	[m/s]
Bender Element: $v_s$	40,8	[m/s]	Bender Element: $v_s$	33	[m/s]	Bender Element: $v_s$	29	[m/s]
UCS, $q_{uf}$	35,47	[kPa]	UCS, $q_{uf}$	31,86	[kPa]	UCS, $q_{uf}$	30,93	[kPa]
UCS, $\tau_{max}$	17,74	[kPa]	UCS, $\tau_{max}$	15,93	[kPa]	UCS, $\tau_{max}$	15,47	[kPa]
Secant modulus, $E_{50}$	630	[kPa]	Secant modulus, $E_{50}$	400	[kPa]	Secant modulus, $E_{50}$	381	[kPa]
Failure strain, $\epsilon_f$	15,24	[%]	Failure strain, $\epsilon_f$	14,29	[%]	Failure strain, $\epsilon_f$	13,99	[%]
P.1.100/200.PSA			P.2.100/200.PSA			P.3.100/200.PSA		
								
Height	108	[mm]	Height	108	[mm]	Height	108	[mm]
Diameter	54	[mm]	Diameter	54	[mm]	Diameter	54	[mm]
Electrical Resistivity, $\rho$	1,67	[ $\Omega$ m]	Electrical Resistivity, $\rho$	1,73	[ $\Omega$ m]	Electrical Resistivity, $\rho$	1,83	[ $\Omega$ m]
Pundit: $v_p$	270	[m/s]	Pundit: $v_p$	290	[m/s]	Pundit: $v_p$	289	[m/s]
Pundit: $v_s$	x	[m/s]	Pundit: $v_s$	x	[m/s]	Pundit: $v_s$	x	[m/s]
Bender Element: $v_s$	72,5	[m/s]	Bender Element: $v_s$	63,4	[m/s]	Bender Element: $v_s$	64,4	[m/s]
UCS, $q_{uf}$	58,84	[kPa]	UCS, $q_{uf}$	50,91	[kPa]	UCS, $q_{uf}$	48,45	[kPa]
UCS, $\tau_{max}$	29,42	[kPa]	UCS, $\tau_{max}$	25,45	[kPa]	UCS, $\tau_{max}$	24,22	[kPa]
Secant modulus, $E_{50}$	1391	[kPa]	Secant modulus, $E_{50}$	913	[kPa]	Secant modulus, $E_{50}$	921	[kPa]
Failure strain, $\epsilon_f$	10,59	[%]	Failure strain, $\epsilon_f$	12,46	[%]	Failure strain, $\epsilon_f$	11,46	[%]

<b>P.1.100/200.BC4</b>			<b>P.2.100/200.BC4</b>			<b>P.3.100/200.BC4</b>		
								
Height	<b>108</b>	[mm]	Height	<b>108</b>	[mm]	Height	<b>108</b>	[mm]
Diameter	<b>54</b>	[mm]	Diameter	<b>54</b>	[mm]	Diameter	<b>54</b>	[mm]
Electrical Resistivity, $\rho$	<b>3,59</b>	[ $\Omega$ m]	Electrical Resistivity, $\rho$	<b>3,03</b>	[ $\Omega$ m]	Electrical Resistivity, $\rho$	<b>3,35</b>	[ $\Omega$ m]
Pundit: $v_p$	<b>278</b>	[m/s]	Pundit: $v_p$	<b>273</b>	[m/s]	Pundit: $v_p$	<b>261</b>	[m/s]
Pundit: $v_s$	<b>x</b>	[m/s]	Pundit: $v_s$	<b>x</b>	[m/s]	Pundit: $v_s$	<b>x</b>	[m/s]
Bender Element: $v_s$	<b>92,4</b>	[m/s]	Bender Element: $v_s$	<b>86,9</b>	[m/s]	Bender Element: $v_s$	<b>89,9</b>	[m/s]
UCS, $q_{uf}$	<b>91,98</b>	[kPa]	UCS, $q_{uf}$	<b>93,31</b>	[kPa]	UCS, $q_{uf}$	<b>89,96</b>	[kPa]
UCS, $\tau_{max}$	<b>45,99</b>	[kPa]	UCS, $\tau_{max}$	<b>46,66</b>	[kPa]	UCS, $\tau_{max}$	<b>44,98</b>	[kPa]
Secant modulus, $E_{50}$	<b>4545</b>	[kPa]	Secant modulus, $E_{50}$	<b>3306</b>	[kPa]	Secant modulus, $E_{50}$	<b>2920</b>	[kPa]
Failure strain, $\epsilon_f$	<b>9,13</b>	[%]	Failure strain, $\epsilon_f$	<b>9,93</b>	[%]	Failure strain, $\epsilon_f$	<b>9,41</b>	[%]
<b>P.1.100/300.BC4</b>			<b>P.2.100/300.BC4</b>			<b>P.3.100/300.BC4</b>		
								
Height	<b>108</b>	[mm]	Height	<b>108</b>	[mm]	Height	<b>108</b>	[mm]
Diameter	<b>54</b>	[mm]	Diameter	<b>54</b>	[mm]	Diameter	<b>54</b>	[mm]
Electrical Resistivity, $\rho$	<b>6,39</b>	[ $\Omega$ m]	Electrical Resistivity, $\rho$	<b>5,15</b>	[ $\Omega$ m]	Electrical Resistivity, $\rho$	<b>4,49</b>	[ $\Omega$ m]
Pundit: $v_p$	<b>274</b>	[m/s]	Pundit: $v_p$	<b>266</b>	[m/s]	Pundit: $v_p$	<b>273</b>	[m/s]
Pundit: $v_s$	<b>x</b>	[m/s]	Pundit: $v_s$	<b>x</b>	[m/s]	Pundit: $v_s$	<b>x</b>	[m/s]
Bender Element: $v_s$	<b>91,9</b>	[m/s]	Bender Element: $v_s$	<b>79,5</b>	[m/s]	Bender Element: $v_s$	<b>74,4</b>	[m/s]
UCS, $q_{uf}$	<b>94,42</b>	[kPa]	UCS, $q_{uf}$	<b>93,09</b>	[kPa]	UCS, $q_{uf}$	<b>101,97</b>	[kPa]
UCS, $\tau_{max}$	<b>47,21</b>	[kPa]	UCS, $\tau_{max}$	<b>46,55</b>	[kPa]	UCS, $\tau_{max}$	<b>50,98</b>	[kPa]
Secant modulus, $E_{50}$	<b>2768</b>	[kPa]	Secant modulus, $E_{50}$	<b>2807</b>	[kPa]	Secant modulus, $E_{50}$	<b>2749</b>	[kPa]
Failure strain, $\epsilon_f$	<b>12,08</b>	[%]	Failure strain, $\epsilon_f$	<b>9,55</b>	[%]	Failure strain, $\epsilon_f$	<b>10,15</b>	[%]
<b>P.1.100/400.BC4</b>			<b>P.2.100/400.BC4</b>			<b>P.3.100/400.BC4</b>		
								
Height	<b>108</b>	[mm]	Height	<b>108</b>	[mm]	Height	<b>108</b>	[mm]
Diameter	<b>54</b>	[mm]	Diameter	<b>54</b>	[mm]	Diameter	<b>54</b>	[mm]
Electrical Resistivity, $\rho$	<b>5,48</b>	[ $\Omega$ m]	Electrical Resistivity, $\rho$	<b>4,85</b>	[ $\Omega$ m]	Electrical Resistivity, $\rho$	<b>4,54</b>	[ $\Omega$ m]
Pundit: $v_p$	<b>301</b>	[m/s]	Pundit: $v_p$	<b>286</b>	[m/s]	Pundit: $v_p$	<b>303</b>	[m/s]
Pundit: $v_s$	<b>x</b>	[m/s]	Pundit: $v_s$	<b>x</b>	[m/s]	Pundit: $v_s$	<b>x</b>	[m/s]
Bender Element: $v_s$	<b>92,8</b>	[m/s]	Bender Element: $v_s$	<b>88,8</b>	[m/s]	Bender Element: $v_s$	<b>86,9</b>	[m/s]
UCS, $q_{uf}$	<b>98,28</b>	[kPa]	UCS, $q_{uf}$	<b>116,09</b>	[kPa]	UCS, $q_{uf}$	<b>106,79</b>	[kPa]
UCS, $\tau_{max}$	<b>49,14</b>	[kPa]	UCS, $\tau_{max}$	<b>58,05</b>	[kPa]	UCS, $\tau_{max}$	<b>53,40</b>	[kPa]
Secant modulus, $E_{50}$	<b>4211</b>	[kPa]	Secant modulus, $E_{50}$	<b>2930</b>	[kPa]	Secant modulus, $E_{50}$	<b>3540</b>	[kPa]
Failure strain, $\epsilon_f$	<b>7,51</b>	[%]	Failure strain, $\epsilon_f$	<b>8,93</b>	[%]	Failure strain, $\epsilon_f$	<b>7,88</b>	[%]



## **Appendix B**

# **Interpretation of Unconfined Compression Strength Testing**

Appendix B gives a complete overview of every interpretation of the Unconfined Compression Strength (UCS) testing.

## Interpreted results from uniaxial compressional strength test

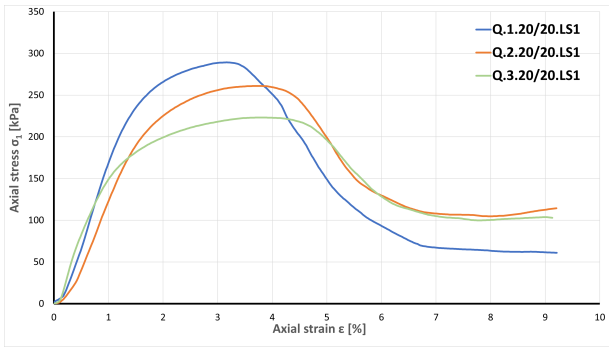
The following pages presents the interpreted results from Uniaxial compressional strength testing conducted in the period of 07.04.2023 - 15.04.2023. Out of the total 108 samples, made over the 9 mixing days, 99 have been tested in the uniaxial. The remaining 9 samples broke beforehand. Results for samples from same batch (up to 3 samples) are plotted together. An overview on how the results are presented, is given in the following table:

Presentation of results

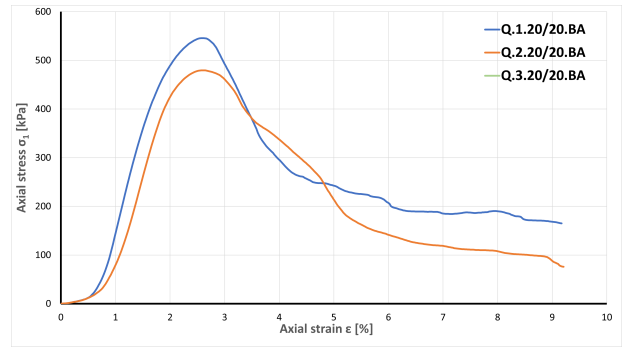
Date	Description
07.04.2023	Quick clay with 20/20 mixes for LS1, BA and PSA*, and 50/50 mixes for BC1
08.04.2023	Quick clay with 40/40 mixes for LS1, BA and PSA*, and 50/100 mixes for BC1
09.04.2023	Quick clay with 60/60 mixes for LS1, BA and PSA*, and 50/200 mixes for BC1
10.04.2023	Onsøy clay with 20/20 mixes for LS1, BA and PSA*, and 50/50 mixes for BC1
11.04.2023	Onsøy clay with 40/40 mixes for LS1, BA and PSA*, and 50/100 mixes for BC1
12.04.2023	Onsøy clay with 60/60 mixes for LS1, BA and PSA*, and 50/200 mixes for BC1
13.04.2023	Peat with 100/50 mixes for LS1, BA and PSA*, and 100/200 mixes for BC4
14.04.2023	Peat with 100/100 mixes for LS1, BA and PSA*, and 100/300 mixes for BC4
15.04.2023	Peat with 100/200 mixes for LS1, BA and PSA*, and 100/400 mixes for BC4

\* Important: All *RPMS* in plot legends are equivalent to *PSA*

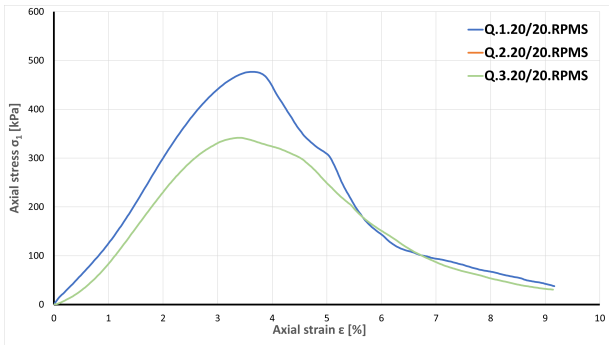
07.04.2023



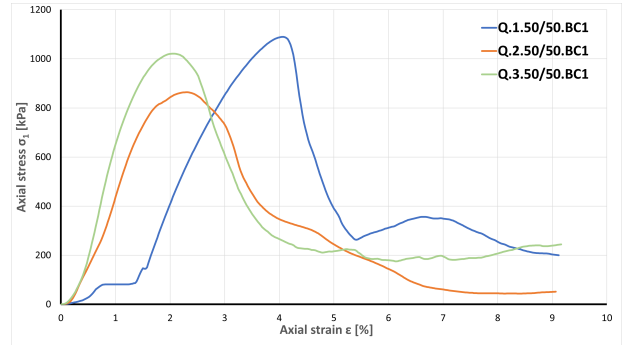
LS1



BA



PSA

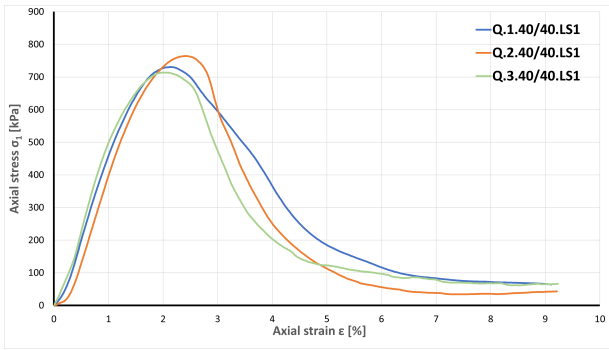


BC1

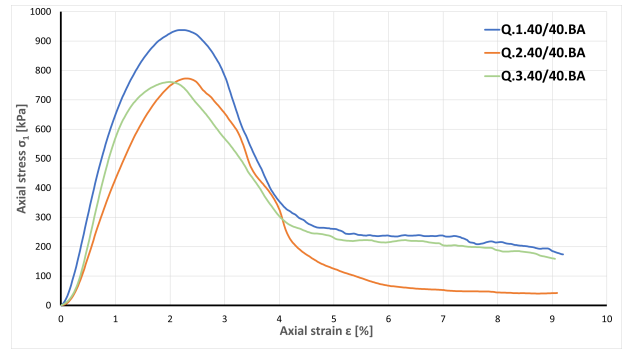
Interpreted results for samples from 07.04.2023

Sample ID	$q_u$ [kPa]	$s_u$ [kPa]	$E_{50}$ [kPa]	$\epsilon_f$ [%]
Q.1.20/20.LS1	289.23	144.62	19886.36	3.19
Q.2.20/20.LS1	261.01	130.51	18716.58	3.72
Q.3.20/20.LS1	223.23	111.62	19774.01	3.79
Q.1.20/20.BA	545.69	272.85	36585.37	2.59
Q.2.20/20.BA	479.47	239.74	35928.14	2.60
Q.3.20/20.BA	-	-	-	-
Q.1.20/20.PSA	473.93	238.46	20689.66	3.62
Q.2.20/20.PSA	-	-	-	-
Q.3.20/20.PSA	341.72	170.86	15290.52	3.41
Q.1.50/50.BC1	1089.63	544.8	59782.6	4.05
Q.2.50/50.BC1	864.17	462.09	55214.72	2.29
Q.3.50/50.BC1	1021.15	510.57	72847.68	2.06

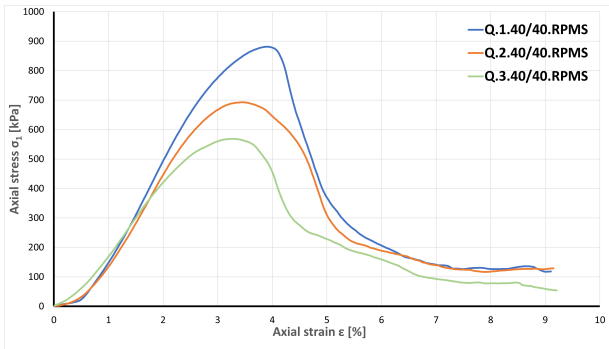
08.04.2023



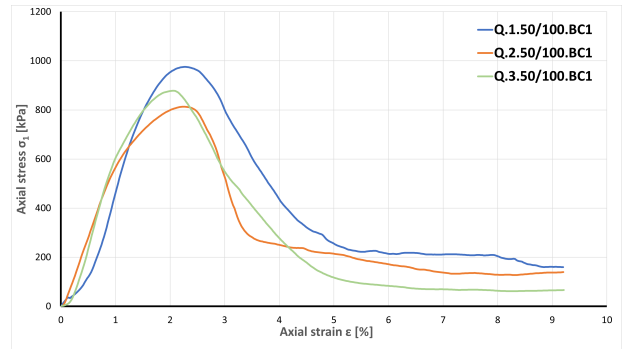
LS1



BA



PSA



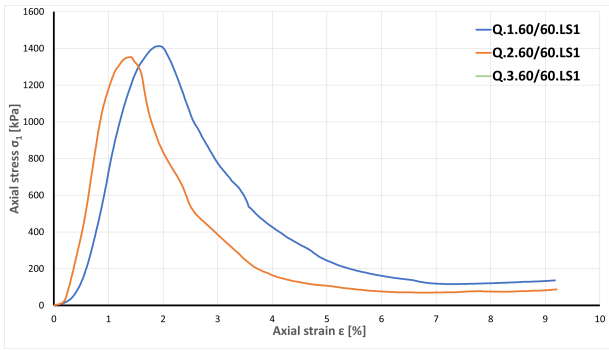
BC1

Interpreted results for samples from 08.04.2023

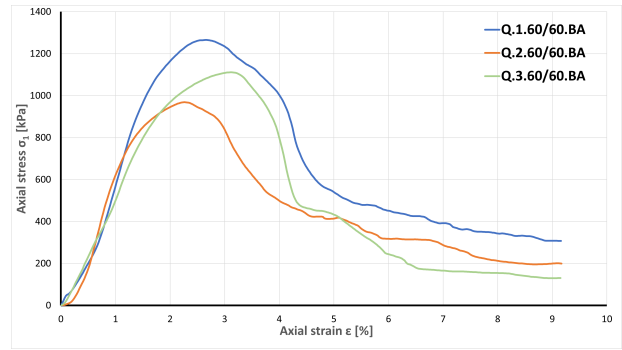
Sample ID	$q_u$ [kPa]	$s_u$ [kPa]	$E_{50}$ [kPa]	$\epsilon_f$ [%]
Q.1.40/40.LS1	730.45	365.23	49773.76	2.15
Q.2.40/40.LS1	764.36	382.00	51428.57	2.40
Q.3.40/40.LS1	713.53	356.77	59139.78	2.05
Q.1.40/40.BA	937.88	468.94	78571.43	2.21
Q.2.40/40.BA	772.97	386.48	55214.72	2.30
Q.3.40/40.BA	760.84	380.42	69182.39	2.00
Q.1.40/40.PSA	881.12	440.56	32163.74	3.92
Q.2.40/40.PSA	692.61	346.31	27607.36	3.46
Q.3.40/40.PSA	568.71	284.35	26829.27	3.29
Q.1.50/100.BC1	975.57	487.78	67901.23	2.26
Q.2.50/100.BC1	813.49	406.75	57324.84	2.25
Q.3.50/100.BC1	878.32	439.16	65476.19	2.07



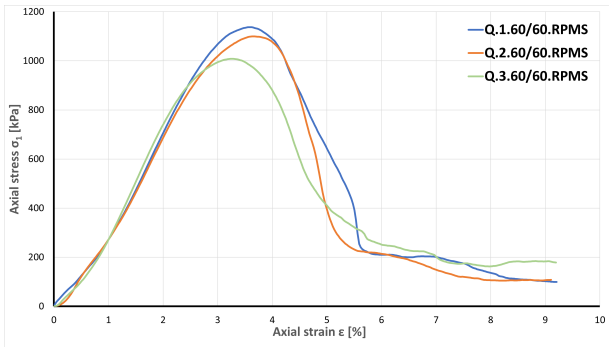
09.04.2023



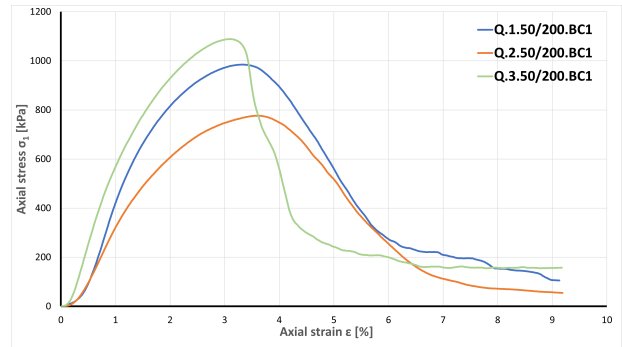
LS1



BA



PSA

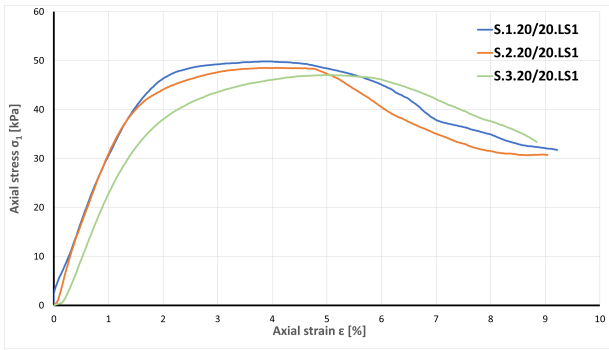


BC1

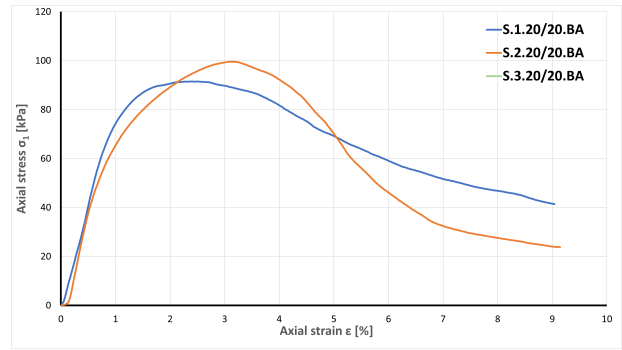
Interpreted results for samples from 09.04.2023

Sample ID	$q_u$ [kPa]	$s_u$ [kPa]	$E_{50}$ [kPa]	$\epsilon_f$ [%]
Q.1.60/60.LS1	1412.46	706.23	98039.22	1.93
Q.2.60/60.LS1	1353.12	676.56	123966.94	1.41
Q.3.60/60.LS1	-	-	-	-
Q.1.60/60.BA	1265.62	632.81	80645.16	2.67
Q.2.60/60.BA	968.91	484.45	74324.32	2.26
Q.3.60/60.BA	1111.33	555.67	56994.82	3.13
Q.1.60/60.PSA	1137.34	568.67	38167.94	3.6
Q.2.60/60.PSA	1099.83	549.91	35830.62	3.65
Q.3.60/60.PSA	1008.24	504.12	47210.3	3.26
Q.1.50/200.BC1	984.63	492.31	55000	3.31
Q.2.50/200.BC1	776.39	388.19	38135.59	3.6
Q.3.50/200.BC1	1088.6	544.31	63953.49	3.1

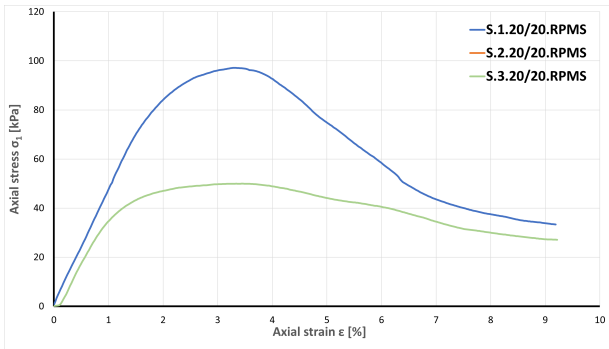
10.04.2023



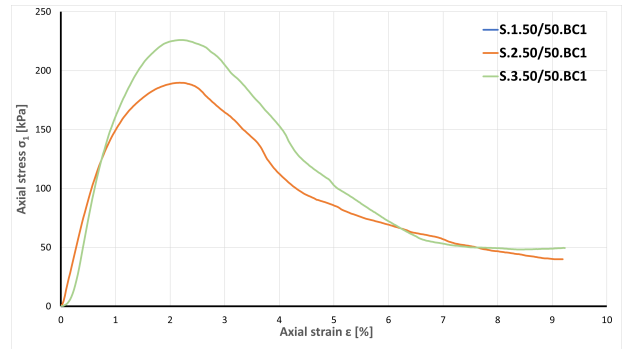
LS1



BA



PSA

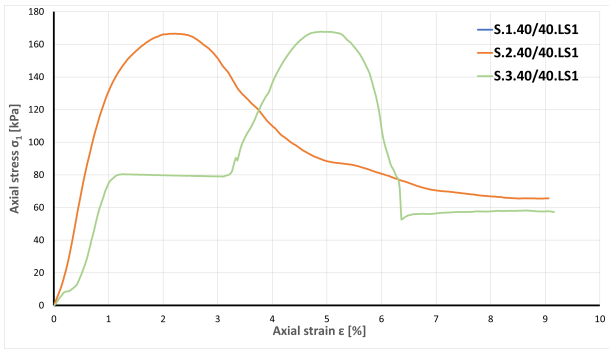


BC1

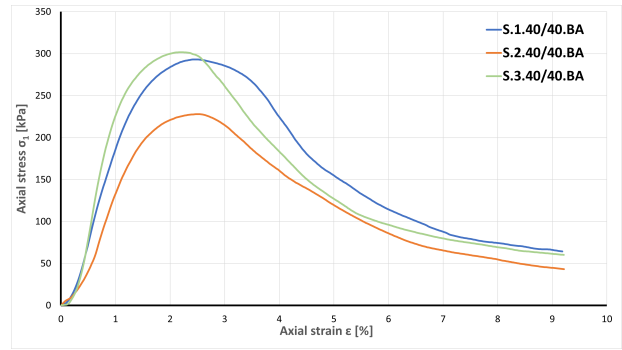
Interpreted results for samples from 10.04.2023

Sample ID	$q_u$ [kPa]	$s_u$ [kPa]	$E_{50}$ [kPa]	$\epsilon_f$ [%]
S.1.20/20.LS1	49.87	24.93	3365.38	3.94
S.2.20/20.LS1	48.53	24.27	3414.63	4.09
S.3.20/20.LS1	47.08	23.54	2702.7	5.04
S.1.20/20.BA	91.5	45.76	8685.65	2.51
S.2.20/20.BA	99.6	49.8	8208.96	3.16
S.3.20/20.BA	-	-	-	-
S.1.20/20.PSA	97.15	48.57	4888.89	3.31
S.2.20/20.PSA	-	-	-	-
S.3.20/20.PSA	49.96	24.98	4511.28	3.44
S.1.50/50.BC1	-	-	-	-
S.2.50/50.BC1	189.75	94.87	20202.02	2.20
S.3.50/50.BC1	225.99	113	20869.57	2.19

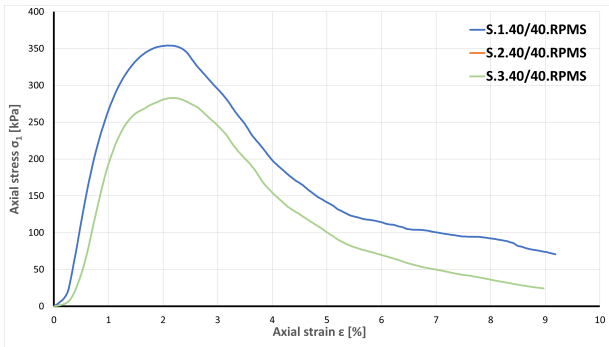
11.04.2023



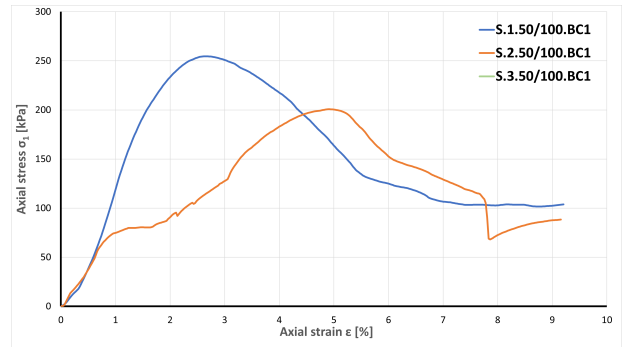
LS1



BA



PSA

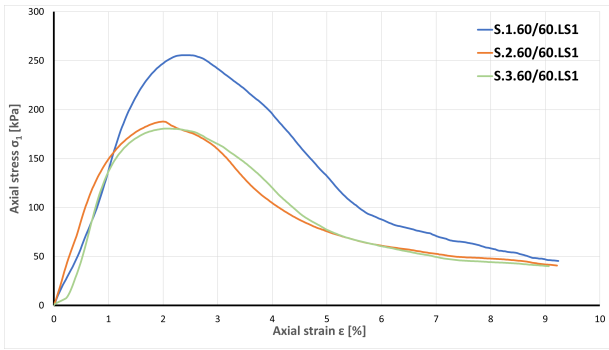


BC1

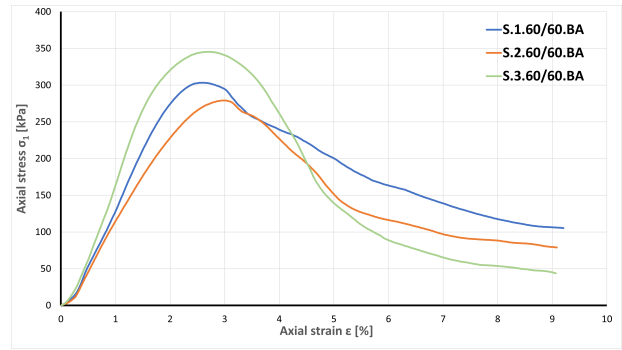
Interpreted results for samples from 11.04.2023

Sample ID	$q_u$ [kPa]	$s_u$ [kPa]	$E_{50}$ [kPa]	$\epsilon_f$ [%]
S.1.40/40.LS1	-	-	-	-
S.2.40/40.LS1	166.53	83.26	15596.33	2.23
S.3.40/40.LS1	167.74	83.87	11258.28	4.87
S.1.40/40.BA	293.1	146.55	20270.27	2.51
S.2.40/40.BA	228.06	114.04	13793.1	2.52
S.3.40/40.BA	301.8	150.9	28571.43	2.21
S.1.40/40.PSA	354.13	177.07	32743.36	2.11
S.2.40/40.PSA	-	-	-	-
S.3.40/40.PSA	282.96	141.48	26229.51	2.16
S.1.50/100.BC1	254.64	127.32	13500	2.64
S.2.50/100.BC1	200.71	100.36	10144.93	4.92
S.3.50/100.BC1	-	-	-	-

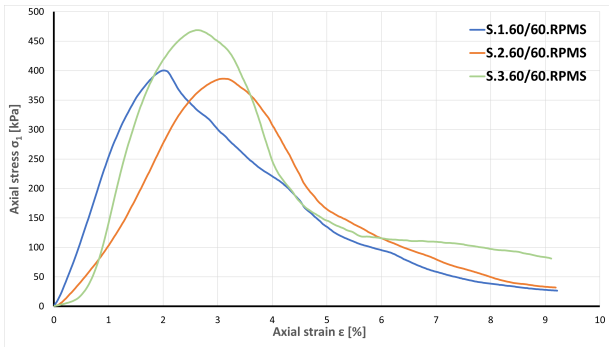
12.04.2023



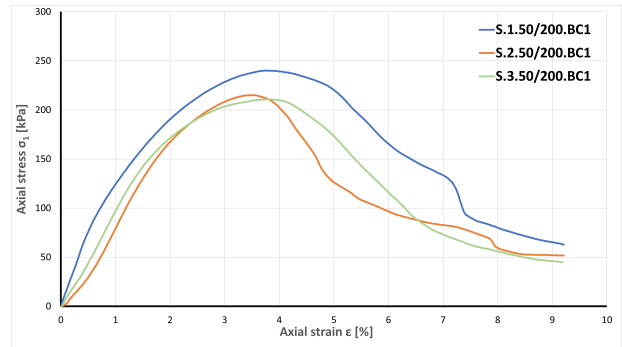
LS1



BA



PSA

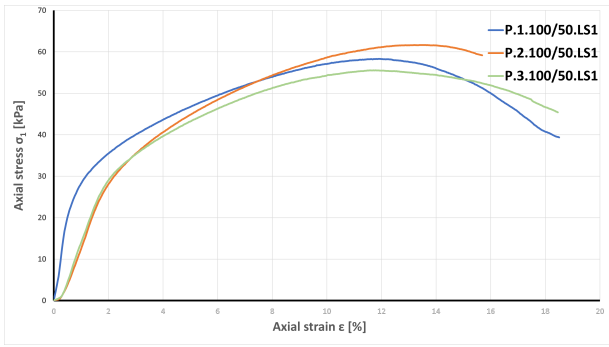


BC1

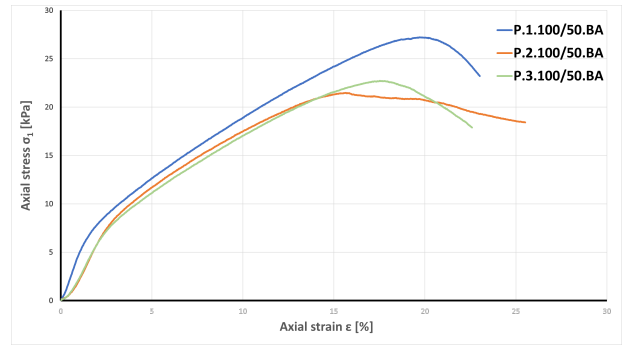
Interpreted results for samples from 12.04.2023

Sample ID	$q_u$ [kPa]	$s_u$ [kPa]	$E_{50}$ [kPa]	$\epsilon_f$ [%]
S.1.60/60.LS1	255.65	127.83	13265.31	2.41
S.2.60/60.LS1	187.8	93.9	18095.24	2
S.3.60/60.LS1	180.7	90.35	17431.19	2.07
S.1.60/60.BA	303.35	151.68	15121.95	2.56
S.2.60/60.BA	279.14	139.57	14222.22	2.99
S.3.60/60.BA	345.38	172.69	19553.07	2.73
S.1.60/60.PSA	400.26	200.13	27891.16	2
S.2.60/60.PSA	386.31	193.16	13793.16	3.1
S.3.60/60.PSA	468.95	234.48	31543.62	2.62
S.1.50/200.BC1	240.02	120.01	12755.1	3.74
S.2.50/200.BC1	215.06	107.53	9652.51	3.49
S.3.50/200.BC1	210.8	105.4	9881.42	3.85

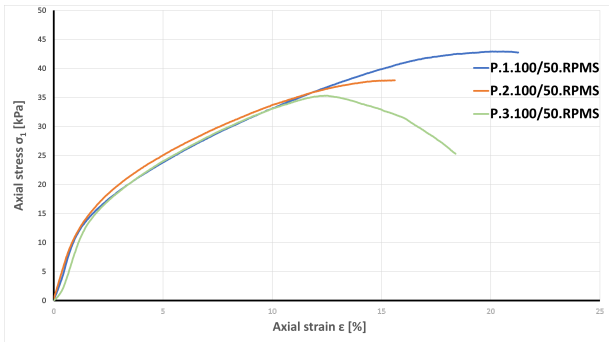
13.04.2023



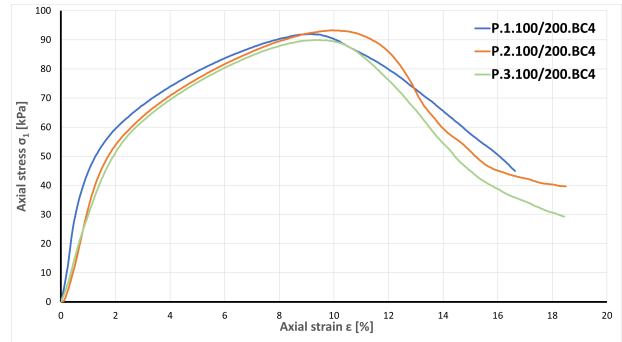
LS1



BA



PSA

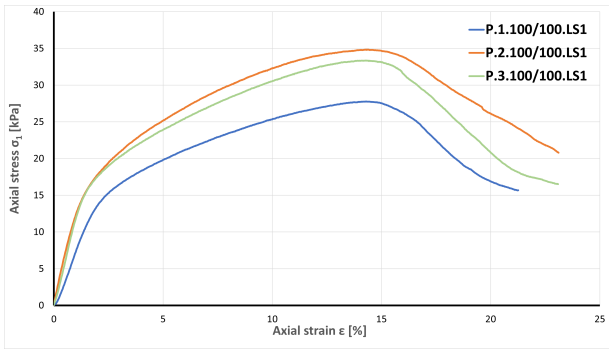


BC1

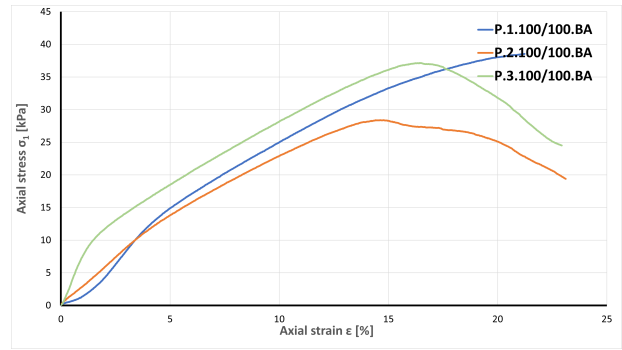
Interpreted results for samples from 13.04.2023

Sample ID	$q_u$ [kPa]	$s_u$ [kPa]	$E_{50}$ [kPa]	$\epsilon_f$ [%]
P.1.100/50.LS1	58.3	29.15	2632	11.91
P.2.100/50.LS1	61.67	30.83	1471	13.53
P.3.100/50.LS1	55.54	27.77	1832	11.79
P.1.100/50.BA	27.21	13.61	252	19.71
P.2.100/50.BA	21.47	10.74	267	15.64
P.3.100/50.BA	22.71	11.36	236	17.51
P.1.100/50.PSA	42.92	21.46	542	20.59
P.2.100/50.PSA	37.97	18.99	719	15.66
P.3.100/50.PSA	35.32	17.66	695	12.41
P.1.100/200.BC4	91.98	45.99	4545	9.13
P.2.100/200.BC4	93.31	46.66	3306	9.93
P.3.100/200.BC4	89.96	44.98	2920	9.41

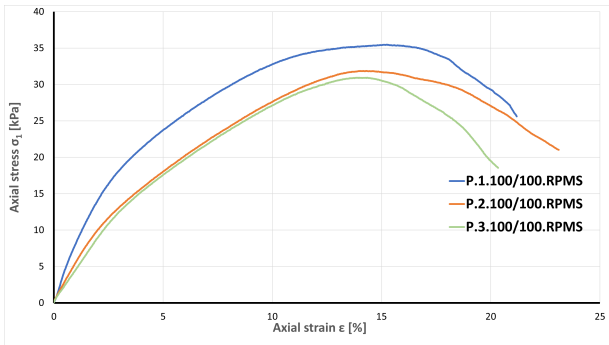
14.04.2023



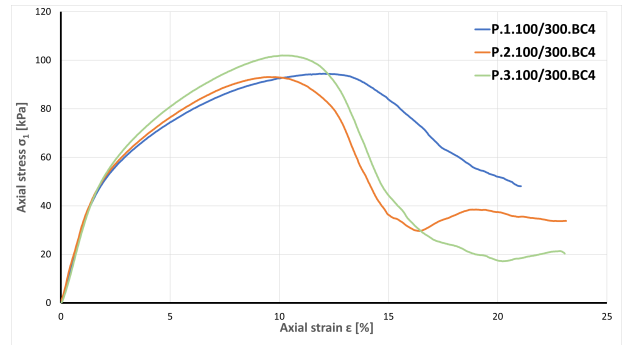
LS1



BA



PSA

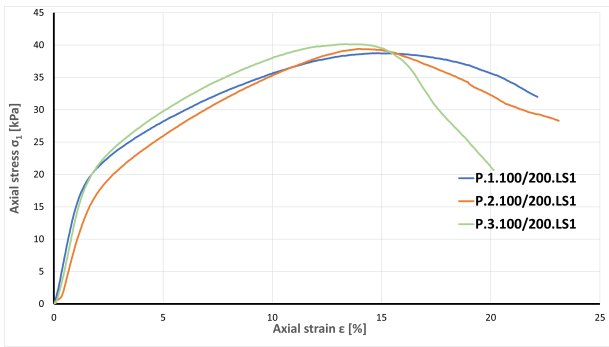


BC1

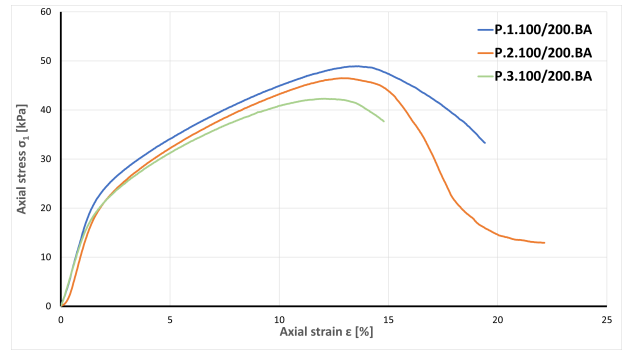
Interpreted results for samples from 14.04.2023

Sample ID	$q_u$ [kPa]	$s_u$ [kPa]	$E_{50}$ [kPa]	$\epsilon_f$ [%]
P.1.100/100.LS1	27.79	13.89	735	14.31
P.2.100/100.LS1	34.84	17.42	947	14.39
P.3.100/100.LS1	33.37	16.68	1006	14.29
P.1.100/100.BA	38.54	19.27	320	21.24
P.2.100/100.BA	28.39	14.2	286	14.61
P.3.100/100.BA	37.14	18.57	372	16.44
P.1.100/100.PSA	35.47	17.74	630	15.24
P.2.100/100.PSA	31.86	15.93	400	14.29
P.3.100/100.PSA	30.93	15.47	381	13.99
P.1.100/300.BC4	94.42	47.21	2768	12.08
P.2.100/300.BC4	93.09	46.55	2807	9.55
P.3.100/300.BC4	101.97	50.98	2749	10.15

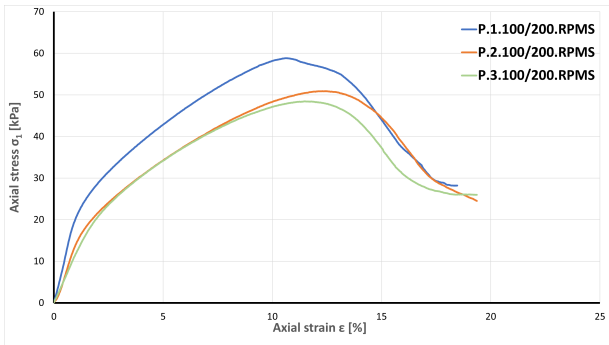
15.04.2023



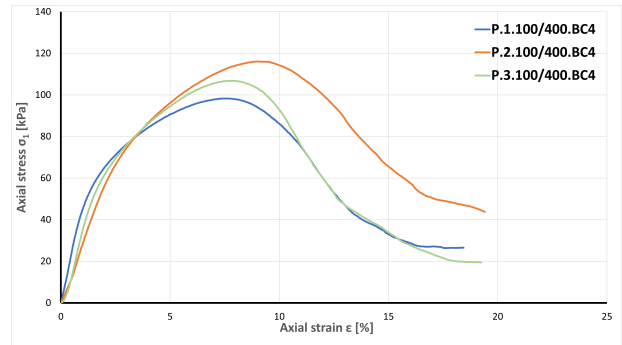
LS1



BA



PSA



BC1

Interpreted results for samples from 15.04.2023

Sample ID	$q_u$ [kPa]	$s_u$ [kPa]	$E_{50}$ [kPa]	$\epsilon_f$ [%]
P.1.100/200.LS1	38.78	19.39	1280	14.86
P.2.100/200.LS1	39.43	19.72	838	13.96
P.3.100/200.LS1	40.15	20.08	1292	13.34
P.1.100/200.BA	48.91	24.45	1185	13.64
P.2.100/200.BA	46.48	23.24	1119	12.86
P.3.100/200.BA	42.3	21.15	1097	12.09
P.1.100/200.PSA	58.84	29.42	1391	10.59
P.2.100/200.PSA	50.91	25.45	913	12.46
P.3.100/200.PSA	48.45	24.22	921	11.46
P.1.100/400.BC4	98.28	49.14	4211	7.51
P.2.100/400.BC4	116.09	58.05	2930	8.93
P.3.100/400.BC4	106.79	53.4	3540	7.88

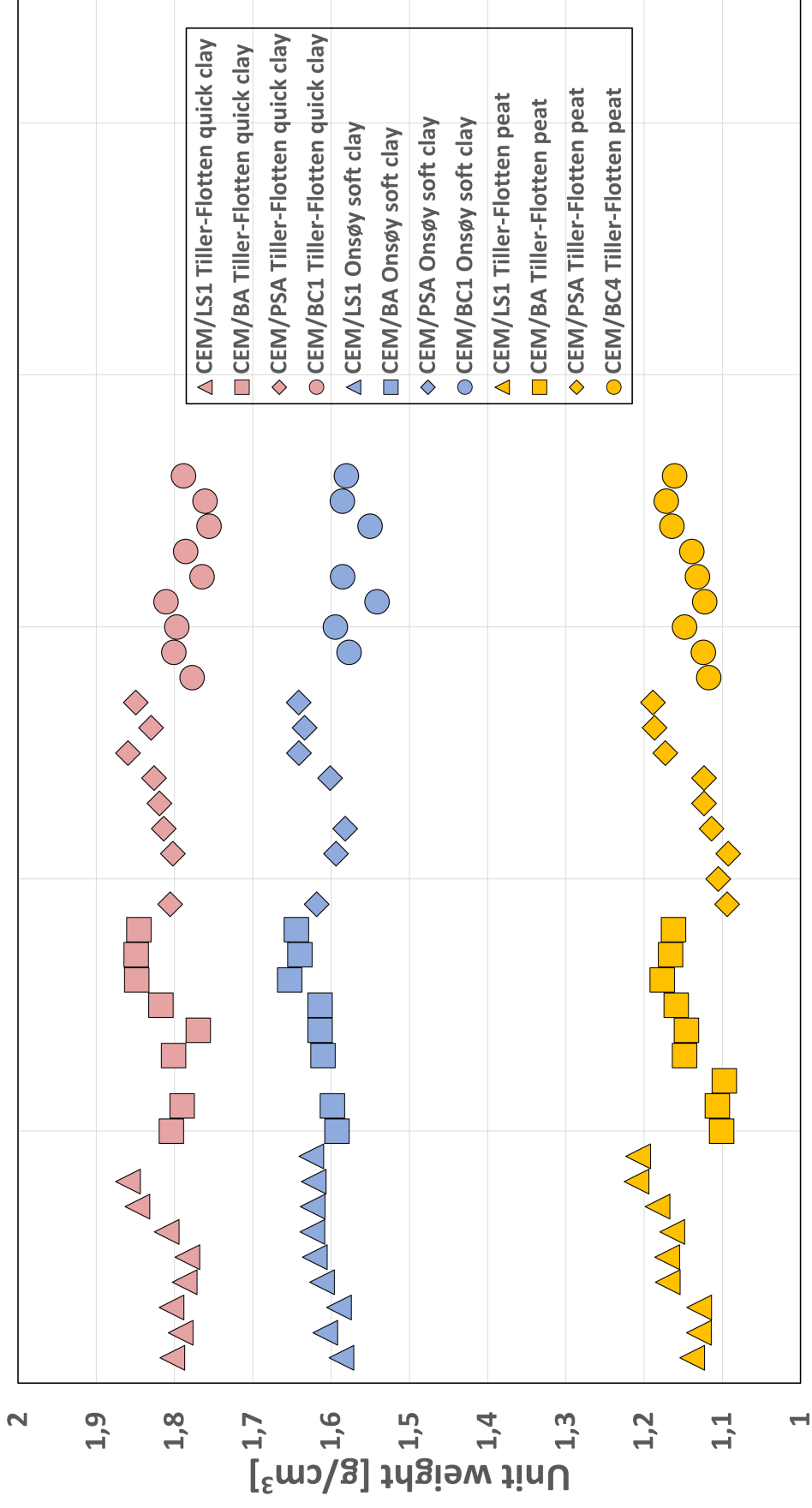




## Appendix C

# Sample Densities

Appendix C gives a summary of all measured densities. The different soil types and binder combinations are labeled according to the legend. The different binder ratios are not labeled, but the binder ratios increases from left to right within one binder combination.

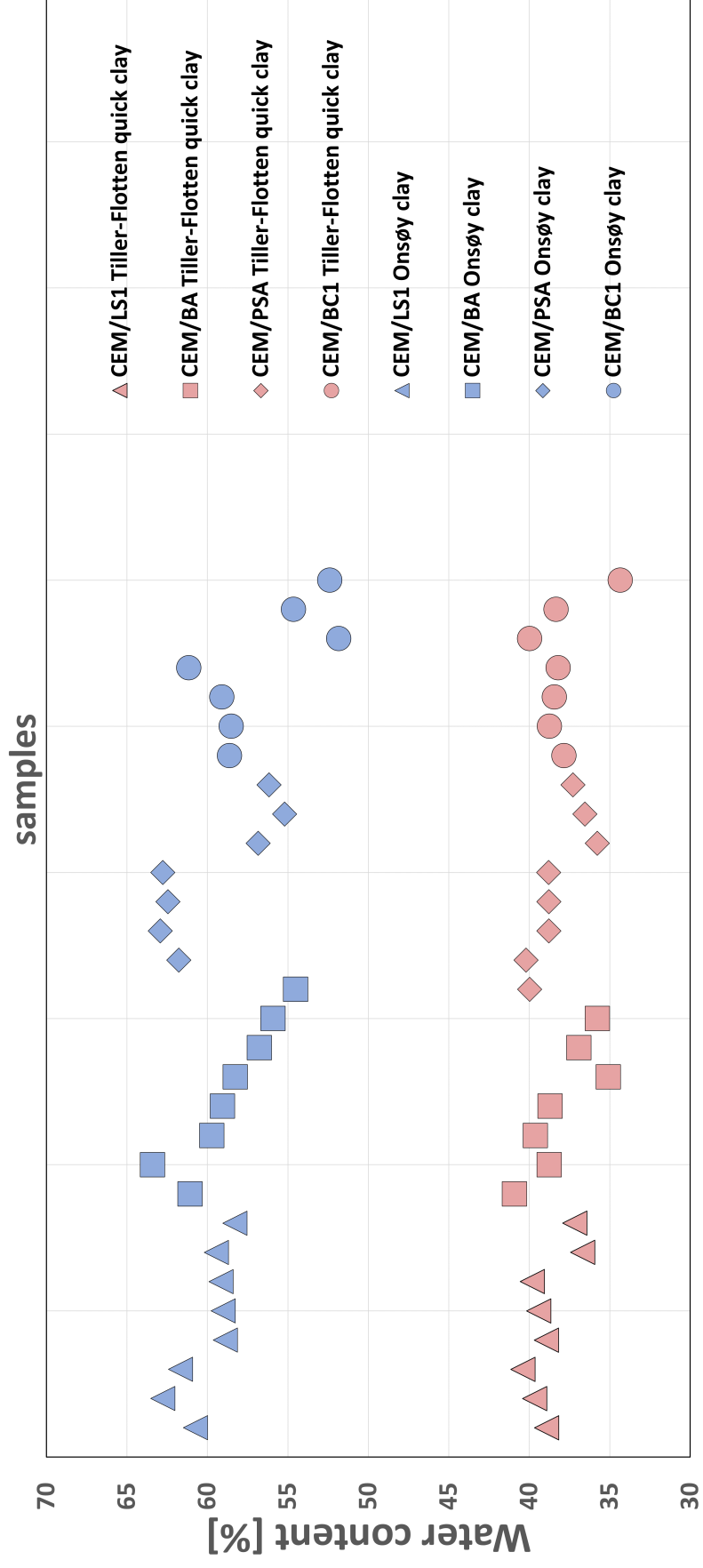


## Appendix D

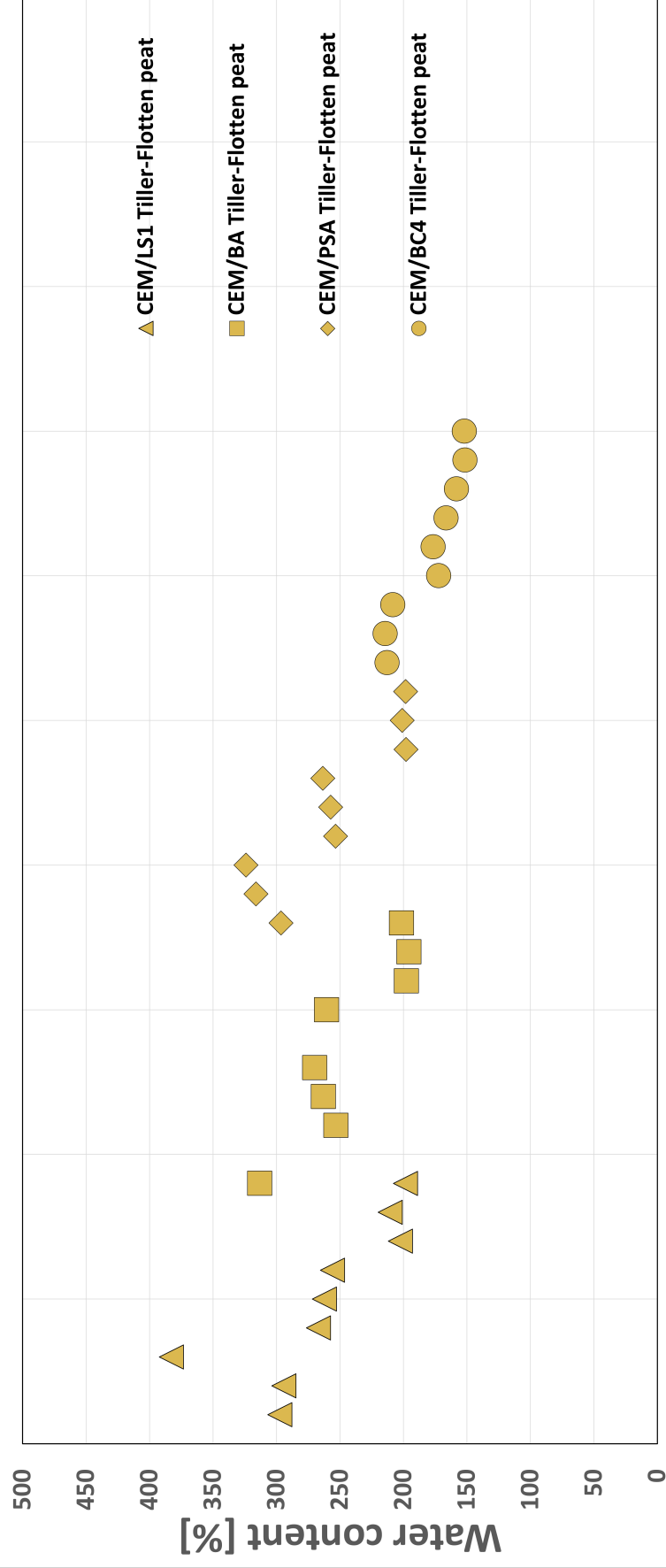
# Water Content of Stabilized Samples

Appendix D gives a presentation of the water content of the stabilized Tiller-Flotten quick clay and peat, and Onsøy soft clay samples. The presentation is divided into two plots, with the quick clay and soft clay together since it is in the same order of magnitude, whereas the peat is significantly higher. Further, the plot is divided to present samples with the same binder combination together, see plot legends. For each binder combination, the lowest binder ratio is the one furthest to the left, and the ratio grows going right. The representation generally shows that the water content decreases with an increase in the binder ratio.

# Water content of stabilized Tiller Flotten quick clay and Onsøy samples



Water content of stabilized Tiller-Flotten peat samples







 **NTNU**

Norwegian University of  
Science and Technology